Title
Analysis of Social and Flow Networks

Author
Askarzadeh, Zahra

Publication Date
2021

Peer reviewed|Thesis/dissertation

UNIVERSITY OF CALIFORNIA,
IRVINE

Analysis of Social and Flow Networks

DISSERTATION

submitted in partial satisfaction of the requirements
for the degree of

DOCTOR OF PHILOSOPHY

in Mechanical and Aerospace Engineering

by

Zahra Askarzadeh

Dissertation Committee:
Professor Tryphon T. Georgiou, Chair
Professor Athanasios Sideris
Professor Haithem Taha

2021

DEDICATION

To Mom and Dad.

TABLE OF CONTENTS

LIST OF FIGURES

LIST OF TABLES

ACKNOWLEDGMENTS

First and foremost, I would like to thank my advisor, Professor Tryphon Georgiou, for guiding me through my research at UCI. His enthusiasm for science gave me motivation to continue pursuing my research. I am very thankful for all the advice that he has given me over the years.

I have been fortunate to have collaborated with a number of great scientists over the years, and I am thankful to each of them for the roles that they have played in my career. I had the privilege to work with Dr. Abhishek Halder and Dr. Rui Fu. I would like to thank them for the memorable collaboration, all the hard work, and the time that we talked about different ideas. I also had the pleasure to work with Dr. Fariba Ariaei. I would like to thank her for her great collaboration and insightful feedbacks.

I would like to thank Dr. Kiyoshi Nakayama for giving me the exciting opportunity of being part of building start-up company, quite a unique experience.

Finally, I would like to thank my Mom, Dad, and sisters, no matter how far we were I received lots of love and support from them. I am forever thankful to my parents for giving me the opportunities and experiences that have made me who I am.

VITA

Zahra Askarzadeh

EDUCATION

Doctor of Philosophy in Mechanical and Aerospace Engineering **2016-2021**
University of California, Irvine *Irvine, USA*

Master of Science in Mechanical and Aerospace Engineering **2016-2019**
University of California, Irvine *Irvine, USA*

Bachelor of Science in Mechanical Engineering **2011-2016**
Sharif University of Technology *Tehran, Iran*

RESEARCH EXPERIENCE

Graduate Research Assistant **2017–2021**
University of California, Irvine *Irvine, California*

TEACHING EXPERIENCE

Teaching Assistant **Fall 2018**
University of California, Irvine *Irvine, California*

Teaching Assistant **Fall 2020**
University of California, Irvine *Irvine, California*

Teaching Assistant **Winter 2021**
University of California, Irvine *Irvine, California*

Teaching Assistant **Summer 2021**
University of California, Irvine *Irvine, California*

REFEREED JOURNAL PUBLICATIONS

Stability Theory of Stochastic Models in Opinion Dynamics **2019**
IEEE Transactions on Automatic Control

Macroscopic Network Circulation for Planar Graphs **2021**
IEEE Transactions on Control of Network Systems

REFEREED CONFERENCE PUBLICATIONS

Opinion Dynamics over Influence Networks **2019**
The 2019 American Control Conference (ACC)

ABSTRACT OF THE DISSERTATION

Analysis of Social and Flow Networks

By

Zahra Askarzadeh

Doctor of Philosophy in Mechanical and Aerospace Engineering

University of California, Irvine, 2021

Professor Tryphon T. Georgiou, Chair

In this thesis, we study problems in analysis of social and flow networks. Specifically, we study models of social interactions between individuals who discuss and form opinions about a sequence of issues. We also study quantifying macroscopic circulation in a given planar graph.

A social network is a medium for the exchange of information, ideas, and influence among its members. In recent years, availability of large amounts of data from online social networks have drawn the attention of many researchers to study opinion formation and the evolutionary behaviors in social networks. In this thesis, we revisit several types of opinion dynamics models and review relevant results from the literature. We then present a set of new results related to both modeling and analysis of social networks. Starting with analyzing DeGroot-Friedkin model, we establish existence and uniqueness of its fixed point using local inverse function theorem and Hadamard's global inverse function theorem. Motivated by DeGroot-Friedkin model, we then propose a group of nonlinear Markov chain models of social interaction for the purpose of assessing opinion evolution in social networks. We seek and develop conditions that determine when such system display oscillations, manifest chaos, or lead to a stable equilibrium that represents consensus. We also provide extensions of proposed models to count for different subgroups of interacting individuals.

Flow networks are typically used to model problems involving the transportation of mass between

nodes, through routes that have limited capacity. Examples of such problems that motivate our research are modeling traffic on a network of roads and blood current in heart. Based on these examples, we introduce a new concept of maximal global circulation and explore 3-partitions that expose this type of macroscopic feature of networks. Herein, graph circulation is motivated by probabilistic flows (Markov chains) on graphs. Our goal is to quantify the large-scale imbalance of network flows and delineate key parts that mediate such global features. While we introduce and propose these notions in a general setting, here, we only work out the case of planar graphs. We explain that a scalar potential can be identified to encapsulate the concept of circulation, quite similarly as in the case of the curl of planar vector fields. Beyond planar graphs, in the general case, the problem to determine global circulation remains at present a combinatorial problem.

Chapter 1

Introduction

A network is a collection of objects (called nodes or vertices) in which some pairs of the objects are connected together. The connections between the vertices are called edges. A network can be used to model many types of relations and dynamical processes in a wide range of areas, e.g., computer science, biological, and social systems. This thesis is focused on problems involving analysis of social networks and flow networks.

Social networks has enabled individuals to be more closely connected and has provided huge amount of data available for analysis regarding how individuals interact over networks. Consequently, there has been increased interest in understanding how individuals form opinion and interact with others in their social network. The study of social interaction is important because it allows researchers to predict behavior of network and may further be motivated by potential marketing applications.

Flow networks are typically used to model problems involving the transportation of mass between nodes, through routes that have limited capacity. Modeling traffic on a network of roads, blood current in heart, fluid in a network of pipes, and airline scheduling are examples of flow networks.

This thesis is concerned with analysis of social networks and flow networks. Specifically, the problems that we address are (i) modeling social interactions between individuals who discuss on a sequence of issues and assessing stability of such models; (ii) quantifying macroscopic circulation in a given planar graph. In the remainder of this chapter, a broad literature survey of each one of these fronts of research is described.

1.1 Literature review on opinion dynamics

Here, we present a broad literature review of classical opinion dynamics models and DeGrootian models which are our focus and motivations of research in Chapters 3 and 4.

1.1.1 Classical opinion dynamics models

Here, we review list of well-known models that have been proposed to illustrate opinion dynamics. These models can be divided into two main groups, the models in which the opinion space is continuous, e.g., the DeGroot [24], Friedkin-Johnsen (FJ) [35], Deffuant and Weisbuch [23], and Hegselmann-Krause model [48] and the models in which the opinion space is discrete, e.g., Sznajd [78] and Galam model [39].

DeGroot model describes opinion formation in a group of interacting individuals as a repeated weighted averaging process. In this model, at each time step every person updates his/her opinion as the weighted sum of their own opinion and those of the neighbors. The Friedkin-Johnsen model is an extension of the DeGroot model in which each agent has different level of stubbornness. The Hegselmann-Krause model and the Deffuant-Weisbuch model are known as bounded confidence models. In these models, if the opinion distance between two individuals is less than the confidence bound, that is, opinion threshold, then these individuals communicate and influence each other's opinion. In these models, the opinion threshold is the main factor that influences opinion consensus and drives stabilization.

The Sznajd model describes the concept of social validation. In this model, If two people have the same opinion, their neighbors will start to agree with them otherwise their neighbors will start to argue with them. In the Galam model, there are two opinions in the opinion space. The update rule has three steps; In the first step, agents are randomly distributed in groups of a specific size. In the second step, the opinion of the each group is updated using majority rule, meaning that at this step each group is agreed on either of the two opinions. Third, agents are reshuffled. And this process will be repeated.

1.1.2 DeGroot-Friedkin model and its variants

The dynamics of DeGroot-Friedkin model has been proposed by Jia et al.[52]. This model extends the DeGroot model by using the mechanism of reflected appraisal from sociology [33]. In this mechanism, individuals' thoughts, emotions, and behaviors are affected by the displayed thoughts, emotions, and behaviors of other individuals. In the literature, there have been several variations and extensions of DeGroot-Friedkin model. For example, Jia et al. [52] analyzed the model for the case that the individuals form opinions with reducible relative interactions. Chen et al. [15] extended the DeGroot-Friedkin model to the case where the relative interaction matrix is switching and stochastic. Xu et al. introduced a modified DeGrootFriedkin model in which reflected appraisal and opinion dynamics take place on a single issue. He analyzed this model for the special case of doubly stochastic influence network [88]. Recently, Jia et al. analyzed it for the general case [52]. Chen et al. [17] proposed continuous time self-appraisal model. DeGroot-Friedkin model was used to analyze a social network with dynamically changing network topology [89].

Halder [45] showed that the DeGroot-Friedkin map can be viewed as entropic mirror descent over the standard simplex. Also, the proposed model [61] which investigates information spread over cybersocial network of agents is adopted from DeGroot-Friedkin model.

One of the important modification of DeGroot-Friedkin model is to investigate the evolution of social power in influence networks with stubborn individuals. Tabatabaei et al.[65] studied the evolution of interpersonal influences in a group of stubborn individuals as they discuss a sequence of issues. Abrahamsson et al. [2] studied the effect of stubborn agents who influence their neighbors but always stick to their initial opinions. Zhou et al. [92] studied the effect of partially stubborn agents on a modified DeGroot model.

In opinion dynamics, sometimes is of interest to guide the forming opinions to reach either a consensus or even more a specific consensus target. Here, we mention related works on this subject which are built on modified DeGroot-Friedkin models. Dong et al. [27] developed a consensus building process in opinion dynamics. Specifically, they proposed a strategy in which they add a minimum number of interactions in the social network to form a consensus based on leadership. Hegselmann et al. [47] studied a social network in which there is at least one strategic agent who can change its opinion in a way that at the end guides as many agents as possible towards a certain interval of the opinion space.

In Chapter 4, which is taken from Askarzadeh et al. [9], we proposed a general class of nonlinear Markov Chain models for evolution of individual's self-confidence in a social network, motivated from the DeGroot-Friedkin model. Our proposed models have two main differences from original DeGroot-Friedkin model. The first difference is that individuals update their self-confidence levels in finite time without waiting for the opinion process to reach a consensus on any particular issue. The second difference is the presence of feedback that enhances or, perhaps, diminishes the influence of particular individuals within the group, and thereby modifies the transition mechanism based on the outcome of past interactions between them.

1.2 Literature review on circulation for planar graphs

In this section, we present a literature review of related topics to circulation on graphs. Circulation itself is a new concept in graphs that we introduce and discuss thoroughly in Chapter 5. Here, we mention two of its applications and the related papers. Then, we present a review of related papers on graph partitioning since the macroscopic circulation relates to partitioning of a graph into three parts as we discuss in Chapter 5.

Perhaps, circulation is nowhere more apparent than in air currents at the planetary scale [14, 72, 90]. The vorticity, locally as well as at earth-scale, very much as in planar vector fields, can be quantified by a suitably defined scalar potential and, as we will explain, this scalar potential helps quantifying maximal circulation macroscopically.

Within the fields of biology and medicine, potential applications of network analysis are also widespread [63, 71]. For instance, circular propagation of action potentials in the heart electrical conduction system, known as "reentry," is a mechanism of pathologic impulse conduction that underlies a self-sustaining cardiac rhythm abnormality. Reentry appears to account for most tachyarrhythmias[1]; these may lead to life-threatening arrhythmias and sudden cardiac death [42, 51, 54]. Potential application of our framework on assessing macroscopic circulation in a directed graph model of cardiac conduction system will be discussed in Section 5.7.

Graph partitioning has been approached with different tools and for a variety of applications, such as, community detection. Earlier contributions abound. We mention Anderson et al. [6, 7] who discussed local partitioning of an undirected and directed graph, respectively, and Chung [28]

[1]Tachycardia is the medical term for an abnormally fast heartbeat of more than 100 times per minute at rest.

who considers directed graphs and generalizes the classical Cheeger inequality in this setting via PageRank and an algorithm proposed in [7]. On the other hand, a notion of global partitioning was considered by Wang et al. [85] via a hierarchical algorithm and a recursive implementation of Spectral graph partitioning, whereas Arora et al. [8] considered partitioning having sparsest cuts. To the best of authors' knowledge, graph partitioning as a way to capture global circulation has not been proposed before; large-scale network circulation is closely connected to a suitable partition of the graph and is developed in the context of academic and real-world examples. We present theory and a computational framework for *embedded planar graphs* by taking advantage of insights drawn from the well-known Helmholtz-Hodge decomposition of vector fields in Chapter 5.

1.3 Contribution and organization

In this section, objectives and contributions of each chapter are discussed.

- In Chapter 3, we analyze stability of DeGroot-Friedkin model where we establish existence and uniqueness of the fixed point for this model. To this end, we first write the inverse map of DeGroot-Friedkin model. Having stablished that the Jacobian of the inverse map is nonzero, we use local inverse function theorem to show existence of the fixed point. We show that the uniqueness of the fixed point follows from Hadamard's global inverse function theorem. We also calculate closed form solution for fixed point of the map for the society of three individuals.

- There are several key contributions in Chapter 4. First, we introduce a class of nonlinear Markov Chain models for the formation of an individual's self-confidence in a social network, motivated by DeGroot-Friedkin. Our proposed setting has two key differences from original DeGroot-Friedkin model. The first one is that individuals update their self-confidence levels in finite-time without waiting for the opinion process to reach a consensus on any particular issue. The second is that feedback is postulated that potentially enhances or, perhaps, diminishes the influence of particular individuals within the group, and thereby modifies the transition mechanism based on the outcome of past interactions between individuals and subgroups. Second, we prove that if Jacobian of these stochastic maps have only positive entries, then these maps are strictly contractive in l_1-norm. Specifically, l_1-distance to the equilibrium serves as a Lyapunov function for these maps. Third, we provide a bound on the induced l_1 -incremental gain of stochastic maps in terms of the induced l_1 -gain of the Jacobian. Fourth, we discuss conditions for local attractiveness of a periodic orbit of the map. Fifth, we extend our proposed models to account for different subgroups of interacting individuals.

- In Chapter 5, we introduce a concept of circulation on graphs. To the best of our knowledge, this concept does not appear to have been studied at any length. Circulation is motivated by its applications in analyzing air currents at the planetary scale and cardiac conduction system for detecting reentry. We discuss how circulation relates to partitioning a graph into three parts. Maximal circulation follows from suitable 3-partition that maximizes the circulation flow. For planar graphs, we propose an algorithm by which macroscopic circulation can be effectively computed via a scalar potential with support on the dual graph. The algorithm quantifies circulation and follows corresponding 3-partitioning of the graph. For general graphs macroscopic circulation and the corresponding graph partitioning remain challenging combinatorial problems. In addition, we show the effect of embedding on macroscopic circulation and how non-equivalent embeddings of a graph leads to different values for macroscopic circulation.

Chapter 2

Background

2.1 Concepts and basics on graph theory

In mathematics, a graph is an abstraction that represents a set of similar things and the connections between them, e.g. cities and the roads connecting them, networks of friendship among people, web sites and their links to other sites. In this chapter, we present an overview on basics of graph theory and graph representation.

2.1.1 Graph definition and basics

A graph, $\mathcal{G}$, is a collection of vertices, $\mathcal{V} = \mathcal{V}(\mathcal{G})$, and edges, $\mathcal{E} = \mathcal{E}(\mathcal{G})$. Each pair $e = (v_i, v_j)$ of vertices in $\mathcal{E}(\mathcal{G})$ is an edge of $\mathcal{G}$, and e is said to join v_i and v_j, v_i is called adjacent to v_j, and v_i and v_j are called neighbors. We can represent vertices with nodes or points. An edge connects two vertices or connects a vertex to itself. We draw the edges as lines, segments, arcs, etc.

Definition 1. Different types of graphs: When a graph has ordered pairs of vertices, it is called a directed graph, otherwise it's called undirected graph. In directed graphs, the edges of the graph represent a specific direction from one vertex to another. When there is an edge representation as (v_i, v_j), the direction is from v_i to v_j. Whereas in undirected graphs, there is no specific direction to represent the edges.

A loop is an edge that connects a vertex to itself. Multiple edges are edges that have the same end nodes, meaning that more than one edge connects two vertices. A graph with neither loops nor multiple edges is called a simple graph. If a graph has multiple edges but no loops then it is called a multigraph. If it has loops (and possible also multiple edges) then it is called a pseudograph.

The graph $\mathcal{G}' = (\mathcal{V}', \mathcal{E}')$ is called a subgraph of $\mathcal{G} = (\mathcal{V}, \mathcal{E})$ if $\mathcal{V}' \subseteq \mathcal{V}$ and $\mathcal{E}' \subseteq \mathcal{E}$. By allowing $\mathcal{V}$ and $\mathcal{E}$ to be infinite sets, we obtain infinite graphs.

Definition 2. Path, connectivity, Distance: A path in an undirected graph $\mathcal{G} = (\mathcal{V}, \mathcal{E})$ is a sequence of nodes $v_1, v_2, \ldots, v_{k-1}, v_k$ with the property that each consecutive pair v_i, v_{i+1} is joined by an edge in $\mathcal{E}$. For directed graphs, we must traverse the edges in the correct direction. Two paths from node v_i to node v_j are internally disjoint if they have no common internal vertex. A cycle is a path $v_1, v_2, \ldots, v_{k-1}, v_k$ in which $v_1 = v_k$, $k > 2$, and the first $k - 1$ nodes are all distinct.

If, for each pair of vertices, we can find a path between them, then the graph is said to be connected. Otherwise graph is disconnected. A connected graph is k-edge-connected if it remains connected after removing fewer than k edges. A connected graph is k-vertex-connected if it remains connected whenever fewer than k vertices are removed. Bridge is an edge that if removed will result in a disconnected graph.

The length of a path is the number of edges in the path. The distance between two vertices v_i and v_j, denoted by $\mathtt{dist}(v_i, v_j)$, is the length of the shortest path joining them.

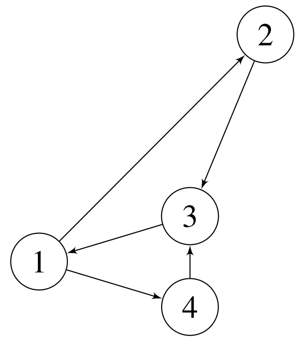

Figure 2.1: Directed graph $\mathcal{G}$

2.1.2 Graph Representation

Here, we review three methods of graph representation and their properties: adjacency matrix, incidence matrix and laplacian matrix.

Adjacency Matrix: Let $\mathcal{G} = (\mathcal{V}, \mathcal{E})$ be a graph where $\mathcal{V} = \{v_1, v_2, ..., v_n\}$ and $\mathcal{E} = \{e_1, e_2, ..., e_m\}$. An Adjacency Matrix, $A = [a_{ij}]_{i,j=1}^{n}$, is an $n \times n$ binary matrix in which value of a_{ij} element is equal to 1 if there exists an edge originating from v_i and terminating to v_j, otherwise the value is 0. For undirected graphs the matrix is symmetric $(A^T = A)$. Summation of numbers in row i is equal to the degree of node i or outdegree (the number of outgoing edges at each vertex) in case of directed graph. Summation of numbers in a column i is equal to the degree of i or indegree (the number of incoming edges at each vertex) in case of directed graph. Given below is Adjacency matrix for the directed graph in Fig. 2.1

$$A = \begin{bmatrix} 0 & 1 & 0 & 1 \\ 0 & 0 & 1 & 0 \\ 1 & 0 & 0 & 0 \\ 0 & 0 & 1 & 0 \end{bmatrix}.$$

Incidence Matrix: The incidence matrix of $\mathcal{G}$ is an $n \times m$ matrix B, where each row corresponds to a vertex and each column corresponds to an edge such that if e_l is an edge between v_i and v_j, $e_l = (v_i, v_j)$, then all elements of column l are 0 except $b_{il} = b_{jl} = 1$ in case of undirected graph and $b_{il} = -1, b_{jl} = 1$ in case of directed graph. Given below is incidence matrix for the directed graph in Fig. 2.1

$$B = \begin{bmatrix} -1 & 0 & 1 & -1 & 0 \\ 1 & -1 & 0 & 0 & 0 \\ 0 & 1 & -1 & 0 & 1 \\ 0 & 0 & 0 & 1 & -1 \end{bmatrix}.$$

Laplacian Matrix: Given a simple graph $\mathcal{G}$ with n vertices, its Laplacian matrix $L_{n\times n}$ is defined as

$$L = D - A$$

In which D is the degree matrix and A is the adjacency matrix of the graph. Degree matrix, D, is a diagonal matrix whose (i, i) entry is equal to the degree of the i_{th} vertex of $\mathcal{G}$, $deg(v_i)$, which counts the number of times an edge terminates at that vertex. In an undirected graph, this means that each loop increases the degree of a vertex by two. In a directed graph, the term degree may refer either to indegree or outdegree. If deg(v) = 0 we call it an isolated vertex.

By definition, row sum of the Laplacian matrix is zero, $L\mathbb{1} = 0$. As a result $\mathbb{1}$ is an eigenvector of the Laplacian with eigenvalue 0. It can be shown that all the other eigenvalues of Laplacian are non-negative. To show this, let $0 = \lambda_1 \leqslant \lambda_2 \leqslant \ldots \leqslant \lambda_n$ be the eigenvalues of the Laplacian matrix. For all $v \in \mathbb{R}^n$,

$$
\begin{aligned}
\sum_{(i,j)\in\mathcal{E}} (v_i - v_j)^2 &= \frac{1}{2}\sum_{i\in\mathcal{V}} \sum_{j\in\mathcal{V}:(i,j)\in\mathcal{E}} (v_i - v_j)^2 \\
&= \frac{1}{2}\sum_{i\in\mathcal{V}} \sum_{j\in\mathcal{V}:(i,j)\in\mathcal{E}} (v_i^2 - 2v_iv_j + v_j^2) \\
&= \frac{1}{2}\left(\sum_{i\in\mathcal{V}} v_i^2 d_i + \sum_{j\in\mathcal{V}} v_j^2 d_j\right) - \sum_{i\in\mathcal{V}}\sum_{j\in\mathcal{V}} v_i a_{ij} v_j \\
&= \sum_{i\in\mathcal{V}} d_i v_i^2 - \sum_{i,j\in\mathcal{V}} a_{ij} v_i v_j \\
&= v^T L v
\end{aligned} \tag{2.1}
$$

The first equality holds because the sum on the right counts each edge twice, once as (i, j) and once as (j, i). Thus, we have shown that $v^T L v \geqslant 0$, $\forall v \in \mathbb{R}^n$. Therefore, by the variational characterisation of eigenvalues, $\lambda_2 \geqslant 0$. As the eigenvalues are arranged in increasing order, it follows that all other eigenvalues are also non-negative. Also, it can be shown that Laplacian of a graph has as many eigenvalues equal to zero as there are connected components in the graph. In particular, if the graph is connected, i.e., it consists of a single connected component, then the eigenvalue zero is simple, and all other eigenvalues are strictly positive. Here, we also discuss the cheeger constant and its connection with Laplacian matrix.

The Cheeger constant h of an undirected finite graph $\mathcal{G}$ is a prominent measure of the connectivity of $\mathcal{G}$, and is defined as

$$
h \coloneqq \min\left\{\frac{|\partial A|}{|A|} : A \subseteq \mathcal{V}(\mathcal{G}), 0 < |A| \leqslant \frac{1}{2}|\mathcal{V}(\mathcal{G})|\right\}
$$

where ∂A is the edge boundary of A. Intuitively, if the Cheeger constant is small but positive, then there exists a bottleneck, in the sense that there are two large sets of vertices with few links (edges) between them. The Cheeger constant is large if any possible division of the vertex set into two subsets has many links between those two subsets.

Computing the Cheeger constant exactly for an arbitrary graph is NP-hard [40, 57]. However, even though we may not be able to compute the Cheeger constant directly we can still get a good estimate for it by using the eigenvalues of the normalized Laplacian. In particular, it is well known that the Cheeger inequalities relate the spectral gap of the Laplacian matrix, λ, of a graph with its Cheeger constant

$$2h \geqslant \lambda \geqslant \frac{h^2}{2\Delta}$$

where Δ is the maximum degree for the nodes in $\mathcal{G}$. Cheeger inequality is one of the main tools for bounding the mixing time for random walks on undirected graphs.

2.2 Concepts and basics on Markov chains

In this section we define various useful concepts and notations. We provide an overview of some known results on Markov chains, while also introducing notation that will be used throughout the thesis to deal with vectors and matrices, and random walks on graphs.

2.2.1 Markov chains

A Markov chain is a sequence of random variables taking value in the finite state-space $\mathcal{X} = \{1, 2, \ldots, n\}$ with the Markov property, meaning that evolution of the Markov process in the future depends only on the present state and does not depend on past history.

Let $X_t \in \{1, ..., n\}$ denote the location of a random walker at time $t \in \{0, 1, 2, ...\}$, then a discrete-time Markov chain is time-homogeneous if $\Pr[X_{t+1} = j | X_t = i] = \Pr[X_t = j | X_{t-1} = i] = \Pi_{i,j}$, where $\Pi = [\Pi_{i,j}] \in \mathbb{R}^{n \times n}$ is the transition matrix of the Markov chain. By definition, each transition matrix Π is row-stochastic, i.e., $\Pi \mathbb{1}_n = \mathbb{1}_n$. A state i has period $k \geqslant 1$ if any chain starting at state i can return to state i only at multiples of the period k, and k is the largest such integer. If $k = 1$, then the state is known as aperiodic, and if $k > 1$, the state is known as periodic. If all states are aperiodic, then the Markov chain is known as aperiodic. A Markov chain is irreducible if for all i, j there exists some t such that $\Pi^t_{i,j} > 0$. In the literature, an irreducible, aperiodic Markov chain is referred to ergodic.

If the Markov chain is irreducible and aperiodic, then there is a unique stationary distribution p, whose entries are non-negative and sum to 1, which is unchanged by the operation of transition matrix Π on it and so is defined by $p\Pi = p$. In particular, p is the unique left eigenvector of Π corresponding to eigenvalue 1.

Let $\pi > 0$ be a probability distribution over $\mathcal{X}$. A Markov chain with transition matrix Π is said to be reversible with respect to π if

$$\forall i, j \in \mathcal{X} : \pi_i \Pi_{i,j} = \pi_j \Pi_{j,i}.$$

Any symmetric matrix Π is trivially reversible (w.r.t. the uniform distribution π). If a Markov chain Π is reversible w.r.t. π, then π is a stationary distribution for Π.

Let $X_t \in \{1, ..., n\}$ denote the location of a random walker at time $t \in \mathbb{R}^+$, then a continuous-time Markov chain is time-homogeneous if $\Pr[X_t = j | X_0 = i] = \Pr[X_{t+s} = j | X_s = i] = \Pi_{ij}(t)$ for all $t \geqslant 0, s \geqslant 0$, where $\Pi(t) = [\Pi_{ij}(t))]_{i,j \in X_t} \in R^{n \times n}$ is the transition matrix of the Markov chain. The evolution of the continuous-time Markov chain is determined by the solution to the first-order differential equation $\Pi'(t) = \Pi(t)Q$, where $\Pi(t) = \exp(Qt)$ and $Q = [q_{ij}]^n_{i,j=1}$ is a transition rate matrix of the process describing the instantaneous rate at which a continuous time Markov chain transitions between states and it satisfies

$$-q_{ii} =: q_i > 0,$$

$$q_{ij} \geqslant 0, \forall i \neq j,$$

$$q_i = \sum_{j \neq i} q_{ij}$$

That is, $Q\mathbb{1}_n = \mathbb{0}_n$, where $\mathbb{1}_n$, $\mathbb{0}_n$ denote column vectors with ones and zeros, respectively. A probability distribution p is stationary if and only if $p^T Q = \mathbb{0}^T$. If the continuous-time Markov chain is ergodic. Then it admits a unique stationary distribution.

The following theorem is used in the proofs of the main results introduced in this thesis.

Theorem 1. *(Perron-Frobenius): Let $A = [a_{ij}]_{n \times n}$ be a matrix with nonnegative elements. Suppose there exist N such that A^N has only positive elements, and let λ_A be its spectral radius. Then*

I) $\lambda_A > 0$ *is an eigenvalue of A;*

II) λ_A *is a simple eigenvalue;*

III) *There exists an eigenvector v corresponding to λ_A with strictly positive entries;*

IV) v *is the only non-negative eigenvector of A;*

V) *Let $B = [b_{ij}]$ be an $n \times n$ matrix with nonnegative elements. If $a_{ij} \leqslant b_{ij}$, $\forall i, j \leqslant n$ and $A \neq B$, then $\lambda_A < \lambda_B$*

2.2.2 Markov chains on graphs

Discrete-time Markov chains can be represented with weighted directed graphs $\mathcal{G} = (\mathcal{V}, \mathcal{E}, \Pi)$ with node sets $\mathcal{V} := \{1, ..., n\}$, edge set $\mathcal{E} \subset \mathcal{V} \times \mathcal{V}$, and transition matrix Π. In this representation, nodes are identified with elements of the state-space. We put a directed edge between states i, j if $\Pi_{i,j} > 0$, with edge-weight $\Pi_{i,j}$, and there is no edge between two states i and j if $\Pi_{i,j} = 0$, meaning that the weight of the edge (i, j) is interpreted as the weight associated with the probability of transition from node i to node j. If the Markov chain is irreducible then its graphical representation $\mathcal{G}(\Pi)$ is strongly connected. In case the graphical representation is an undirected graph, then it is equivalent to $\mathcal{G}(\Pi)$ being connected. For an irreducible Markov chain Π, if $\mathcal{G}(\Pi)$ is undirected then aperiodicity is equivalent to $\mathcal{G}(\Pi)$ being non-bipartite.

Continuous-time Markov chains can be represented with weighted directed graphs $\mathcal{G} = (\mathcal{V}, \mathcal{E}, \mathcal{Q})$ with node sets $\mathcal{V} := \{1, ..., n\}$, edge set $\mathcal{E} \subset \mathcal{V} \times \mathcal{V}$, and associated transition rate matrix $Q = [Q_{i,j}]_{i,j=1}^{n}$. As before, nodes are identified with elements of the state-space. We put a directed edge between states i, j if $q_{i,j} > 0$, with edge-weight $q_{i,j}$, and there is no edge between two states i and j if $q_{i,j} = 0$, meaning that the weight of the edge (i, j) is interpreted as the rate of transition from node i to node j. One could also look at the entry $-1/q_{i,i}$ as the average time at which the walker leaves node i and $1/q_{i,j}$ as the average time for a jump from i to j.

Chapter 3

Dynamics of DeGroot-Friedkin Map

3.1 Introduction

Studying models of interactions among agents in complex networks has been received lots of attention in literature over the last several decades [3, 4, 5, 34, 53, 81, 82]. The subject of this chapter, opinion dynamics, is included in this category and relates to many problems in different areas including economics, sociology, politics and etc. Proposed models of opinion dynamics concern on how individual's opinion evolve over time. The first model was proposed by French, which was an averaging model. This model has been changed and today it is known widely as DeGroot model [24]. Other important models of opinion dynamics which have received attention in literature are Abelson [1], Friedkin-Johnsen (FJ) [37], and Hegselmann-krause model [48].

Our research in this chapter is motivated by the DeGroot-Friedkin model, which is proposed and characterized in [53]. This model is for studying evolution of self appraisal and social power for a group of individuals who form opinion on a sequence of issues. DeGroot-Friedkin model has two stages. In the first one, the averaging rule by DeGroot is used to update opinions of individuals for a particular issue, and in the second one, reflected appraisal mechanism by Friedkin is used to update social power of individuals for the next issue [53, 68, 69].

In this chapter, we first review DeGroot model and Friedkin Mechanism as an introduction to explain DeGroot-Friedkin model. For the special case of two and three individuals discussing on a sequence of issues, we drive closed form solution for the fixed point of DeGroot-Friedkin model. Then, for the general case, we analyze equilibria and stability of the model. Our stability analysis is an alternative approach to the one proposed by Jia [53]. Lastly, we review an extension of DeGroot-Friedkin model to study evolution of individuals' self-confidence over time.

Notation

The set of real-valued n-dimensional vectors is denoted by $\mathbb{R}^n$, and its corresponding non-negative orthant as $\mathbb{R}^n_+$. The notation $^\top$ is used for matrix transpose, $\odot$ for Hadamard product, $\det(\cdot)$ for determinant, and $\mathrm{diag}(\cdot)$ for diagonal matrix. For $i = 1, \ldots, n$, we use ε_i to denote the i^{th} standard basis vector in n-dimensions. The symbols $\mathbb{1}$ and $\mathbb{0}$ denote the column vectors of all ones, and all zeros, respectively. The standard $(n-1)$-simplex, whose vertices are $\varepsilon_1, \ldots, \varepsilon_n$, is given by $\mathcal{S}_{n-1} := \{\boldsymbol{x} \in \mathbb{R}^n \ : \ \mathbf{0} \leqslant \boldsymbol{x} \leqslant \mathbf{1}, \mathbb{1}^\top \boldsymbol{x} = 1\}$. We denote the $(n-1)$-sphere centered at the origin with radius r by $\mathbb{S}^{n-1}(r) := \{\boldsymbol{x} \in \mathbb{R}^n \ : \ \boldsymbol{x}^\top \boldsymbol{x} = r^2\}$, and its non-negative orthant part by $\mathbb{S}^{n-1}_+(r) := \mathbb{S}^{n-1}(r) \bigcap \mathbb{R}^n_+$. The interior of a set $\mathcal{X}$ is denoted by $\mathcal{X}^o$, the standard Euclidean norm is denoted by $\|\cdot\|$, and we use the following notation for Kronecker Delta: $\delta_{ij} = 1$ for $i = j$, and 0 otherwise. The notation $\sum\limits_{\text{symm}}$ stands for symmetric sum.

3.2 DeGroot-Friedkin Model

In this section, we review a dynamical model for the evolution of the social influence network called DeGroot-Friedkin model. We start with describing the well-known DeGroot model. Then we explain how Jia et al. [53] for the first time combined this model with Friedkin mechanism to introduce DeGroot-Friedkin model.

3.2.1 DeGroot Model

We consider a society consist of n individuals where everybody has an opinion on a sequence of subjects, $s \in \{0, 1, 2, 3, \ldots\}$. The opinion of individuals about subject s at time t is represented by a vector of probabilities $x(s,t)$. Each individual has a fixed set of neighbors and communicate with them. The relation between individuals can be represented by a directed graph in which nodes represent individuals and the directed edges represent neighbor relations. The weights of directed edges represent the weight that individuals put on each other's opinions and is represented by an influence matrix $\Pi(s)$ where $\Pi_{ij}(s)$ is the weight that individual i puts on individual j's opinion. This matrix is issue-dependent and row stochastic meaning that its rows consists of nonnegative real numbers, with each row summing to 1. DeGroot averaging model describes the evolution of individuals' opinion about each issue s as follow

$$x_i(s, t+1) = \Pi_{ii}(s) x_i(s,t) + \sum_{j=1, j\neq i}^{n} \Pi_{ij}(s) x_j(s,t), \tag{3.1}$$

or in a matrix representation as

$$x(s,t+1) = \Pi(s)x(s,t) \tag{3.2}$$

with initial condition of $x(s,0)$. In this model, there is a psychological meaning for the elements of influence matrix. Diagonal element Π_{ii} is representing the self-confidence of individual i and the off diagonal element Π_{ij} is representing interpersonal weight which indicates how much individual i's opinion is affected by opinion of individual j based on j's displayed opinions.

For simplicity, for the self-confidence $\Pi_{ii}(s)$ of the i_{th} individual, we use the notation of $p_i(s) \in [0,1]$. we decompose the off-diagonal entries as $\Pi_{ij}(s) = (1 - p_i(s))C_{ij}$. The reason is that Π is assumed to be row stochastic, meaning that $1 - p_i(s)$ is the total amount that individual i's opinion is affected by others. In this decomposition, the C_{ij} coefficients are the relative interpersonal weights that the i_{th} individual assigns to other individuals. With $C_{ii} = 0$, the matrix C, which we refer to as the relative interaction matrix, is row-stochastic with zero diagonal. Notice that, while the self-confidence are issue-dependent, the matrix C is issue-independent, that is, constant. With these notations and assumptions, each influence matrix in the sequence is written as

$$\Pi(p(s)) = diag(p(s)) + (I_n - diag(p(s)))C. \tag{3.3}$$

Hence, the DeGroot Dynamic over a specific issue can be rewritten as

$$x(s,t+1) = \left(diag(p(s)) + (I_n - diag(p(s)))C\right) x(s,t). \tag{3.4}$$

It is well known that for the DeGroot model, the limit of opinions for each issue s is

$$\lim_{t\to\infty} x(s,t) = \lim_{t\to\infty} \Pi(p(s))^t x(s,0) = \nu(p(s))' x(s,0) \mathbb{1}_n \tag{3.5}$$

in which $\nu(p(s))$ is the left eigenvector for the influence matrix $\Pi(p(s))$ associated with eigenvalue one. From Perron-Frobenius theorem, $\nu(p(s))$ has strictly positive entries and is unique.

Hence, the individuals' opinions converge to a convex-combination of their initial opinion. And the $\nu(p(s))_i$ coefficients represent the amount that each individual controls the final outcomes for a particular issue s. Particularly, these coefficients manifest the social power of the individuals in determining the final opinions.

3.2.2 DeGroot-Friedkin Model

DeGroot-Friedkin Model describes how self-confidence of individuals evolve across sequence of issues. This model combines the DeGroot model for describing opinion evolution over a single issue and Friedkin model to describe how the individuals' self-confidence evolve over a sequence of issues.

Based on psychological mechanism of reflected appraisal introduced by Friedkin, the evolution of the self-confidence from issue to issue can be explained. In this mechanism, we wait till consensus is achieved on a particular issue s then we update the self-confidence of individuals for the next issue. This update is based on the contribution that the individuals had over the prior issue outcome, mathematically

$$p(s+1) = \nu(p(s))$$

where $\nu(p(s))$ is the left eigenvector of the influence matrix in 3.3.

Jia et al. provided the explicit mathematical expression for DeGroot-Friedkin model, see Lemma 2.2 in [53]. Here, we summarize their result and use the same explicit mathematical expression for our analysis:

DeGroot-Friedkin model is a continous map $\mathbf{p}(s) \mapsto \mathbf{p}(s+1) = \mathbf{f}(\mathbf{p}(s), \mathbf{c})$, where $s = 0, 1, 2, \ldots$ is the issue index, $\mathbf{p}(0) \in \mathcal{S}_{n-1}$ is the given initial condition, the parameter vector $\mathbf{c} \in \mathcal{S}^{o}_{n-1}$ is the Perron-Frobenius left eigenvector of the relative interaction matrix C, which is row stochastic, zero diagonal, and irreducible and hence the elements of $\mathbf{c}$ are positive proper fractions which sum up to one. The continuous map $\mathbf{f} : \mathcal{S}_{n-1} \mapsto \mathcal{S}_{n-1}$ is given by

$$\mathbf{f}(\mathbf{p}(s), \mathbf{c}) = \begin{cases} \varepsilon_i & \text{if } \mathbf{p} = \varepsilon_i \, \forall\, i \in \{1, \ldots, n\}, \\ \left(\dfrac{c_1}{1 - p_1(s)}, \ldots, \dfrac{c_n}{1 - p_n(s)} \right)^{\top} \Big/ \displaystyle\sum_{i=1}^{n} \dfrac{c_i}{1 - p_i(s)} & \text{otherwise.} \end{cases} \tag{3.6}$$

Here, we use this explicit mathematical expression, first we find the fixed point of the map for the case $n = 2$ and 3, second for the general case we provide a rigorous and comprehensive analysis of the equilibria and stability. Note that this stability analysis is an alternative approach to the proposed analysis by Jia [53].

Fixed Points of DeGroot-Friedkin model for $n = 2$ and 3

Case for $n = 2$:

In this case, we write the fixed point equation for (3.6) as

$$\left.\begin{aligned} \tfrac{c_2 p_1^*}{1 - p_2^*} &= c_1 \Leftrightarrow p_1^* + \tfrac{c_1}{c_2} p_2^* = \tfrac{c_1}{c_2} \\ \tfrac{c_1 p_2^*}{1 - p_1^*} &= c_2 \Leftrightarrow \tfrac{c_2}{c_1} p_1^* + p_2^* = \tfrac{c_2}{c_1} \end{aligned}\right\} \Leftrightarrow \begin{pmatrix} 1 & \frac{c_1}{c_2} \\ \frac{c_2}{c_1} & 1 \end{pmatrix} \begin{pmatrix} p_1^* \\ p_2^* \end{pmatrix} = \begin{pmatrix} \frac{c_1}{c_2} \\ \frac{c_2}{c_1} \end{pmatrix}, \tag{3.7}$$

wherein the determinant of the square matrix is always zero, meaning (3.7) has either infinitely many solutions or no solution. Since $c_1 = c_2 = \frac{1}{2}$, equation (3.7) has infinitely many solutions. In other words, the DeGroot-Friedkin dynamics is degenerate for $n = 2$ case since any point on the simplex $\mathcal{S}_1$ is a fixed point.

Case for $n = 3$:

For this case, the fixed point equation for (3.6) can be written as

$$\frac{c_2 p_1^*}{1-p_2^*} + \frac{c_3 p_1^*}{1-p_3^*} = c_1 \Leftrightarrow (c_2+c_3)p_1^* + c_1 p_2^* + c_1 p_3^* - c_1 = \sum_{\text{symm}} c_1 p_2^* p_3^*, \tag{3.8}$$
$$\frac{c_3 p_2^*}{1-p_3^*} + \frac{c_1 p_2^*}{1-p_1^*} = c_2 \Leftrightarrow c_2 p_1^* + (c_1+c_3)p_2^* + c_2 p_3^* - c_2 = \sum_{\text{symm}} c_1 p_2^* p_3^*, \tag{3.9}$$
$$\frac{c_1 p_3^*}{1-p_1^*} + \frac{c_2 p_3^*}{1-p_2^*} = c_3 \Leftrightarrow c_3 p_1^* + c_3 p_2^* + (c_1+c_2)p_3^* - c_3 = \sum_{\text{symm}} c_1 p_2^* p_3^*. \tag{3.10}$$

Motivated by the common quadratic nonlinearity in (3.8), (3.9) and (3.10), we subtract (3.9) from (3.8), and (3.10) from (3.9), and use the condition that $p_1^* + p_2^* + p_3^* = 1$, to get a system of linear equations:

$$\begin{pmatrix} c_3 & c_3 & c_1 - c_2 \\ c_2 - c_3 & c_1 & -c_1 \\ 1 & 1 & 1 \end{pmatrix} \begin{pmatrix} p_1^* \\ p_2^* \\ p_3^* \end{pmatrix} = \begin{pmatrix} c_1 - c_2 \\ c_2 - c_3 \\ 1 \end{pmatrix}, \tag{3.11}$$

wherein the determinant of the 3×3 matrix is $1 - 2\|c\|^2$. If $1 - 2\|c\|^2 \neq 0$, the unique solution of (3.11) follows from Cramer's rule as

$$\mathbf{p}^* = \frac{1}{1 - 2\|c\|^2} \begin{pmatrix} c_1^2 - (c_2 - c_3)^2 \\ c_2^2 - (c_1 - c_3)^2 \\ c_3^2 - (c_2 - c_1)^2 \end{pmatrix}. \tag{3.12}$$

In addition, it is necessary to impose the condition that $p_i^* \in (0,1)$. For example, for $p_1^* > 0$, we need to have $1 - 2||c||^2 < 0$ and $c_1^2 - (c_2 - c_3)^2 < 0$ or $1 - 2||c||^2 > 0$ and $c_1^2 - (c_2 - c_3)^2 > 0$. The first set of conditions reach to the contradiction of $p_1^* < 0$ but for the second set of conditions we have $(c_1 - c_2 + c_3)(c_1 + c_2 - c_3) > 0 \Rightarrow c_2 < \frac{1}{2}$ and $c_3 < \frac{1}{2}$, similarly, we can obtain that $c_1 < \frac{1}{2}$. Notice that without considering zero diagonal elements for $\mathbf{C}$, we obtain that c_i should be less that $\frac{1}{2}$.

Lemma 2. *The set* $\mathcal{S}_2 \bigcap \mathbb{S}_+^2(\frac{1}{\sqrt{2}})$ *is the incircle of the equilateral triangular face of* $\mathcal{S}_2$.

Proof. Notice that the equilateral triangular face of $\mathcal{S}_2$ has sides of length $\sqrt{2}$. From basic geometry, the incenter of the equilateral triangular face of $\mathcal{S}_2$ coincides with the centroid $(\frac{1}{3}, \frac{1}{3}, \frac{1}{3})$, and the inradius is equal to the ratio of the area of the equilateral triangle and its semi-perimeter, that is, $\frac{\frac{\sqrt{3}}{4} \times 2}{\frac{1}{2} \times 3 \times \sqrt{2}} = \frac{1}{\sqrt{6}}$. Thus, it suffices to prove that the sets $\mathcal{S}_2$ and $\mathbb{S}_+^2(\frac{1}{\sqrt{2}})$ intersect, and that the intersection is a circle centered at $(\frac{1}{3}, \frac{1}{3}, \frac{1}{3})$ with radius $\frac{1}{\sqrt{6}}$.

Due to symmetry, the distance between the center of $\mathbb{S}_+^2(\frac{1}{\sqrt{2}})$ to $\mathcal{S}_2$, is equal to the distance of the origin to centroid $(\frac{1}{3}, \frac{1}{3}, \frac{1}{3})$, that is, $\frac{1}{\sqrt{3}}$. Since $\frac{1}{\sqrt{3}} < \frac{1}{\sqrt{2}}$, hence $\mathcal{S}_2$ and $\mathbb{S}_+^2(\frac{1}{\sqrt{2}})$ intersect, and the intersection is a circle of radius $\sqrt{(\frac{1}{\sqrt{2}})^2 - (\frac{1}{\sqrt{3}})^2} = \frac{1}{\sqrt{6}}$ centered at $(\frac{1}{3}, \frac{1}{3}, \frac{1}{3})$. Hence the statement. $\square$ $\square$

Fixed Points for the General Case.

To show the existence and uniqueness of fixed point $\mathbf{p}^* \in \mathcal{S}_{n-1}^o$, we start by rewriting the fixed point equation corresponding to (3.6) as a map $\mathbf{p}^* \mapsto \mathbf{c}$, given by the linear equation

$$\mathbf{X}\mathbf{c} = \mathbf{c}, \tag{3.13}$$

where $\mathbf{X}$ is a zero-diagonal $n \times n$ matrix with $(i, j)^{\text{th}}$ entry

$$\mathbf{X}_{ij} = \begin{cases} \frac{p_i^*}{1-p_j^*} & \text{for } i \neq j, \\ 0 & \text{otherwise.} \end{cases} \tag{3.14}$$

Notice that since $\mathbf{p}^* \in \mathcal{S}_{n-1}^{o}$, the expression (3.14) is well-defined. Furthermore, since any column of $\mathbf{X}$ has sum one, and all entries of the column are non-negative, hence each entry must lie in interval $[0, 1]$. Thus, $\mathbf{X}$ is a column stochastic matrix with zero-diagonal, which implies that $c_i = \sum_{j \neq i} \mathbf{X}_{ij} c_j \leqslant \sum_{j \neq i} c_j = 1 - c_i$, and hence $0 < c_i \leqslant \frac{1}{2}$ for all $i = 1, \ldots, n$. Consequently, solving (3.13) for $\mathbf{c}$ has the interpretation of computing the right Perron-Frobenius eigenvector for the column stochastic matrix $\mathbf{X}$. In what follows, we first use (3.13) to solve for $\mathbf{c}$ as a function of $\mathbf{p}^*$ in closed-form, and then utilize that solution to establish the existence and uniqueness of the inverse map $\mathbf{c} \mapsto \mathbf{p}^*$.

Lemma 3. *Considering the map in 3.13, we can solve for* c *as a function of* p^* *in closed-form of*

$$c_i = k p_i^* (1 - p_i^*)$$

where $k = \frac{1}{1 - ||\mathbf{p}^*||^2}$.

Proof. Writing $c_i = c_i \left(\frac{1}{1-p_i^*} - \frac{p_i^*}{1-p_i^*} \right)$, and since $p_i^* \neq 1$, we can transcribe (3.13) as the system of equations

$$\frac{c_i}{1 - p_i^*} = p_i^* \sum_{j=1}^{n} \frac{c_j}{1 - c_j}, \quad \forall i = 1, \ldots, n. \tag{3.15}$$

Introducing change-of-variable $\gamma_i := \frac{c_i}{1-p_i^*}$, notice that (3.15) gives $\gamma_i \propto p_i^*$, i.e., $\gamma_i = k p_i^*$ where k is a normalization constant. We thus obtain $c_i = k p_i^* (1 - p_i^*)$ and $k = \frac{1}{1 - ||\mathbf{p}^*||^2}$. □ □

Lemma 4. *For* $\mathbf{D} = \operatorname{diag}(d_1, \ldots, d_n)$*, and* $n \times 1$ *vectors* $\boldsymbol{u}, \boldsymbol{v}$*, we have*

$$\det\left(\mathbf{D} + \boldsymbol{u}\boldsymbol{v}^\top\right) = \begin{cases} \left(1 + \sum_{i=1}^{n} \frac{u_i v_i}{d_i}\right) \prod_{i=1}^{n} d_i & \text{if } \mathbf{D} \text{ is nonsingular,} \\ u_i v_i \prod_{\substack{j=1 \\ j \neq i}}^{n} d_j & \text{if only the } i^{th} \text{ diagonal element of } \mathbf{D} \text{ is zero,} \\ 0 & \text{otherwise.} \end{cases} \tag{3.16}$$

Proof. First, let us consider the case of $\mathbf{D}$ being nonsingular. Then

$$\begin{aligned} \det\left(\mathbf{D} + \boldsymbol{u}\boldsymbol{v}^\top\right) = \det\left(\mathbf{D}\left(\mathbf{I} + \mathbf{D}^{-1}\boldsymbol{u}\boldsymbol{v}^\top\right)\right) &= \det(\mathbf{D}) \det\left(\mathbf{I} + \mathbf{D}^{-1}\boldsymbol{u}\boldsymbol{v}^\top\right) \\ &= \det(\mathbf{D})\left(1 + \boldsymbol{v}^\top \mathbf{D}^{-1}\boldsymbol{u}\right) &(3.17a) \\ &= \left(1 + \sum_{i=1}^{n} \frac{u_i v_i}{d_i}\right) \prod_{i=1}^{n} d_i, &(3.17b) \end{aligned}$$

where (3.17a) follows from Sylvester's determinant identity.

Next, consider the case when exactly one (say i^{th}) diagonal entry of $\mathbf{D}$ is zero, and rest $(n-1)$ diagonal entries are non-zero. Let R and C be the shorthand for row and column, respectively. Performing elementary column operations $C_j \mapsto C_j - \frac{v_j}{v_i} C_i$ for all j such that $1 \leqslant j < i$, followed by elementary row operations $R_k \mapsto R_k - \frac{u_k}{u_i} R_i$ for all k such that $n \geqslant k > i$, we transform $\det(\mathbf{D} + \boldsymbol{u}\boldsymbol{v}^\top)$ to a upper-triangular determinant with diagonal entries $d_1, \ldots, d_{i-1}, u_i v_i, d_{i+1}, \ldots, d_n$, and thus the determinant evaluates to the product of these entries.

Finally, consider the case when more than one diagonal entry of $\mathbf{D}$ are zero. Then at least two rows of $\mathbf{D} + \boldsymbol{u}\boldsymbol{v}^\top$ are same as the corresponding rows of $\boldsymbol{u}\boldsymbol{v}^\top$, and are linearly dependent. Hence in this case, the determinant equals zero.

□

Theorem 5. *Given $\mathbf{c} \in \mathcal{S}_{n-1} \bigcap (0, \frac{1}{2}]^n$, dynamics (3.6) admits a unique fixed point $\mathbf{p}^* \in \mathcal{S}_{n-1}^{o}$.*

Proof. Using Lemma 3, direct calculation yields the Jacobian for map $\mathbf{p}^* \mapsto \mathbf{c}$ as

$$J_{\mathbf{p}^* \mapsto \mathbf{c}} := \frac{\partial c_i}{\partial p_j^*} = \frac{1 - 2p_i^*}{1 - \|\mathbf{p}^*\|^2}\delta_{ij} \; + \; \frac{2p_i^* \left(1 - p_i^*\right) p_j^*}{\left(1 - \|\mathbf{p}^*\|^2\right)^2}, \quad \forall\, i, j = 1, \ldots, n, \tag{3.18}$$

which can be written in "diagonal-plus-rank one" form

$$\mathrm{diag}\left(\frac{\mathbf{1} - 2\mathbf{p}^*}{1 - \|\mathbf{p}^*\|^2}\right) \; + \; \frac{2\mathbf{p}^* \odot \left(\mathbf{1} - \mathbf{p}^*\right)}{\left(1 - \|\mathbf{p}^*\|^2\right)^2} \left(\mathbf{p}^*\right)^\top. \tag{3.19}$$

At this point, two cases need to be considered, viz. **Case I:** none of the entries in $\mathbf{p}^*$ is equal to $\frac{1}{2}$, and **Case II:** exactly one of the entries in $\mathbf{p}^*$ is equal to $\frac{1}{2}$. Nothing else is possible other than these two cases since $\mathbf{p}^* \in \mathcal{S}_{n-1}^{o}$. We next show that $\det(J_{\mathbf{p}^* \mapsto \mathbf{c}}) \neq 0$.

For **Case I**, the diagonal matrix in (3.19) is invertible, and using Lemma 4, we get

$$\det\left(J_{\mathbf{p}^* \mapsto \mathbf{c}}\right)\Big|_{\text{Case I}} = \frac{\prod_{i=1}^{n} \left(1 - 2p_i^*\right)}{\left(1 - \|\mathbf{p}^*\|^2\right)^n} \left(1 + \frac{2}{1 - \|\mathbf{p}^*\|^2} \sum_{i=1}^{n} \frac{(p_i^*)^2 \left(1 - p_i^*\right)}{1 - 2p_i^*}\right). \tag{3.20}$$

We now have two sub-cases: viz. **Case I.A:** $0 < p_i^* < \frac{1}{2}$ for all $i = 1, \ldots, n$, and **Case I.B:** $\frac{1}{2} < p_i^* < 1$ for exactly one $i \in \{1, \ldots, n\}$ and $0 < p_j^* < \frac{1}{2}$ for all $j \neq i$. For **Case I.A**, each term in (3.20) is positive, and so is the determinant. For **Case I.B**, the question arises whether

$$1 + \frac{2}{1 - \|\mathbf{p}^*\|^2} \sum_{i=1}^{n} \frac{(p_i^*)^2 \left(1 - p_i^*\right)}{1 - 2p_i^*} \tag{3.21}$$

may become equal to zero or not. In fact, we now demonstrate that (3.21) is non-zero for any $\mathbf{p}^*$ under **Case I**. To this end, notice that for (3.21) to be equal to zero, we must have

$$
\begin{aligned}
& \sum_{i=1}^{n} \frac{(p_i^*)^2(1-p_i^*)}{1-2p_i^*} = \frac{\|\mathbf{p}^*\|^2-1}{2} \\
\Rightarrow \quad & \sum_{i=1}^{n} \left(\frac{1}{2}(p_i^*)^2 - \frac{1}{4}p_i^* - \frac{1}{8}\right) - \frac{1}{8}\sum_{i=1}^{n} \frac{1}{2p_i^*-1} = -\frac{1}{2} + \frac{\|\mathbf{p}^*\|^2}{2} \\
\Rightarrow \quad & \sum_{i=1}^{n} \frac{1}{2p_i^*-1} = 2-n \;\Leftrightarrow\; \sum_{i=1}^{n}\left(y_i - \frac{1}{y_i}\right) = 0 \;\Leftrightarrow\; \sum_{i=1}^{n} \cos\theta_i = \sum_{i=1}^{n} \sec\theta_i, \quad (3.22)
\end{aligned}
$$

where $y_i := 2p_i^* - 1 \equiv \cos\theta_i \in (-1,1)\setminus\{0\}$ for all $i = 1,\ldots,n$. In other words, (3.22) must have solution for $p_i^* \in (0,1)\setminus\{\frac{1}{2}\}$ under constraint $\sum_{i=1}^{n} p_i^* = 1$, or equivalently for $y_i \equiv \cos\theta_i \in (-1,1)\setminus\{0\}$ under constraint $\sum_{i=1}^{n}\sec\theta_i = 2-n$. Noticing that

$$
\begin{aligned}
& \sum_{i=1}^{n} \prod_{j\neq i} \left(1-2p_j^*\right) = n - 2\left[(n-1)\sum_{\text{symm}} p_1^*\right] + 2^2\left[(n-2)\sum_{\text{symm}} p_1^* p_2^*\right] + \ldots \\
& +(-1)^{n-2}\left[(n-(n-2))\sum_{\text{symm}} p_1^*\ldots p_{n-2}^*\right] + (-1)^{n-1}2^{n-1}\left[(n-(n-1))\sum_{\text{symm}} p_1^*\ldots p_{n-1}^*\right],
\end{aligned}
$$

we rewrite (3.22) as

$$
\begin{aligned}
& \sum_{\text{symm}} p_1^* p_2^* p_3^* - 2\times 2^1 \sum_{\text{symm}} p_1^* p_2^* p_3^* p_4^* + 3\times 2^2 \sum_{\text{symm}} p_1^* p_2^* p_3^* p_4^* p_5^* - \ldots \\
& +(n-3)(-1)^{n-4}\, 2^{n-4} \sum_{\text{symm}} p_1^*\ldots p_{n-1}^* + (n-2)(-1)^{n-3}\, 2^{n-3} p_1^*\ldots p_n^* = 0. \quad (3.23)
\end{aligned}
$$

Since $p_i^* \in (0,1) \setminus \{\frac{1}{2}\}$, introducing $z_i := \frac{1}{p_i^*} \in (1,\infty) \setminus \{2\}$, we further rewrite (3.23) as

$$\begin{aligned}
&\sum_{\text{symm}} z_1 \dots z_{n-3} - 2 \times 2^1 \sum_{\text{symm}} z_1 \dots z_{n-4} + 3 \times 2^2 \sum_{\text{symm}} z_1 \dots z_{n-5} - \dots \\
&+(n-3)(-1)^{n-4}\, 2^{n-4} \sum_{\text{symm}} z_1 + (n-2)(-1)^{n-3}\, 2^{n-3} = 0. \qquad (3.24)
\end{aligned}$$

Noting $z_i > 1$, we substitute $z_i(\lambda) = 1 + \lambda x_i$ in (3.24), where $\lambda > 0$ is a free parameter, to obtain

$$\begin{aligned}
&\sum_{r=0}^{n-3} \binom{n-r}{(n-3)-r} \lambda^r \sum_{\text{symm}} p_1^* \dots p_r^* - 2 \times 2^1 \sum_{r=0}^{n-4} \binom{n-r}{(n-4)-r} \lambda^r \sum_{\text{symm}} p_1^* \dots p_r^* + \dots \\
&+(n-3)(-1)^{n-4}\, 2^{n-4} \sum_{r=0}^{1} \binom{n-r}{1-r} \lambda^r \sum_{\text{symm}} p_1^* + (n-2)(-1)^{n-3}\, 2^{n-3} = 0, \qquad (3.25)
\end{aligned}$$

which follows from the fact that for $k = 1, \dots, n-3$, we have

$$\begin{aligned}
&\sum_{\text{symm}} z_1 z_2 \dots z_k = \sum_{\text{symm}} (1+\lambda p_1^*)(1+\lambda p_2^*) \dots (1+\lambda p_k^*) = \binom{n}{k} + \binom{n-1}{k-1} \lambda \sum_{\text{symm}} p_1^* \\
&+\binom{n-2}{k-2} \lambda^2 \sum_{\text{symm}} p_1^* p_2^* + \dots + \binom{n-(k-1)}{k-(k-1)} \lambda^{k-1} \sum_{\text{symm}} p_1^* \dots p_{k-1}^* + \lambda^k \sum_{\text{symm}} p_1^* \dots p_k^* \qquad (3.26)
\end{aligned}$$

Rearranging (3.25), we arrive at

$$
\begin{aligned}
&\lambda^0\Bigg[\binom{n}{n-3} - 2\times 2^1\binom{n}{n-4} + \ldots + (n-3)(-1)^{n-4}\,2^{n-4}\binom{n}{1} + (n-2)(-1)^{n-3}\,2^{n-3}\Bigg] + \\
&\lambda\Bigg[\binom{n-1}{n-4} - 2\times 2^1\binom{n-1}{n-5} + \ldots + (n-3)(-1)^{n-4}\,2^{n-4}\Bigg]\sum_{\text{symm}} p_1^* + \ldots + \lambda^{n-3}\sum_{\text{symm}} p_1^*\ldots p_{n-3}^* \\
&= \sum_{k=0}^{n-3}(-1)^{(n-3)-k}\,2^{(n-3)-k}\,((n-3)-(k-1))\sum_{r=0}^{k}\binom{n-r}{k-r}\lambda^r\sum_{\text{symm}} x_1^*\ldots x_r^* \\
&= \sum_{k=3}^{n} a(k)\lambda^{n-k}\sum_{\text{symm}} x_1^*\ldots x_{n-k}^* = 0,
\end{aligned}
\tag{3.27}
$$

where

$$
a(k) := \sum_{j=1}^{k-2}\binom{k}{k-j-2}(-1)^{j-1}\,2^{j-1}j. \tag{3.28}
$$

Let $\phi(t) := \sum_{j=1}^{k-2}\binom{k}{k-j-2}t^j$, and notice that $a(k) = \phi'(-2) = \frac{1}{4}\left(1-(-1)^k\right)(k-1) \geqslant 0$ for all $k = 3, \ldots, n$. In addition, for fixed $n \geqslant 3$, since all the $a(k)$'s cannot vanish at the same time, (3.27) does not have any solution for $\lambda > 0$ and $p_i^* \in (0,1)\setminus\{\frac{1}{2}\}$. Consequently, (3.22) does not have any solution for $p_i^* \in (0,1)\setminus\{\frac{1}{2}\}$, and thus (3.21) remains non-zero for any $\mathbf{p}^*$ under **Case I**.

For **Case II**, the diagonal matrix in (3.19) has exactly one zero (say the i^{th} entry) along its diagonal, and the rest of the diagonal entries are non-zero. Using Lemma 4, we then have

$$
\det\left(J_{\mathbf{p}^*\mapsto\mathbf{c}}\right)\Big|_{\text{Case II}} = \frac{2(p_i^*)^2\,(1-p_i^*)}{(1-\|\mathbf{p}^*\|^2)^{n+1}}\prod_{\substack{j=1\\ j\neq i}}^{n}\left(1-2p_j^*\right), \tag{3.29}
$$

which is non-zero for all $\mathbf{p}^* \in \mathcal{S}_{n-1}^{o}$, since none of the p_j^* inside the $(n-1)$-term product in (3.29) is equal to $\frac{1}{2}$ due to $j \neq i$.

Having established that $\det(J_{\mathbf{p}^* \mapsto \mathbf{c}}) \neq 0$, by local inverse function theorem, we conclude that for any $\mathbf{c} \in \mathcal{S}_{n-1} \bigcap (0, \frac{1}{2}]^n$, there exists $\mathbf{p}^* \in \mathcal{S}_{n-1}^o$. Uniqueness of $\mathbf{p}^*$ follows from a version of Hadamard's global inverse function theorem (see [**?** , Thm. 6.2.8]), since $\mathcal{S}_{n-1} \bigcap (0, \frac{1}{2}]^n$ is simply connected, $\det(J_{\mathbf{p}^* \mapsto \mathbf{c}}) \neq 0$ everywhere in $\mathcal{S}_{n-1}^o$, and the map $\mathbf{p}^* \mapsto \mathbf{c}$ is proper. The last condition ("properness") requires that each compact set in $\mathcal{S}_{n-1} \bigcap (0, \frac{1}{2}]^n$ has compact pre-image in $\mathcal{S}_{n-1}^o$, which is met since the pre-image is necessarily bounded, and closed (boundary points of a compact set in $\mathcal{S}_{n-1} \bigcap (0, \frac{1}{2}]^n$ comes from boundary of the pre-image in $\mathcal{S}_{n-1}^o$, thanks to $\det(J_{\mathbf{p}^* \mapsto \mathbf{c}}) \neq 0$). This concludes the proof.

□

3.3 Extension of DeGroot-Friedkin Model

In DeGroot-Friedkin model opinion consensus is achieved on a particular issue s before individuals' self-confidence are updated. In other words, we need to wait for many or infinite number of time steps before updating the individuals' self-confidence. In practice, when a group of individuals discuss on a sequence of issues, they don't necessarily converge on a particular opinion and they may discuss an issue for a finite number of times. In order to count for these situations, Xu et al. [88] introduced a modified DeGroot-Friedkin Model. In this model, individuals' self-confidence are updated and they are set to be equal to the perceived social power for issue s after T times discussions

$$p_i(s+1) = x_i(s, T).$$

This means that individuals self-confidence are updated along the time of discussions and we don't need to wait for opinion consensus on a particular issue s. Note that if we tends T to the infinitely we will recover DeGreoot-Friedkin model. Based on this assumption, 3.4 can be rewritten as

$$p(s+1) = \left(diag(p(s)) + (I_n - diag(p(s)))C\right) p(s) \tag{3.30}$$

Based on the modified DeGroot-Friedkin Model in 3.30, in the next chapter, we propose a group of nonlinear models to capture evolution of individuals' self-confidence. Then, we assess stability of them.

3.4 Summary

In this section, we had a review on DeGroot model and DeGroot-Friedkin model. For the special case of three individuals, we found closed form solution for the fixed point of the DeGroot-Friedkin model. Then, we developed a complete analysis for uniqueness and existence of the fixed point of DeGroot-Friedkin model. Our proposed approach is an alternative to analysis of Jia et al. [53]. We also discussed a modified DeGroot-Friedkin model proposed by Xu et al. [88], which allows individuals to update their self-confidence levels after each discussion on a particular issue. Based on this idea, in the next chapter we introduce a group of nonlinear models that describe self-confidence evolution in a group. A comprehensive analysis of the proposed models is the main focus of the next chapter.

Chapter 4

Stability Theory of Stochastic Models in Opinion Dynamics

4.1 Introduction

Models of social interactions and the formation of opinions in large groups have been receiving increasing attention in recent years (see [3, 5, 17, 34, 53, 70] and the references therein). As the basis for social exchanges, an averaging mechanism has been postulated in the literature, whereby the outcome represents a weighted sum of individual preferences or beliefs. In turn, the averaging mechanism itself is modified by the outcome of past interactions, reflecting relative increase or decrease in the confidence and, thereby, influence of particular individuals. Such feedback models can be traced to [24, 32, 36, 48].

Averaging schemes leading to consensus are broadly relevant in coordination of dynamical systems such as co-operating drones or ground robots, sensor networks, formation flight, and distributed frequency regulation in power grid, see, e.g. [12, 13, 91]. The distinguishing feature of social interaction models has been the postulate of a suitable nonlinear effect that enhances or, perhaps, diminishes the influence of particular individuals in the group. The purpose of this chapter is first to step back, and view the dynamics as a nonlinear random walk. We then develop a stability theory for corresponding stochastic maps by resorting to the ℓ_1 metric. The key element of our approach is to consider the differential of the stochastic maps and assess whether these are contractive in ℓ_1.

More specifically, we consider a discrete-time (or rather, discrete-indexed, where the index may represent issue being considered) process $\{X_t \mid t \in \mathbb{Z}_+\}$ taking values on a finite state-space $\mathcal{X} = \{1, 2, \ldots, n\}$. We denote by $\mathbf{p}(t)$ the marginal probability vector, i.e., its entry $p_i(t) = \Pr(X_t = i)$ is the occupation probability of state i at iteration index t, and postulate a transition mechanism that depends nonlinearly on the occupation probability (a.k.a. belief state) of the process according to the rule:

$$\Pi_{ij} := \Pr(X_{t+1} = j \mid X_t = i) = \rho_i(t)\delta_{ij} + (1 - \rho_i(t))C_{ij}, \tag{4.1a}$$

$$\rho_i(t) := r(p_i(t)), \tag{4.1b}$$

where $\mathbf{C} := [C_{ij}]_{i,j=1}^n$ is a row-stochastic matrix[1], δ_{ij} equals one for $i = j$ and zero otherwise, and $r(\cdot)$ is a differentiable function

$$r \ : \ [0, 1] \mapsto [0, 1].$$

In general, the mapping $r(\cdot)$ needs to be neither onto nor invertible (nor independent of i, as taken at the early part of the chapter, for simplicity). Typical examples include

$$r(x) = x, \ 1 - x, \ 1 - e^{-\gamma x}, \ \text{or} \ e^{-\gamma x}, \ \text{for some } \gamma > 0. \tag{4.2}$$

[1]A matrix $\mathbf{C}$ is referred to as stochastic (or, row-stochastic, for specificity) provided $C_{ij} \geqslant 0$ for all (i, j) and $\sum_j C_{ij} = 1$. Such matrices map the probability simplex into itself (or into another, if not square).

Equation (4.1a) represents a model for a "lazy" random walk where the transition probabilities C_{ij} are modified to increase/decrease the "prior" return-probability from C_{ii} to $\rho_i + C_{ii}(1 - \rho_i)$, in a way that depends on the probability of the corresponding state, since $\rho_i(t) = r(p_i(t))$. For this reason, we refer to $r(\cdot)$ as the *reinforcement function*. Thus, the essence of the above model is that the random walk adapts the return probability of each state so as to promote or discourage residence in states with high marginal probability. An alternative interpretation of the time t-marginal probabilities is as representing confidence or influence which, accordingly, is modified constructively or destructively by the likelihood of the particular state of the process. It has been argued, for instance, that high confidence and success in an argument, begets higher confidence.

The model in (4.1) provides an example of a discrete-time, discrete-space *nonlinear Markov semigroup* that maps the probability simplex on $\mathcal{X}$ into itself [55]. In general, for a nonlinear Markov semigroup to define finite-dimensional distributions (and thereby a random process), one needs to decide on a stochastic representation as in (4.1), which may not be unique. Then, once the transition probabilities are specified as a nonlinear function of the state, the stochastic process can be defined in the form of a time inhomogeneous-Markov chain [55, Chapter 1]. Such *nonlinear Markov* models arise naturally as limits of interacting particle systems that model processes with mass-preserving interactions [55, Section 1.3]. Herein, we will not be concerned with the probabilistic nature and properties of such systems, but instead focus on the dynamical response and stability of equilibria on the probability simplex. Thus, for the most part, we will focus on stochastic maps with transition probabilities as above.

In the context of opinion dynamics, the matrix $\mathbf{C} = [C_{ij}]_{i,j=1}^n$ in (4.1), encodes the influence of neighboring nodes–a standing assumption throughout is that $\mathbf{C}$ corresponds to a *strongly connected aperiodic Markov chain*. With regard to the reinforcement mechanism, of particular interest are exponentially-scaled transition kernels (introduced here)

$$\Pi_{ij}(x) = (1 - e^{-\gamma x_i})\delta_{ij} + e^{-\gamma x_i} C_{ij}, \text{ and its “opposite”} \tag{4.3a}$$

$$\overline{\Pi}_{ij}(x) = e^{-\gamma x_i}\delta_{ij} + (1 - e^{-\gamma x_i}) C_{ij}, \tag{4.3b}$$

as well as the linearly-scaled kernels

$$\Pi_{ij}(x) = \gamma x_i \delta_{ij} + (1 - \gamma x_i) C_{ij}, \text{ and} \tag{4.4a}$$

$$\overline{\Pi}_{ij}(x) = (1 - \gamma x_i)\delta_{ij} + \gamma x_i C_{ij} \tag{4.4b}$$

which have been considered in, e.g., [53]. Naturally, in all these cases, $\mathbf{\Pi} = [\Pi_{ij}]_{i,j=1}^{n}$ and $\overline{\mathbf{\Pi}} = \left[\overline{\Pi}_{ij}\right]_{i,j=1}^{n}$ are row-stochastic (i.e., rows sum to one). Those two models will be analyzed in some detail as they provide rather insightful examples of the dynamics that one can expect of such models. We highlight ranges of parameters where globally stable behavior is observed and where the process tends towards a stationary distribution and, others, where multiple equilibria, periodic orbits, or chaotic behavior is observed. Local stability of equilibria (i.e., local stationarity of distributions), if that is the case, can be assessed using the theory developed in Section 4.2.

The evolution of the marginal probability (column) vector $\mathbf{p}(t)$ corresponding to (4.1) (also, (4.3) and (4.4)) is as follows:

$$\mathbf{p}(t+1) = \mathbf{\Pi}(\mathbf{p}(t))^{\mathsf{T}} \mathbf{p}(t), \tag{4.5a}$$

with

$$\mathbf{\Pi}(\mathbf{p}(t))^{\mathsf{T}} = \mathbf{D}(\mathbf{p}(t)) + \mathbf{C}^{\mathsf{T}}(\mathbf{I} - \mathbf{D}(\mathbf{p}(t))), \tag{4.5b}$$

and a diagonal matrix

$$\mathbf{D}(\mathbf{p}(t)) = \mathrm{diag}(\mathbf{r}(\mathbf{p}(t))), \tag{4.5c}$$

where "$(\cdot)^{\mathsf{T}}$" as usual denotes transposition. As noted, throughout, $\mathbf{C}$ is row stochastic and corresponds to a strongly connected and aperiodic chain. The starting point for the evolution is $\mathbf{p}_0 \in \mathcal{S}_{n-1}$, where

$$\mathcal{S}_{n-1} := \{\mathbf{x} \in \mathbb{R}^n \mid x_i \geqslant 0, \ \sum_i x_i = 1\}$$

denotes the probability simplex. By $\mathcal{S}^{o}_{n-1}$ we will denote the (open) interior of $\mathcal{S}_{n-1}$.

A closely related alternative model for the evolution of influence and opinion dynamics that has appeared in the literature, is to postulate the transition mechanism

$$\mathbf{p}(t+1) = \left[\mathbf{\Pi}(\mathbf{p}(t))^{\mathsf{T}}\right]_{\mathrm{FP}}, \tag{4.6}$$

where the notation $\left[\mathbf{\Pi}^{\mathsf{T}}\right]_{\mathrm{FP}}$ represents the mapping $\mathbf{\Pi}^{\mathsf{T}} \mapsto \mathbf{q} \in \mathcal{S}_{n-1}$ of an irreducible (row) stochastic matrix $\mathbf{\Pi}$ to its corresponding Frobenius-Perron eigenvector, i.e., to the unique probability (column) vector $\mathbf{q}$ that satisfies $\mathbf{\Pi}^{\mathsf{T}}\mathbf{q} = \mathbf{q}$. The relation between the two update-mechanisms, (4.5a) and (4.6), can be understood by virtue of the fact that $\left(\mathbf{\Pi}(\mathbf{p}(t))^{\mathsf{T}}\right)^k \mathbf{p}(t)$ is approximately equal to the right Frobenius-Perron eigenvector of $\mathbf{\Pi}(\mathbf{p}(t))^{\mathsf{T}}$ for sufficiently large k, and hence a suitable modification of the dynamics in (4.5a) (i.e., by introducing a suitably high exponent) approximates the dynamics in (4.6). We will not be concerned with the update mechanism in (4.6), as our primary interest is in the general transition mechanism (4.5a). It is reasonable to expect that stochastic maps in either form, (4.5a), or (4.6), for specific choices of kernel $\Pi_{ij}(\cdot)$ and generalizations (see Sections 4.5-4.6), have appealing properties as models of opinion dynamics.

The exposition in our manuscript proceeds as follows. In Section 4.2, we provide conditions that ensure contractivity in ℓ_1 (Theorem 6 and Propositions 11, 12), quantify the ℓ_1-gain (Theorem 14), and give conditions for attractiveness of a periodic orbit (Proposition 13). We discuss "exponential influence" models in Section 4.3 and DeGroot-Friedkin models in Section 4.4. In both sections we present and analyze representative dynamical behaviors via examples. We comment briefly on the continuous-time counterpart of such models and, in Section 4.6 we introduce local coupling in the reinforcement mechanism to model grouping between colluding subgroups in opinion forming, and comment on extensions of the theory to account for such interactions. Section 4.8 provides concluding remarks and directions.

4.2 ℓ_1-contractivity

We consider stochastic maps of the particular form

$$\mathbf{f} : \mathcal{S}_{n-1} \to \mathcal{S}_{n-1} : \mathbf{p} \mapsto \mathbf{f}(\mathbf{p}) := \mathbf{\Pi}(\mathbf{p})^{\mathsf{T}}\mathbf{p} = \mathbf{q}, \tag{4.7a}$$

where $\mathbf{\Pi}(p)$ is of the form

$$\mathbf{\Pi}(\mathbf{p})^{\mathsf{T}} = \mathbf{C}_0^{\mathsf{T}}\mathbf{D}(\mathbf{p}) + \mathbf{C}_1^{\mathsf{T}}(\mathbf{I} - \mathbf{D}(\mathbf{p})), \tag{4.7b}$$

with $\mathbf{C}_0$, $\mathbf{C}_1$ both row stochastic, and $\mathbf{D}(\mathbf{p})$ diagonal with entries bounded by one; the expression (4.5b) is the special case where $\mathbf{C}_0$ is the identity matrix. Note that $\mathbf{\Pi}(\mathbf{p})$ has nonnegative entries with rows summing to one for all $\mathbf{p} \in \mathcal{S}_{n-1}$. Under suitable conditions, which often hold for the type of dynamics that we consider, $\mathbf{f}$ turns out to be contractive, and even strictly contractive[2] in

[2] The map $\mathbf{f}$ is strictly contractive on $S \subset \mathcal{S}_{n-1}$ if there exists $\epsilon > 0$ that may depend on S so that

$$(1-\epsilon)\|\mathbf{p}^b - \mathbf{p}^a\|_1 \geqslant \|\mathbf{f}(\mathbf{p}^b) - \mathbf{f}(\mathbf{p}^a)\|_1,$$

ℓ_1, in $\mathcal{S}_{n-1}$ or subsets thereof as specified.

Denote by $\mathcal{T}$ the tangent space of the probability simplex, i.e.,

$$\mathcal{T} := \{\boldsymbol{\delta} \in \mathbb{R}^n \mid \mathbb{1}^\mathsf{T}\boldsymbol{\delta} = 0\}$$

with $\mathbb{1}$ the column vector of ones. The Jacobian of $\mathbf{f}(\cdot)$ is

$$\begin{aligned} \mathrm{d}\mathbf{f} \, : \, \mathcal{T} \to \mathcal{T} \, : \, (\delta_j)_{j=1}^n \mapsto & \left(\sum_{i=1}^n \Pi_{ij}\delta_i \right)_{j=1}^n \\ & + \left(\sum_{i,k=1}^n \frac{\partial \Pi_{ij}}{\partial p_k} p_i \delta_k \right)_{j=1}^n \end{aligned}$$

where, by interchanging indices, the latter term can be written as

$$\left(\sum_{k,i=1}^n \frac{\partial \Pi_{kj}}{\partial p_i} p_k \delta_i \right)_{j=1}^n .$$

Thus, $\mathrm{d}\mathbf{f}$ can be written in a matrix form as

$$\mathrm{d}\mathbf{f} \, : \, \boldsymbol{\delta} \mapsto \left(\underbrace{\boldsymbol{\Pi}^\mathsf{T} + \left[\frac{\partial \boldsymbol{\Pi}^\mathsf{T}}{\partial p_1}\mathbf{p}, \ldots, \frac{\partial \boldsymbol{\Pi}^\mathsf{T}}{\partial p_n}\mathbf{p} \right]}_{\mathbf{Q}^\mathsf{T}} \right) \boldsymbol{\delta}. \tag{4.8}$$

Since $\mathbb{1}^\mathsf{T}\mathbf{C}_i^\mathsf{T} = \mathbb{1}^\mathsf{T}$, for $i \in \{0, 1\}$, the columns on the second entry in the expression for $\mathbf{Q}^\mathsf{T}$ satisfy

$$\begin{aligned} \mathbb{1}^\mathsf{T} \left(\frac{\partial \boldsymbol{\Pi}^\mathsf{T}}{\partial p_j}\mathbf{p} \right) &= \mathbb{1}^\mathsf{T} \left(\mathbf{C}_0^\mathsf{T} \frac{\partial \mathbf{D}}{\partial p_j}\mathbf{p} - \mathbf{C}_1^\mathsf{T} \frac{\partial \mathbf{D}}{\partial p_j}\mathbf{p} \right) \\ &= \mathbb{1}^\mathsf{T} \frac{\partial \mathbf{D}}{\partial p_j}\mathbf{p} - \mathbb{1}^\mathsf{T} \frac{\partial \mathbf{D}}{\partial p_j}\mathbf{p} = 0. \end{aligned}$$

for all $\mathbf{p}^a, \mathbf{p}^b \in S$. It is contractive if the statement holds for $\epsilon = 0$.

Hence,[3]

$$\mathbb{1}^\mathsf{T}\mathbf{Q}^\mathsf{T} = \mathbb{1}^\mathsf{T}\mathbf{\Pi}^\mathsf{T} = \mathbb{1}^\mathsf{T}. \tag{4.9}$$

The following serves as a key ingredient in subsequent developments.

Theorem 6. *Let* $\mathbf{f}(\cdot)$ *be as in* (4.7) *with* $\mathbf{D}(\mathbf{p})$ *continuously differentiable, and suppose that the Jacobian matrix* $\mathbf{Q}$ *defined in* (4.8) *has strictly positive entries in* $\mathcal{S}^o_{n-1}$. *The following hold:*

(a) $\mathbf{f}$ *is strictly contractive in* ℓ_1 *in compact subsets of* $\mathcal{S}^o_{n-1}$.

(b) Provided $\mathbf{f}$ *has a fixed point in* $\mathcal{S}^o_{n-1}$, *this fixed point is the only fixed point and it is globally attracting.*

Proof. Consider two probability vectors $\mathbf{p}^a$ and $\mathbf{p}^b$ in $\mathcal{S}^o_{n-1}$, and let $\boldsymbol{\alpha} := (\mathbf{p}^b - \mathbf{p}^a)_+$ be the vector with the positive entries of the difference $\mathbf{p}^b - \mathbf{p}^a$ and $\boldsymbol{\beta} := -(\mathbf{p}^b - \mathbf{p}^a)_-$ contain the entries that originally appear with negative sign, while setting the remaining entries to be zero in both cases. Thus,

$$\mathbf{p}^b - \mathbf{p}^a = \boldsymbol{\alpha} - \boldsymbol{\beta},$$

but in this representation $\boldsymbol{\alpha}$ and $\boldsymbol{\beta}$ have non-negative entries and have no common support, i.e., $\boldsymbol{\alpha}_i\boldsymbol{\beta}_i = 0$ as they are not simultaneously $\neq 0$. Since $\mathbb{1}^\mathsf{T}(\mathbf{p}^b - \mathbf{p}^a) = 0$, it follows that $\mathbb{1}^\mathsf{T}\boldsymbol{\beta} = \mathbb{1}^\mathsf{T}\boldsymbol{\alpha}$, hence,

$$\|\boldsymbol{\beta}\|_1 = \|\boldsymbol{\alpha}\|_1 =: \gamma$$

[3] It is easy to see that this property also holds for maps that are composition of maps with the structure in (4.7).

and

$$\begin{aligned}
\|\mathbf{p}^b - \mathbf{p}^a\|_1 &= \sum_i |p_i^b - p_i^a| \\
&= \|\boldsymbol{\beta} - \boldsymbol{\alpha}\|_1 \\
&= \sum_i \beta_i + \sum_i \alpha_i \\
&= \|\boldsymbol{\beta}\|_1 + \|\boldsymbol{\alpha}\|_1 \\
&= 2\gamma.
\end{aligned}$$

Now consider a path $\mathbf{p}(\lambda) = (1-\lambda)\mathbf{p}^a + \lambda\mathbf{p}^b$ for $\lambda \in [0,1]$ and consider comparing the distance between $\mathbf{p}^b$ and $\mathbf{p}^a$ to the length of the path

$$\mathbf{q}(\lambda) = \boldsymbol{\Pi}(\mathbf{p}(\lambda))^T \mathbf{p}(\lambda),\ \lambda \in [0,1].$$

Clearly,

$$d\mathbf{p}(\lambda) = (\boldsymbol{\alpha} - \boldsymbol{\beta})d\lambda,$$

and thus

$$\begin{aligned}
\int_{\lambda=0}^{1} \|d\mathbf{p}(\lambda)\|_1 &= \int_0^1 \|\boldsymbol{\alpha} - \boldsymbol{\beta}\|_1 d\lambda \\
&= \|\boldsymbol{\alpha} - \boldsymbol{\beta}\|_1 \int_0^1 d\lambda = \|\mathbf{p}^b - \mathbf{p}^a\|_1.
\end{aligned}$$

The entries of $\mathbf{Q}$ are bounded away from zero in any compact subset of $\mathcal{S}_{n-1}^o$, hence we can assume that they are greater than $\frac{\epsilon}{n}$ along the path, for some $\epsilon > 0$ which may depend on the compact subset. Then,

$$\begin{aligned}
\int_{\lambda=0}^{1} \|\mathrm{d}\mathbf{q}(\lambda)\|_1 &= \int_0^1 \|\mathbf{Q}(\mathbf{p}(\lambda))^\mathsf{T}(\boldsymbol{\alpha}-\boldsymbol{\beta})\|_1 \mathrm{d}\lambda \\
&\leqslant (1-\epsilon)\int_0^1 \left(\|\mathbf{Q}(\mathbf{p}(\lambda))^\mathsf{T}\boldsymbol{\beta}\|_1 + \|\mathbf{Q}(\mathbf{p}(\lambda))^\mathsf{T}\boldsymbol{\alpha})\|_1\right) \mathrm{d}\lambda \qquad (4.10)\\
&= (1-\epsilon)\int_0^1 (\|\boldsymbol{\beta}\|_1 + \|\boldsymbol{\alpha}\|_1)\mathrm{d}\lambda \qquad (4.11)\\
&= (1-\epsilon)\|\mathbf{p}^b - \mathbf{p}^a\|_1.
\end{aligned}$$

To see why the inequality (4.10) holds, note that for each λ,

$$\boldsymbol{\nu}^\beta := \mathbf{Q}(\mathbf{p}(\lambda))^\mathsf{T}\boldsymbol{\beta} \text{ and } \boldsymbol{\nu}^\alpha := \mathbf{Q}(\mathbf{p}(\lambda))^\mathsf{T}\boldsymbol{\alpha}$$

are vectors with positive entries, while $\|\boldsymbol{\nu}^\beta\|_1 = \|\boldsymbol{\beta}\|_1 = \gamma$, and $\|\boldsymbol{\nu}^\alpha\|_1 = \|\boldsymbol{\alpha}\|_1 = \gamma$ since $\mathbf{Q}$ is row stochastic. The entries of $\boldsymbol{\nu}^\beta$ are strictly larger than $\frac{\epsilon}{n}\|\boldsymbol{\beta}\|_1 = \frac{\epsilon\gamma}{n}$ and, similarly, the entries of $\boldsymbol{\nu}^\alpha$ are strictly larger than the same value, $\frac{\epsilon}{n}\|\boldsymbol{\alpha}\|_1 = \frac{\epsilon\gamma}{n}$. Therefore,

$$\begin{aligned}
\|\boldsymbol{\nu}^\beta - \boldsymbol{\nu}^\alpha\|_1 &\leqslant \|\boldsymbol{\nu}^\beta\|_1 + \|\boldsymbol{\nu}^\alpha\|_1 - 2\epsilon\gamma \\
&= 2\gamma(1-\epsilon),
\end{aligned}$$

establishing the claimed inequality. Finally, the metric property of $\|\cdot\|_1$ implies that

$$\|\mathbf{q}(1) - \mathbf{q}(0)\|_1 \leqslant \int_{\lambda=0}^{1} \|\mathrm{d}\mathbf{q}(\lambda)\|_1,$$

where $\mathbf{q}(1) = \boldsymbol{\Pi}(\mathbf{p}^b)^\mathsf{T}\mathbf{p}^b$ and $\mathbf{q}(0) = \boldsymbol{\Pi}(\mathbf{p}^a)^\mathsf{T}\mathbf{p}^a$. Hence,

$$\|\boldsymbol{\Pi}(\mathbf{p}^b)^\mathsf{T}\mathbf{p}^b - \boldsymbol{\Pi}(\mathbf{p}^a)^\mathsf{T}\mathbf{p}^a\|_1 \leqslant (1-\epsilon)\|\mathbf{p}^b - \mathbf{p}^a\|_1.$$

This proves the first claim (part (a)).

Now assuming that $\mathbf{f}$ has a fixed point $\mathbf{p}^a$ in $\mathcal{S}^o_{n-1}$, consider any other point $\mathbf{p}^b \in \mathcal{S}_{n-1}$ and the path $\mathbf{p}(\lambda) = (1-\lambda)\mathbf{p}^a + \lambda\mathbf{p}^b$ for $\lambda \in [0,1]$ as before. Since $\mathbf{p}^a$ is in the interior of $\mathcal{S}_{n-1}$ there is an $\epsilon_1 > 0$ such that $\mathcal{B}_{\ell_1}(\mathbf{p}, \epsilon_1) := \{\mathbf{p} \in \mathcal{S}_{n-1} \mid \|\mathbf{p} - \mathbf{p}^a\|_1 \leqslant \epsilon_1\}$ is also in the interior of $\mathcal{S}_{n-1}$. The elements of $\mathbf{Q}(\mathbf{p})$ are greater than, $\frac{\epsilon_2}{n}$, for some $0 < \epsilon_2 < 1$, in $\mathcal{B}_{\ell_1}(\mathbf{p}, \epsilon_1)$. Split the path $\{\mathbf{p}(\lambda) \mid \lambda \in [0,1]\}$ into two parts: $\{\mathbf{p}(\lambda) \mid \lambda \in [0,\lambda_1]\}$ that is contained in $\mathcal{B}_{\ell_1}(\mathbf{p}, \epsilon_1)$ and $\{\mathbf{p}(\lambda) \mid \lambda \in [\lambda_1, 1]\}$ that is not. The portion of the path that is in $\mathcal{B}_{\ell_1}(\mathbf{p}, \epsilon_1)$ contracts when mapped via $\mathbf{f}$ by $1-\epsilon_2$, whereas the length of remaining is nonincreasing. Thus,

$$\begin{aligned}
\|\mathbf{f}(\mathbf{p}^b) - \mathbf{f}(\mathbf{p}^a)\|_1 &\leqslant \int_0^{\lambda_1} \|d\mathbf{q}(\lambda)\|_1 + \int_{\lambda_1}^1 \|d\mathbf{q}(\lambda)\|_1 \\
&\leqslant (1-\epsilon_2)\int_0^{\lambda_1} \|d\mathbf{p}(\lambda)\|_1 + \int_{\lambda_1}^1 \|d\mathbf{p}(\lambda)\|_1 \\
&\leqslant (1-\epsilon_2)\lambda_1\|\mathbf{p}^b - \mathbf{p}^a\|_1 + (1-\lambda_1)\|\mathbf{p}^b - \mathbf{p}^a\|_1 \\
&\leqslant (1-\epsilon_2\lambda_1)\|\mathbf{p}^b - \mathbf{p}^a\|_1.
\end{aligned}$$

Finally, we notice that $1-\epsilon_2\lambda_1 \leqslant 1 - \epsilon_2\epsilon_1/2$ since $\|\mathbf{p}^b - \mathbf{p}^a\|_1 \leqslant 2$. In total, the ℓ_1-distance between $\mathbf{p}^a$ and the elements of the sequence $\mathbf{p}^b$, $\mathbf{f}(\mathbf{p}^b)$, $\mathbf{f}(\mathbf{f}(\mathbf{p}^b))$, $\ldots$, reduces to zero exponentially fast with a rate of at least $1-\epsilon_2\epsilon_1/2$. This proves the second part (part (b)). $\square$

Remark 7. *We note that analogous results to Theorem 6 for ℓ_1-contractivity for monotone nonlinear compartmental continuous-time systems were proven in Como etal. [19, 20] (e.g., see [20, Lemma 1]), and that similar ideas underlie the differential Finsler-Lyapunov framework of Forni and Sepulchre [30, 31] as well as work on monotone and hierarchical systems [21, 60, 75]. While our approach in this chapter is to derive conditions on the differential map $\boldsymbol{\delta} \mapsto \mathbf{Q}(\mathbf{p})^\top\boldsymbol{\delta}$ so as to guarantee ℓ_1-contractivity of the map $\mathbf{p} \mapsto \boldsymbol{\Pi}(\mathbf{p})^\top\mathbf{p}$ on $\mathcal{S}_{n-1}$, it would be interesting to investigate a discrete-time Finsler-Lyapunov function approach analogous to the continuous-time case known in the literature (see e.g., Theorem 1 in [30]). Thus, the objective would be to construct* *a Finsler-Lyapunov function* $V(\mathbf{p}, \boldsymbol{\delta}) : \mathcal{S}_{n-1} \times \mathcal{T} \to \mathbb{R}_{\geqslant 0}$ *for the augmented map* $\begin{pmatrix} \mathbf{p}, & \boldsymbol{\delta} \end{pmatrix} \mapsto \begin{pmatrix} \boldsymbol{\Pi}(\mathbf{p})^\mathsf{T}\mathbf{p}, & \mathbf{Q}(\mathbf{p})^\mathsf{T}\boldsymbol{\delta} \end{pmatrix}$ *so as to guarantee* ℓ_1*-contractivity of the map* $\mathbf{p} \mapsto \boldsymbol{\Pi}(\mathbf{p})^\mathsf{T}\mathbf{p}$*.*

Remark 8. *If* $\mathbf{f}$ *is a general nonlinear map, the Jacobian matrix* $\mathbf{Q}$ *may fail to be stochastic for two reasons. First, the elements of* $\mathbf{Q}$ *may fail to be non-negative. Second, the normalization* (4.9) *may fail unless* $\boldsymbol{\Pi}$ *has a particular structure, as for instance the one in* (4.7)*. A simple example to demonstrate the failure of* (4.9) *is*

$$\begin{pmatrix} p_1 \\ p_2 \end{pmatrix} \mapsto \begin{pmatrix} p_1 & p_2 \\ p_2 & p_1 \end{pmatrix} \begin{pmatrix} p_1 \\ p_2 \end{pmatrix}.$$

For this example one can readily see that $\mathbb{1}^\mathsf{T}\mathbf{Q}^\mathsf{T} = 2\mathbb{1}^\mathsf{T} \neq \mathbb{1}^\mathsf{T}$*.*

Remark 9. *At times it is easy to ensure that* $\mathbf{f}$ *in Theorem 6 has a fixed point in the interior of* $\mathcal{S}_{n-1}$*. For instance, if* $\mathbf{C}_0 = \mathbf{I}$ *is the identity matrix, and since* $\mathbf{C}_1^\mathsf{T}(\mathbf{I} - \mathbf{D})\mathbf{p} = (\mathbf{I} - \mathbf{D})\mathbf{p}$ *and* $\mathbf{C}_1$ *corresponds to a simply connected aperiodic chain,* $(\mathbf{I} - \mathbf{D})\mathbf{p}$ *is the corresponding Frobenius-Perron eigenvector and therefore lies in the interior of* $\mathcal{S}_{n-1}$*. Conclusions can be drawn for* $\mathbf{p}$*, accordingly, depending on* $\mathbf{D}$*.*

Corollary 10. *Let* $\boldsymbol{\Pi}(\mathbf{p})$ *be row-stochastic and differentiable in* $\mathbf{p}$*, and suppose that the Jacobian of the map* $\mathbf{f}(\cdot)$ *in* (4.7a) *has non-negative entries. Then,* $\mathbf{f}$ *is contractive (but not necessarily strictly contractive) in the* ℓ_1*-metric.*

Stronger statements that build on the theorem are stated next. All results hold for functional forms that are more general than the exponential and linear models considered in this chapter.

Proposition 11. *Let matrix* $\boldsymbol{\Pi}(\mathbf{p})$ *be row-stochastic and continuously differentiable in* $\mathbf{p}$*. Suppose*

$\mathbf{f}$ *has a fixed point* $\mathbf{p}^\star$ *in* $\mathcal{S}^o_{n-1}$, *and for a suitable integer* m *the differential (Jacobian) of the* m*th iterant*

$$\mathbf{f}^m(\mathbf{p}) := \overbrace{\mathbf{f}(\mathbf{f}(\ldots\mathbf{f}}^{m}(\mathbf{p}))) \tag{4.12}$$

has strictly positive entries for all $\mathbf{p} \in \mathcal{S}^o_{n-1}$. *Then,* $\mathbf{p}^\star$ *is the unique fixed point of* $\mathbf{f}$ *and it is globally stable.*

Proof. By assumption, $\mathbf{p}^\star$ is a fixed point of $\mathbf{f}^m$ since $\mathbf{f}^m(\mathbf{p}^\star) = \mathbf{f}^{m-1}(\mathbf{p}^\star) = \cdots = \mathbf{p}^\star$. Now applying Theorem 6 to $\mathbf{f}^m$ we conclude that $\mathbf{p}^\star$ is the unique fixed point of $\mathbf{f}^m$ and is globally stable. Therefore, $\mathbf{p}^\star$ is also a unique fixed point of $\mathbf{f}$, and the global stability of $\mathbf{p}^\star$ with respect to $\mathbf{f}$ follows from the continuity of $\mathbf{f}$. $\square$

Proposition 12. *Let matrix* $\mathbf{\Pi}(\mathbf{p})$ *be row-stochastic and continuously differentiable in* $\mathbf{p}$. *Suppose that* $\mathbf{p}^\star$ *in* $\mathcal{S}^o_{n-1}$ *is a fixed point of* $\mathbf{f}$ *in* (4.7a) *and that, for a suitable integer* m, *the* m*th power*

$$(\mathrm{d}\mathbf{f}|_{\mathbf{p}^\star})^m$$

of the Jacobian of $\mathbf{f}$ *evaluated at* $\mathbf{p}^\star$ *has strictly positive entries. Then* $\mathbf{p}^\star$ *is a locally attractive equilibrium.*

Proof. The expression $(\mathrm{d}\mathbf{f}|_{\mathbf{p}^\star})^m$ is precisely the Jacobian of the m^{th} iterate, i.e.,

$$(\mathrm{d}\mathbf{f}|_{\mathbf{p}^\star})^m = \mathrm{d}\,\overbrace{\mathbf{f}(\mathbf{f}(\ldots\mathbf{f}))}^{m}|_{\mathbf{p}^\star}.$$

By continuity, the entries of $\mathrm{d}\mathbf{f}^m$, with $\mathbf{f}^m := \overbrace{\mathbf{f}(\mathbf{f}(\ldots\mathbf{f}))}^{m}$, will remain positive in a neighborhood of $\mathbf{p}^\star$. It is then clear that $\mathbf{f}^m$, which is stochastic and satisfies the conditions of Theorem 6, has $\mathbf{p}^\star$ as a (locally) attractive fixed point. Therefore, using the continuity of $\mathbf{f}$, we conclude that $\mathbf{p}^\star$ is a locally attractive fixed point for $\mathbf{f}$. $\square$

Proposition 13. *Let matrix* $\Pi(\mathbf{p})$ *be row-stochastic and continuously differentiable in* $\mathbf{p}$*, and assume that* $\mathbf{p}^i$*, for* $i = 0, 1, 2, \ldots, m-1$*, is a periodic orbit for* $\mathbf{f}$ *in* (4.7a)*, i.e.,*

$$\mathbf{p}^{(i+1)\mathrm{mod}(m)} = \mathbf{f}(\mathbf{p}^{(i)\mathrm{mod}(m)}).$$

Suppose that the product of the Jacobians

$$\left(\mathrm{d}\mathbf{f}|_{\mathbf{p}^{(i+m)\mathrm{mod}(m)}}\right) \ldots \left(\mathrm{d}\mathbf{f}|_{\mathbf{p}^{(i)\mathrm{mod}(m)}}\right)$$

has strictly positive entries for some i*. Then, the periodic orbit is locally attractive.*

Proof. Under the stated condition, for any i, $\mathbf{p}^i$ is a locally attractive fixed point for the mth iterant, $\overbrace{\mathbf{f}(\mathbf{f}(\ldots\mathbf{f}))}^{m}|_{\mathbf{p}^i}$. The fact that the orbit is locally attractive now follows from the continuity of $\mathbf{f}$. $\square$

We provide next a bound on the induced ℓ_1-incremental gain of stochastic maps in terms of the induced ℓ_1-gain of the Jacobian

$$\|\mathrm{d}\mathbf{f}|_{\mathcal{T}}\|_{(1)} := \max\{\|\mathbf{Q}^{\mathsf{T}}\boldsymbol{\delta}\|_1 \mid \mathbb{1}^{\mathsf{T}}\boldsymbol{\delta} = 0, \|\boldsymbol{\delta}\|_1 = 1\}.$$

This strengthens substantially the applicability of the framework since it relaxes the positivity requirement on the Jacobian, albeit this relaxed condition may be more challenging to verify globally.

Theorem 14. *Let* $\mathbf{f}$ *be a differentiable stochastic map as in* (4.7a) *and as before the Jacobian* $\mathrm{d}\mathbf{f}(\mathbf{p})|$ *is represented by a matrix* $\mathbf{Q}(\mathbf{p})^{\mathsf{T}}$*. For any* $\mathbf{p}^b, \mathbf{p}^a \in \mathcal{S}_{n-1}$*,*

$$\|\mathbf{f}(\mathbf{p}^b) - \mathbf{f}(\mathbf{p}^a)\|_1 \leqslant \max_{\mathbf{p}\in\mathcal{S}_{n-1}} \|\mathrm{d}\mathbf{f}(\mathbf{p})|_{\mathcal{T}}\|_{(1)}\|\mathbf{p}^b - \mathbf{p}^a\|_1,$$

and, in general,

$$\|\mathrm{d}\mathbf{f}|_{\mathcal{T}}\|_{(1)} = \frac{1}{2}\max_{j,k}\sum_{i=1}^{n}|(\mathbf{Q}(\mathbf{p}))_{ji} - (\mathbf{Q}(\mathbf{p}))_{ki}|. \tag{4.13}$$

Proof. The first claim is straightforward since, with $\boldsymbol{\alpha}$, $\boldsymbol{\beta}$ as in the proof of Theorem 6,

$$\begin{aligned}
\|\mathbf{f}(\mathbf{p}^b) - \mathbf{f}(\mathbf{p}^a)\|_1 &\leqslant \int_{\lambda=0}^{1}\|\mathrm{d}\mathbf{q}(\lambda)\|_1 \\
&= \int_0^1 \|\mathbf{Q}(\mathbf{p}(\lambda))^\mathsf{T}(\boldsymbol{\beta} - \boldsymbol{\alpha})\|_1 \mathrm{d}\lambda \\
&\leqslant \left(\max_{\mathbf{p}\in\mathcal{S}_{n-1}}\|\mathrm{d}\mathbf{f}(\mathbf{p})|_{\mathcal{T}}\|_{(1)}\right)\int_0^1\|\boldsymbol{\beta} - \boldsymbol{\alpha}\|_1\mathrm{d}\lambda \\
&= \left(\max_{\mathbf{p}\in\mathcal{S}_{n-1}}\|\mathrm{d}\mathbf{f}(\mathbf{p})|_{\mathcal{T}}\|_{(1)}\right)\|\mathbf{p}^b - \mathbf{p}^a\|_1.
\end{aligned}$$

Any $\boldsymbol{\delta} \in \mathcal{T}$ with $\|\boldsymbol{\delta}\|_1 = 1$ can be written as $\boldsymbol{\delta} = \frac{1}{2}(\boldsymbol{\beta} - \boldsymbol{\alpha})$ with $\boldsymbol{\alpha}$, $\boldsymbol{\beta}$ having nonnegative entries and $\|\boldsymbol{\alpha}\|_1 = \|\boldsymbol{\beta}\|_1 = 1$, as before, and at any given $\mathbf{p} \in \mathcal{S}_{n-1}$,

$$\begin{aligned}
\|\mathrm{d}\mathbf{f}|_{\mathcal{T}}\|_{(1)} &= \max\{\|\mathbf{Q}^\mathsf{T}(\mathbf{p})\boldsymbol{\delta}\|_1 \mid \boldsymbol{\delta} \in \mathcal{T}\} \\
&= \frac{1}{2}\max\{\|\mathbf{Q}^\mathsf{T}\boldsymbol{\beta} - \mathbf{Q}^\mathsf{T}\boldsymbol{\alpha}\|_1 \mid \boldsymbol{\alpha}, \boldsymbol{\beta} \in \mathcal{S}_{n-1}\}.
\end{aligned} \tag{4.14}$$

The claim follows by convexity. To see this, note that $\|\mathbf{Q}^\mathsf{T}\boldsymbol{\beta} - \boldsymbol{\nu}\|_1$, for $\boldsymbol{\nu}$ constant, is a convex function of $\boldsymbol{\beta} \in \mathcal{S}_{n-1}$. Therefore the maximal value will be attained at an extreme point, i.e., a vertex, and likewise when maximizing with respect to $\boldsymbol{\alpha}$. Thus, the extremal will be at a point where both $\boldsymbol{\beta}$ and $\boldsymbol{\alpha}$ have a single nonzero element (and thereby select a corresponding row of $\mathbf{Q}$). $\square$

We note that the expression (4.13) for the induced ℓ_1-norm of linear maps is the so-called Markov-

Dobrushin coefficient of ergodicity [25, 41, 62, 77] that characterizes the contraction rate of Markov operators with respect to this norm (also, total variation). For nonlinear operators on probability simplices (nonlinear Markov Chains), the same is true. The above propositions provide candidate certificates for stability of equilibria $\mathbf{p}^\star$ and highlight the fact that the ℓ_1-distance is a natural Finsler-Lyapunov function in the sense of Forni and Sepulchre [30]. The essence is that ℓ_1-contractivity of the nonlinear dynamics $\mathbf{p}_{\text{next}} = \mathbf{f}(\mathbf{p})$, and stability of fixed points or periodic orbits, may be deduced from the infinitesimal properties of $\mathbf{f}$ in the ℓ_1-metric. The approach is illustrated in the next sections.

4.3 Exponential-influence models

In this section we analyze the model in (4.5a) for the cases where the *reinforcement* function $r(x)$ is either $1 - e^{-\gamma x}$ or $e^{-\gamma x}$, for some $\gamma > 0$. The first choice satisfies $r(0) = 0$ and $r'(0) = \gamma$, and thereby strengthens the return probabilities[4] for states with relatively large marginal probability at corresponding times t. The second choice has $r(0) = 1$ and $r'(0) = -\gamma$, has the tendency to do the opposite.

Throughout we assume that $\mathbf{C}$ is an irreducible aperiodic row-stochastic matrix, and we denote by $\mathbf{c}$ the unique (positive) Frobenius-Perron left eigenvector, i.e., $\mathbf{c}$ satisfies

$$\mathbf{C}^T \mathbf{c} = \mathbf{c}.$$

It is normalized so that $\mathbb{1}^T \mathbf{c} = 1$ and, because of the irreducibility assumption, $\mathbf{c}$ has positive entries.

[4]Naturally, the rates also depend on the choice of $\mathbf{C}$.

4.3.1 Case $\mathbf{r}(\mathbf{x}) = \mathbf{1} - \mathbf{e}^{-\text{ﬂ}\mathbf{x}}$ for $\mathbf{0} < \text{ﬂ} \leqslant \mathbf{1}$.

Proposition 15. *With* $\mathbf{C}$ *as above and for any* $\gamma \in (0, 1]$ *consider the map*

$$\mathbf{p}(t) \mapsto \mathbf{f}(\mathbf{p}(t)) = \mathbf{p}(t+1), \text{ where} \tag{4.15a}$$

$$\mathbf{f}(\mathbf{p}(t)) = \left(\operatorname{diag}(\mathbb{1} - e^{-\gamma \mathbf{p}(t)}) + \mathbf{C}^{\mathsf{T}} \operatorname{diag}(e^{-\gamma \mathbf{p}(t)})\right) \mathbf{p}(t). \tag{4.15b}$$

The following hold:

i) $\mathbf{f}(\cdot)$ *is contractive in* ℓ_1*,*

ii) $\mathbf{f}$ *has a unique fixed point* $\mathbf{p}^\star$ *with entries satisfying* $e^{-\gamma p_i^\star} p_i^\star = \kappa c_i$*, for some* $\kappa > 0$*,*

iii) starting from an arbitrary $\mathbf{p}(0) \in \mathcal{S}_{n-1}$*,*

$$\mathbf{p}^\star = \lim_{t \to \infty} \mathbf{p}(t).$$

Proof. The Jacobian $d\mathbf{f}$ is of the form

$$\begin{aligned}
\boldsymbol{\delta} \mapsto & \left(\operatorname{diag}(\mathbf{r}(\mathbf{p}) + \mathbf{p} \odot \mathbf{r}'(\mathbf{p}))\right. \\
& \quad \left. + \mathbf{C}^{\mathsf{T}} (\mathbf{I} - \operatorname{diag}(\mathbf{r}(\mathbf{p}) + \mathbf{p} \odot \mathbf{r}'(\mathbf{p})))\right) \boldsymbol{\delta} \\
= & \underbrace{\left(\operatorname{diag}(\mathbb{1} - e^{-\gamma \mathbf{p}} + \gamma \mathbf{p} \odot e^{-\gamma \mathbf{p}}) + \mathbf{C}^{\mathsf{T}} \operatorname{diag}(e^{-\gamma \mathbf{p}} - \gamma \mathbf{p} \odot e^{-\gamma \mathbf{p}})\right)}_{\mathbf{Q}(\mathbf{p})^{\mathsf{T}}} \boldsymbol{\delta},
\end{aligned}$$

where $\odot$ denotes the entry-wise multiplication of vectors, and for a vector $\boldsymbol{\nu} = (\nu_i)_{i=1}^n$, $e^{\boldsymbol{\nu}}$ denotes the vector with entries e^{ν_i}. Since both functions $1 - e^{-\gamma x} + \gamma x e^{-\gamma x}$ and $e^{-\gamma x} - \gamma x e^{-\gamma x}$ take non-negative values on $[0, 1]$, $\mathbf{Q}(\mathbf{p})^{\mathsf{T}}$ is a (column) stochastic matrix. Thus, $\mathbf{f}$ is contractive.

Any fixed point of $\mathbf{f}$ must satisfy

$$\mathbf{p} = \left(\operatorname{diag}(1 - e^{-\gamma \mathbf{p}}) + \mathbf{C}^{\mathsf{T}}(e^{-\gamma \mathbf{p}}))\right) \mathbf{p}. \tag{4.16}$$

Rearranging terms we see that $\mathbf{p}e^{-\gamma \mathbf{p}}$ is proportional to $\mathbf{c}$ (the Frobenius-Perron vector of $\mathbf{C}$), and therefore,

$$p_i e^{-\gamma p_i} = \kappa c_i, \; i = 1, \dots, n. \tag{4.17}$$

The function $xe^{-\gamma x}$ is monotonic on $[0,1]$ and hence, for any

$$\kappa \leqslant \frac{1/(\gamma e)}{\max\limits_i\{c_i\}} =: \kappa_{\max},$$

there is a unique solution $\{p_i \mid i = 1, \dots, n\}$ of (4.17). Let now $s(\kappa) := \sum_i p_i$. The function $s(\kappa)$ is monotonically increasing as a function of κ and has $s(0) = 0$. For $\kappa = \kappa_{\max}$ one of the p_i's is equal to 1 and hence $s(\kappa_{\max}) \geqslant 1$. Thus, the equation $s(\kappa) = 1$ has a unique solution that corresponds to the probability vector $\mathbf{p}^\star$ that satisfies (4.16). Thus the fixed point $\mathbf{p}^\star$ is unique.

Further, $\mathbf{Q}$ inherits irreducibility from $\mathbf{C}^\mathsf{T}$ in $\mathcal{S}^o_{n-1}$ since it has the same pattern of positive entries; in addition it is aperiodic, irrespective of $\mathbf{C}$, because its diagonal is not zero. Hence, independently of $\mathbf{p}$, there exists integer m such that

$$\mathbf{Q}(\overbrace{\mathbf{f}(\dots \mathbf{f}(\mathbf{p}))}^{m-1})^\mathsf{T} \dots \mathbf{Q}(\mathbf{f}(\mathbf{p}))^\mathsf{T}\mathbf{Q}(\mathbf{p})^\mathsf{T} \tag{4.18}$$

has all entries positive. The expression in (4.18) is precisely the differential of the mth iterant (cf. (4.12)). By Proposition 11, $\mathbf{p}^\star$ is globally attractive. $\square$

Remark 16. *More in the style of DeGroot-Friedkin models [24, 32] of the general form (4.6), one may consider a model*

$$\mathbf{p}(t+1) = \left[\mathrm{diag}(\mathbb{1} - e^{-\gamma \mathbf{p}(t)}) + \mathbf{C}^\mathsf{T}\,\mathrm{diag}(e^{-\gamma \mathbf{p}(t)})\right]_{\mathrm{FP}}. \tag{4.19}$$

Then, $\operatorname{diag}(\mathbb{1} - e^{-\gamma \mathbf{p}(t)}) + \mathbf{C}^T \operatorname{diag}(e^{-\gamma \mathbf{p}(t)}))$ *is irreducible and therefore, an alternative formula for* $\mathbf{p}(t+1)$ *is*

$$\mathbf{p}(t+1) = \lim_{m \to \infty} \left(\operatorname{diag}(\mathbb{1} - e^{-\gamma \mathbf{p}(t)}) + \mathbf{C}^T \operatorname{diag}(e^{-\gamma \mathbf{p}(t)}))\right)^m \mathbf{p}(t).$$

Comparing with (4.15)*, the fixed point* $\mathbf{p}^\star$ *in Proposition 15 is also a fixed point for* (4.19).

4.3.2 Case $\mathbf{r(x) = 1 - e^{-\gamma x}}$ for $\gamma > 1$.

The case $\gamma > 1$ is substantially different. Here, there can be several attractive points of equilibrium for the nonlinear dynamics in (4.15) and even more complicated nonlinear behavior. In fact, we suggest that *such a behavior may be more appropriate for models of opinion dynamics* as it is reasonable to expect a different outcome depending on the starting point (that encapsulates confidence/beliefs of individuals). We illustrate the behavior with two numerical examples for 3-state Markov chains to highlight differences with the case when $\gamma \leqslant 1$.

Example

We consider the dynamics in (4.15) for a 3-state Markov chain (i.e., $n = 3$) with $\gamma = 4$ and

$$\mathbf{C} = \begin{bmatrix} 0.8 & 0.1 & 0.1 \\ 0.4 & 0.2 & 0.4 \\ 0.4 & 0.4 & 0.2 \end{bmatrix}. \tag{4.20}$$

The left Frobenius-Perron eigenvector of $\mathbf{C}$ is $(2/3, 1/6, 1/6)^{\mathsf{T}}$. The fixed-point conditions for possible stationary distributions become

$$
\begin{aligned}
&e^{-4p_1^\star} p_1^\star = \kappa \frac{2}{3}, \\
&e^{-4p_2^\star} p_2^\star = \kappa \frac{1}{6}, \\
&2p_2^\star + p_1^\star = 1.
\end{aligned}
$$

Upon eliminating κ between the first two, and substituting p_1 in terms of p_2, we obtain

$$
\frac{1 - 2p_2^\star}{p_2^\star} e^{-4(1-3p_2^\star)} = 4. \tag{4.21}
$$

This equation has the unique solution

$$
\mathbf{p}^\star := (0.9904, 0.0048, 0.0048)^{\mathsf{T}}.
$$

It turns out that this is a locally attractive fixed point. This can be verified by evaluating the Jacobian of $\mathbf{f}$ at $\mathbf{p}^\star$ as

$$
d\mathbf{f}|_{\mathbf{p}^\star} = \begin{bmatrix} 1.0113 & 0.3849 & 0.3849 \\ -0.0056 & 0.2303 & 0.3849 \\ -0.0056 & 0.3849 & 0.2303 \end{bmatrix}.
$$

Even though the Jacobian has negative entries it is still strictly contractive. Indeed, we explicitly evaluate the induced gain using Theorem 14 and this is

$$
\|d\mathbf{f}|_{\mathcal{T}}\|_{(1)} = \frac{1}{2} \max\{1.2528, 1.2528, 0.3092\} = 0.6264 < 1.
$$

Thus $\mathbf{p}^\star$ is a stable fixed point. This analysis is consistent with simulations shown in Fig. 4.1. In the figure we depict trajectories (in different color) starting from random initial conditions that clearly tend to $\mathbf{p}^\star$.

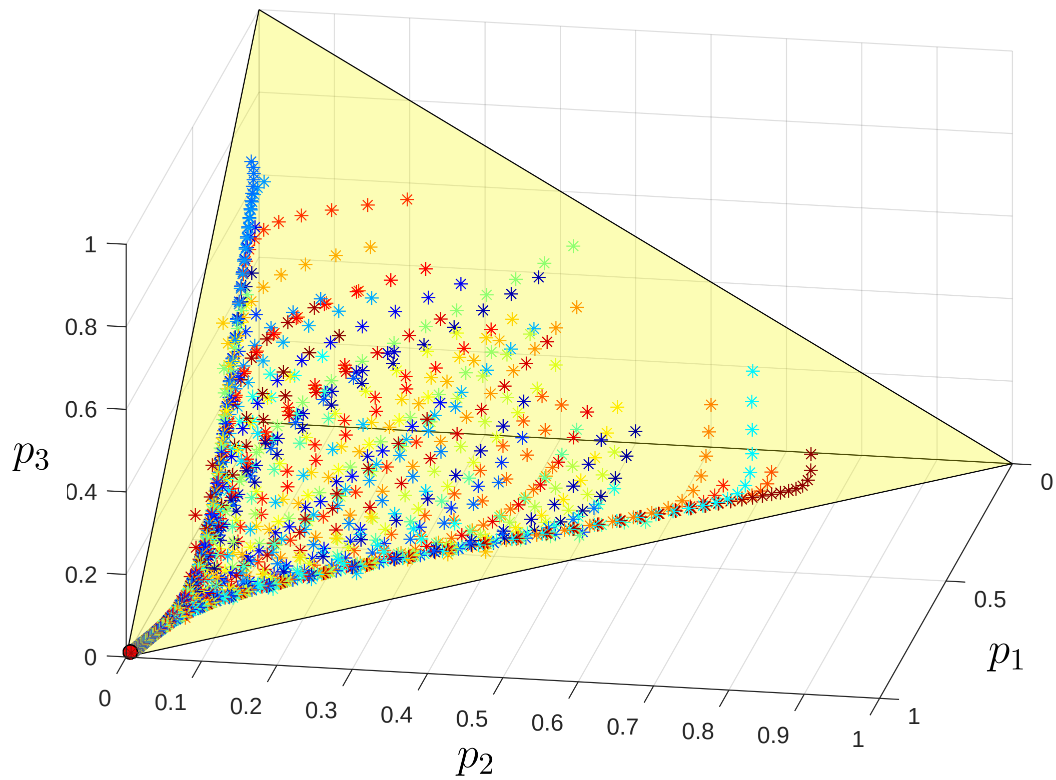

Figure 4.1: Convergence of trajectories to a unique fixed point for the 3-state exponential model (4.15) with $\gamma = 4$ and influence matrix $\mathbf{C}$ given by (4.20).

Example

Once again we consider a 3-state Markov chain with $\gamma = 4$, but this time we take

$$\mathbf{C} = \begin{bmatrix} 0 & 0.5 & 0.5 \\ 0.5 & 0 & 0.5 \\ 0.5 & 0.5 & 0 \end{bmatrix}. \tag{4.22}$$

The fixed-point equations have 7 solutions (taking into account symmetries). Out of those, three are attractive fixed points with coordinates cyclically selected from $\{1 - \alpha, \alpha/2, \alpha/2\}$ for $\alpha = 0.046$. The remaining four are unstable fixed points. One is at the center $(1/3, 1/3, 1/3)^{\mathsf{T}}$ (due to symmetry), and the rest have coordinates cyclically selected from $\{1-\alpha, \alpha/2, \alpha/2\}$ for $\alpha = 0.874$. Just like the previous example, we can verify stability by computing the Jacobian $\mathrm{d}\mathbf{f}$ at fixed points. For instance, for the fixed point $\mathbf{p}^{\star}_{\alpha} = (0.954, 0.023, 0.023)^{\mathsf{T}}$, we have

$$\mathrm{d}\mathbf{f}|_{\mathbf{p}^{\star}_{\alpha}} = \begin{bmatrix} 1.0620 & 0.4141 & 0.4141 \\ -0.0310 & 0.1718 & 0.4141 \\ -0.0310 & 0.4141 & 0.1718 \end{bmatrix},$$

and

$$\|\mathrm{d}\mathbf{f}|_{\mathcal{T}}\|_{(1)} = \frac{1}{2}\max\{1.2958, 1.2958, 0.4846\} = 0.6479 < 1.$$

Applying Theorem 14, we conclude that $\mathbf{p}_{\mathfrak{a}}^{\star}$ is a stable fixed point. For another fixed point $\mathbf{p}_{\mathfrak{b}}^{\star} = (0.1260, 0.4370, 0.4370)^{\mathsf{T}}$, we have

$$\mathrm{d}\mathbf{f}|_{\mathbf{p}_{\mathfrak{b}}^{\star}} = \begin{bmatrix} 0.7004 & -0.0651 & -0.0651 \\ 0.1498 & 1.1302 & -0.0651 \\ 0.1498 & -0.0651 & 1.1302 \end{bmatrix},$$

and

$$\|\mathrm{d}\mathbf{f}|_{\mathcal{T}}\|_{(1)} = \frac{1}{2}\max\{1.9608, 1.9608, 2.3907\} = 1.1954 > 1.$$

Numerical evidence shown in Fig. 4.2 confirms that $\mathbf{p}_{\mathfrak{a}}^{\star}$ is stable and $\mathbf{p}_{\mathfrak{b}}^{\star}$ is unstable. Convergence of trajectories depends on the initial conditions with respect to the basins of attraction for the three stable fixed points. The qualitative behavior of the trajectories around the four unstable and three stable fixed points is illustrated in Fig. 4.3.

4.3.3 Case $\mathbf{r}(\mathbf{x}) = \mathbf{e}^{-\beta \mathbf{x}}$ for $\beta \leqslant 1$.

In this case there is a unique fixed point and it is always globally attractive. We summarize our conclusions as follows:

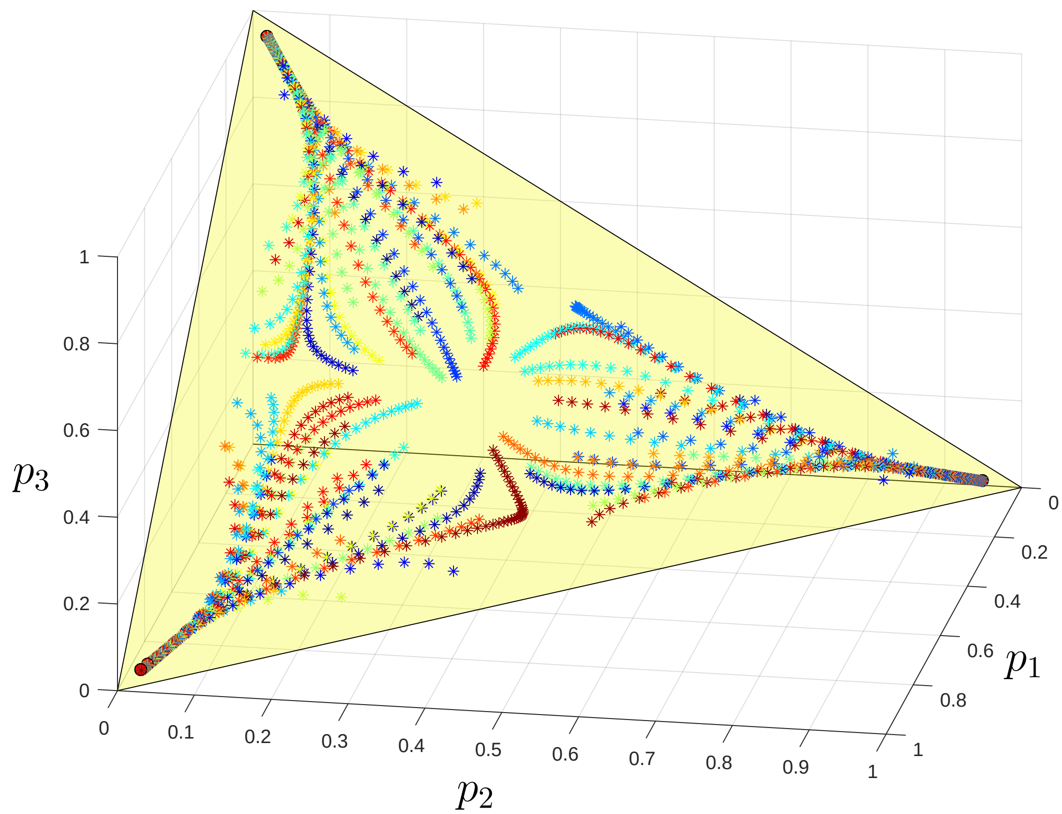

Figure 4.2: For the 3-state exponential model (4.15) with $\gamma = 4$ and influence matrix $\mathbf{C}$ given by (4.22), trajectories converge to one of the three stable fixed points.

Proposition 17. *For any* $\gamma \in [0, 1]$ *consider*

$$\mathbf{p}(t) \mapsto \mathbf{f}(\mathbf{p}(t)) = \mathbf{p}(t+1), \text{ where} \tag{4.23a}$$

$$\mathbf{f}(\mathbf{p}(t)) = \left(\operatorname{diag}(e^{-\gamma \mathbf{p}(t)}) + \mathbf{C}^T \operatorname{diag}(\mathbb{1} - e^{-\gamma \mathbf{p}(t)})\right) \mathbf{p}(t). \tag{4.23b}$$

The map $\mathbf{f}$ *is contractive in* ℓ_1 *and, starting from an arbitrary* $\mathbf{p}(0) \in \mathcal{S}_{n-1}$, *the limit* $\mathbf{p}^\star = \lim_{t\to\infty} \mathbf{p}(t)$ *exists, is unique, and its entries satisfy* $\left(1 - e^{-\gamma p_i^\star}\right) p_i^\star = \kappa c_i$, *for some* $\kappa > 0$.

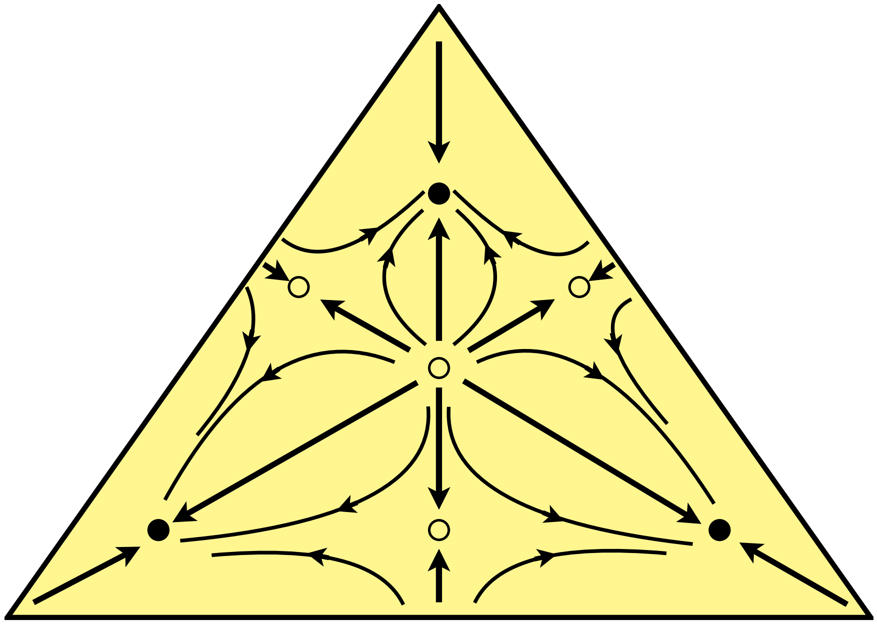

Figure 4.3: The qualitative behavior of dynamics (4.15) with $\gamma > 1$ as observed in Fig. 4.2, where three stable fixed points (solid circles) and four unstable fixed points (empty circles) coexist on the simplex.

Proof. First, the Jacobian matrix $\mathbf{Q}(\mathbf{p})^\top$ is of the form

$$\operatorname{diag}(e^{-\gamma \mathbf{p}} - \gamma \mathbf{p} \odot e^{-\gamma \mathbf{p}}) + \mathbf{C}^\top \operatorname{diag}(\mathbb{1} - e^{-\gamma \mathbf{p}} + \gamma \mathbf{p} \odot e^{-\gamma \mathbf{p}}).$$

Notice that $\mathbf{Q}(\mathbf{p})^\top$ is differentiable in $\mathbf{p}$, and for $\gamma \leqslant 1$, is a (column) stochastic matrix with non-negative entries. Therefore, by Corollary 10, the map (4.23) is contractive in ℓ_1 and inherits irreducibility from $\mathbf{C}^\top$ in $\mathcal{S}^\circ_{n-1}$. Following a similar line of argument as in Proposition 15, uniqueness of the fixed point for map (4.23) is guaranteed. Next, we write the stationarity conditions

$$\mathbf{p}^\star = \left(\operatorname{diag}\left(e^{-\gamma \mathbf{p}^\star}\right) + \mathbf{C}^\top \operatorname{diag}\left(\mathbb{1} - e^{-\gamma \mathbf{p}^\star}\right)\right) \mathbf{p}^\star,$$

equivalently,

$$\left(\mathbb{1} - e^{-\gamma \mathbf{p}^\star}\right) \odot \mathbf{p}^\star = \mathbf{C}^\top \left(\mathbb{1} - e^{-\gamma \mathbf{p}^\star}\right) \odot \mathbf{p}^\star,$$

to obtain that

$$\left(1 - e^{-\gamma p_i^\star}\right) p_i^\star = \kappa c_i, \quad i = 1, \ldots, n, \tag{4.24}$$

where c_i denotes the i-th entry of the Frobenius-Perron vector of $\mathbf{C}$ and $\kappa = \sum_{i=1}^{n} \left(1 - e^{-\gamma p_i^\star}\right) p_i^\star$.

□

4.3.4 Case $\mathbf{r(x) = e^{-\text{fl}x}}$ for fl > 1.

In this case too there exists a unique fixed point in any dimension (any n). This follows easily as the fixed-point conditions are the same,

$$\left(1 - e^{-\gamma p_i^\star}\right) p_i^\star = \kappa c_i.$$

Then, for all $\gamma > 0$, $(1-e^{-\gamma x})x$ is a monotonically increasing starting at 0 for $x = 0$. Solving for a given κ, the sum $\sum_{i=1}^{n} p_i^\star(\kappa)$ is also monotonically increasing function of κ and its value exceeds 1 for a suitable κ. Thus, there is a unique solution $p_i^\star(\kappa)$ which is a probability vector (and the $p_i^\star$'s sum up to 1).

However, interestingly, the nonlinear dynamics now display diverse behaviors. Below we give three examples. In the first two the unique fixed point is attractive, but they differ, in that assurances for stability are drawn (for the second example) by computing the norm of the differential of higher iterants (2nd in this case). In the third example we observe a $2-$periodic attractive orbit.

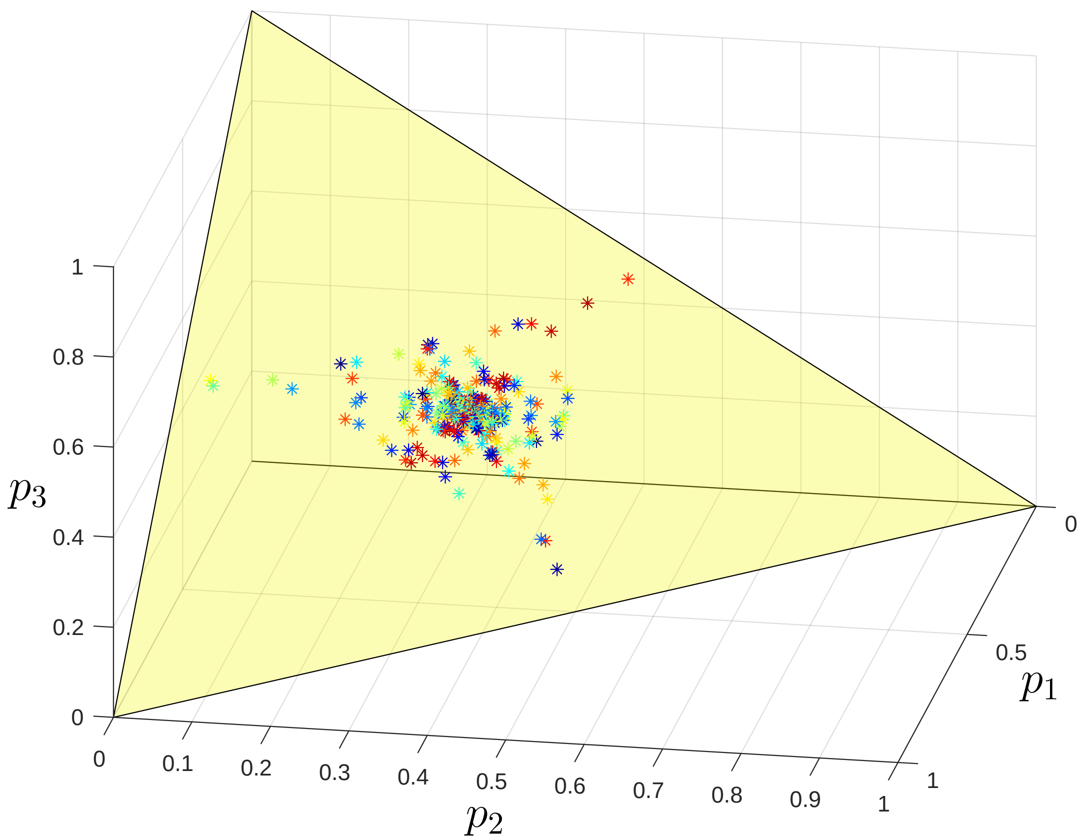

Figure 4.4: For the 3-state exponential model (4.23) with $\gamma = 4$ and influence matrix $\mathbf{C}$ given by (4.25), trajectories converge to the unique stable fixed point $\mathbf{p}^\star = (1/3, 1/3, 1/3)^\mathsf{T}$.

Example

We consider a 3-state Markov chain with $\gamma = 4$, and

$$\mathbf{C} = \begin{bmatrix} 0 & 0.5 & 0.5 \\ 0.5 & 0 & 0.5 \\ 0.5 & 0.5 & 0 \end{bmatrix}. \tag{4.25}$$

Since $\mathbf{C}$ is doubly stochastic, the unique fixed point for (4.24) is $\mathbf{p}^\star = (1/3, 1/3, 1/3)^\mathsf{T}$, and we have

$$\mathrm{d}\mathbf{f}|_{\mathbf{p}^\star} = \begin{bmatrix} -0.0880 & 0.5440 & 0.5440 \\ 0.5440 & -0.0880 & 0.5440 \\ 0.5440 & 0.5440 & -0.0880 \end{bmatrix},$$

and

$$\|\mathrm{d}\mathbf{f}|_{\mathbf{p}^\star}\|_{(1)} = \frac{1}{2}\max\{1.2640, 1.2640, 1.2640\} = 0.6320 < 1.$$

Using Theorem 14, we conclude that $\mathbf{p}^\star$ is a stable fixed point.

Example

For $\gamma = 4$, now take

$$\mathbf{C} = \begin{bmatrix} 0 & 0 & 1 \\ 0.5 & 0.5 & 0 \\ 0.5 & 0.5 & 0 \end{bmatrix}.$$

The unique fixed point is again $\mathbf{p}^\star = (1/3, 1/3, 1/3)^\mathsf{T}$. Here,

$$\mathrm{d}\mathbf{f}|_{\mathbf{p}^\star} = \begin{bmatrix} -0.0880 & 0.5440 & 0.5440 \\ 0 & 0.4560 & 0.5440 \\ 1.0880 & 0 & -0.0880 \end{bmatrix},$$

and

$$\|\mathrm{d}\mathbf{f}|_{\mathbf{p}^\star}\|_{(1)} = 1.1760.$$

However,

$$\|\mathrm{d}\mathbf{f}^2|_{\mathbf{p}^\star}\|_{(1)} = 0.7911.$$

This ensures local attractiveness.

Example

Once again we consider a 3-state Markov chain with $\gamma = 4$, but we now take

$$\mathbf{C} = \begin{bmatrix} 0 & 0 & 1 \\ 0.8 & 0 & 0.2 \\ 0.8 & 0.2 & 0 \end{bmatrix}. \tag{4.26}$$

Uniqueness of a fixed point is guaranteed. This turns out to be

$$\mathbf{p}^\star = (0.4173, 0.1537, 0.4298)^\mathsf{T}.$$

It turns out that

$$\mathrm{d}\mathbf{f}|_{\mathbf{p}^\star} = \begin{bmatrix} -0.1261 & 0.6333 & 0.9031 \\ 0 & 0.2084 & 0.2258 \\ 1.1261 & 0.1583 & -0.1289 \end{bmatrix}$$

has ℓ_1-norm equal to 1.255, and so do the differentials of higher order iterants. However, a stable 2-periodic orbit now appears alternating between

$$\mathbf{p}^{\mathfrak{a}} = (0.1943, 0.1042, 0.7015)^{\mathsf{T}} \text{ and } \mathbf{p}^{\mathfrak{b}} = (0.6450, 0.2005, 0.1545)^{\mathsf{T}}.$$

The periodic orbit is locally attractive. The Jacobians at these two points are

$$\mathrm{d}\mathbf{f}|_{\mathbf{p}^{\mathfrak{a}}} = \begin{bmatrix} 0.1024 & 0.4923 & 0.8873 \\ 0 & 0.3846 & 0.2218 \\ 0.8976 & 0.1231 & -0.1092 \end{bmatrix}$$

and

$$\mathrm{d}\mathbf{f}|_{\mathbf{p}^{\mathfrak{b}}} = \begin{bmatrix} -0.1197 & 0.7290 & 0.6352 \\ 0 & 0.0888 & 0.1588 \\ 1.1197 & 0.1822 & 0.2060 \end{bmatrix},$$

respectively, and it can be verified that the norm of their product is $\|\mathrm{d}\mathbf{f}|_{\mathbf{p}^{\mathfrak{a}}}\mathrm{d}\mathbf{f}|_{\mathbf{p}^{\mathfrak{b}}}\|_{(1)} = 0.8750$. Interestingly, $\|\mathrm{d}\mathbf{f}|_{\mathbf{p}^{\mathfrak{b}}}\mathrm{d}\mathbf{f}|_{\mathbf{p}^{\mathfrak{a}}}\|_{(1)} = 0.7120$, which is different, but < 1 too (as expected). Stability can be ascertained by Proposition 13. An expalantion, as pointed out by an anonymous referee, is that as a particular state gets “more probable”, it actually is associated with “less confidence”, and hence there is indecision oscillating between alternatives.

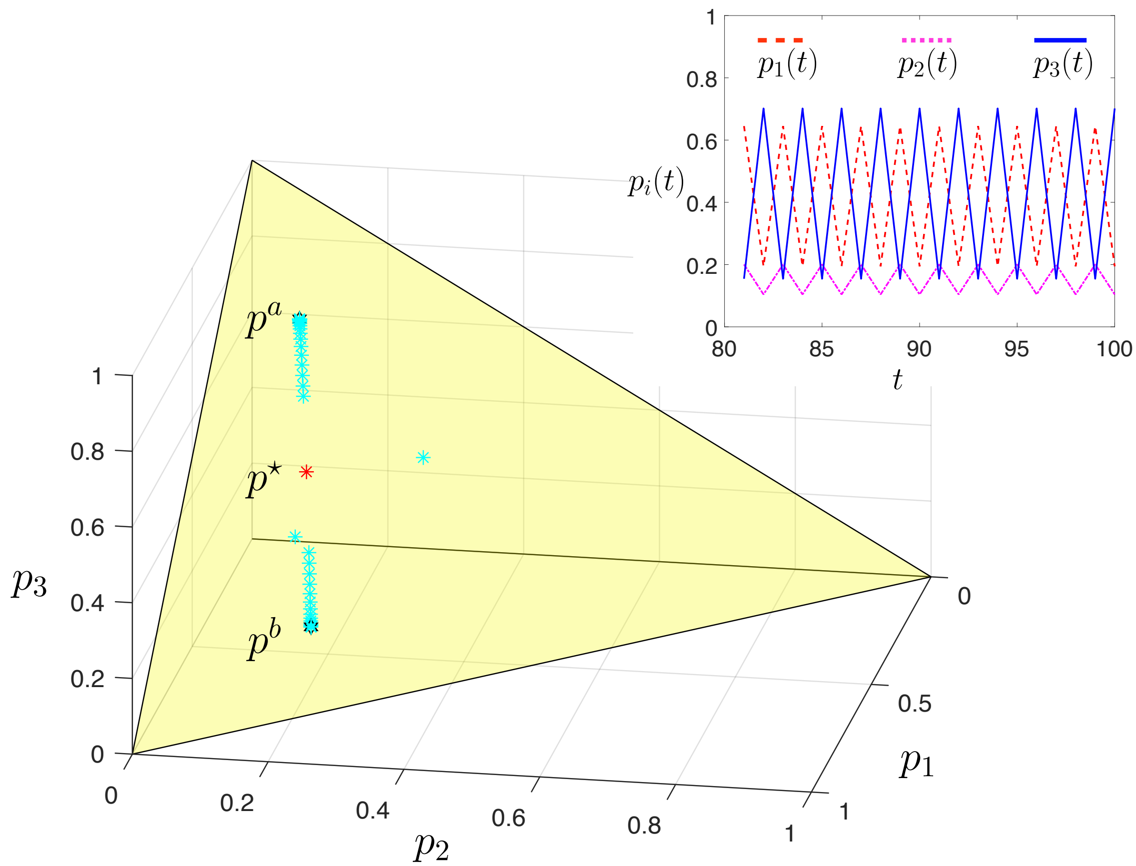

Figure 4.5: For the 3-state exponential model (4.23), $\gamma = 4$, and $\mathbf{C}$ given by (4.26), the unique fixed point $\mathbf{p}^\star = (0.4173, 0.1537, 0.4298)^\top$ is unstable and there is an attractive 2-periodic orbit between $\mathbf{p}^a$ and $\mathbf{p}^b$, verified by the time history (inset graph).

4.4 DeGroot-Friedkin Model and its Variants

We now consider the two classes of nonlinear Markov chains with $r(x) = \gamma x$ and $1 - \gamma x$, for $0 < \gamma \leqslant 1$. The bounds $0 < \gamma \leqslant 1$ ensure that $\mathbf{\Pi}(\mathbf{p})$ (in (4.5a)) remains stochastic for all values of the probability vector $\mathbf{p}$ and any $\mathbf{C}$. For small values of γ, $\gamma x \simeq 1 - e^{-\gamma x}$ and, evidently, these models approximate the corresponding exponential models of Section 4.3.

4.4.1 Case $\mathbf{r}(\mathbf{x}) =$ flx

The case where $r(x) = x$ and $\mathbf{C}$ is restricted to be *doubly stochastic* has been studied in [88] and referred to as a *modified/one-step DeGroot-Friedkin* model. Existence and stability of the fixed point were analyzed and, in particular, it was conjectured that the equilibrium is stable for any irreducible row stochastic matrix $\mathbf{C}$ (see [88]). Herein, we consider the general class where $r(x) = \gamma x$. For this class of models, very much as in the case of the exponential models, we can ascertain ℓ_1 strict-contractivity for a range of values for γ, while for other values, we can ascertain stability on a case by case basis. We begin with the following proposition for general irreducible stochastic $\mathbf{C}$ and $\gamma \leqslant \frac{1}{2}$.

Proposition 18. *For $\gamma \leqslant \frac{1}{2}$ consider*

$$\mathbf{p}(t) \mapsto \mathbf{f}(\mathbf{p}(t)) = \mathbf{p}(t+1), \text{ where} \tag{4.27a}$$

$$\mathbf{p}(t+1) = \big(\mathrm{diag}(\gamma\mathbf{p}(t)) + \mathbf{C}^{\mathsf{T}}\,\mathrm{diag}(\mathbb{1} - \gamma\mathbf{p}(t))\big)\,\mathbf{p}(t). \tag{4.27b}$$

The map $\mathbf{f}$ is contractive in ℓ_1, the iteration for $t = 0, 1, \ldots$ converges to a unique fixed point $\mathbf{p}^\star = \lim_{t\to\infty}\mathbf{p}(t)$, and

$$(1 - \gamma p_i^\star)\, p_i^\star = \kappa c_i, \text{ for a suitable } \kappa > 0. \tag{4.28}$$

Proof. As before, the Jacobian $d\mathbf{f}$ is now

$$\boldsymbol{\delta} \mapsto \underbrace{\big(\mathrm{diag}(2\gamma\mathbf{p}) + \mathbf{C}^{\mathsf{T}}\,\mathrm{diag}(\mathbb{1} - 2\gamma\mathbf{p})\big)}_{\mathbf{Q}^{\mathsf{T}}(\mathbf{p})}\,\boldsymbol{\delta}.$$

For $0 < \gamma \leqslant \frac{1}{2}$, $\mathbf{Q}(\mathbf{p})$ is element-wise non-negative. Corollary 10 ensures that $\mathbf{f}$ is contractive in

ℓ_1. The unique fixed point $\mathbf{p}^\star$ satisfies

$$\mathbf{C}^\mathsf{T}(\mathbb{1} - \gamma\mathbf{p}^\star) \odot \mathbf{p}^\star = (\mathbb{1} - \gamma\mathbf{p}^\star) \odot \mathbf{p}^\star,$$

and therefore, $p_i^\star$ satisfies $(1 - \gamma p_i^\star)\, p_i^\star = \kappa c_i$ with $\kappa = 1 - \gamma \|\mathbf{p}^\star\|_2^2$. The global stability of $\mathbf{p}^\star$ follows a similar argument as in Proposition 15. □

For the range $\gamma \in [\frac{1}{2}, 1]$ all-encompassing conclusions cannot be drawn and examples have to be worked out on a case by case basis. However, more can be said based on the induced norm of $\mathrm{d}\mathbf{f}$ even when the elements of $\mathrm{d}\mathbf{f}$ may have negative entries. Specifically, it is possible to obtain a closed-form expression for $\max_{\mathbf{p} \in \mathcal{S}_{n-1}} \|\mathrm{d}\mathbf{f}|_\mathcal{T}\|_{(1)}$ for $\gamma \in (\frac{1}{2}, 1]$. If $\mathbf{C}$ has zero diagonal (a standard assumption in DeGroot-Friedkin literature), then for $\frac{1}{2} < \gamma < \frac{1}{2}\,(1 + \min_{i \neq j} C_{ji})$, it can be shown that the map $\mathbf{f}$ remains ℓ_1-contractive and consequently $\mathbf{p}^\star$ in (4.28) remains globally attractive. In passing, we note that for $\gamma = 1$, trivially, the vertices of $\mathcal{S}_{n-1}$ are fixed points while, in general, when $\gamma \neq 1$, this is not the case. Also, when $\mathbf{C}$ is doubly stochastic and $\gamma \neq 1$, $\frac{1}{n}\mathbb{1}$ is the unique[5] fixed point of (4.27).

4.4.2 Case $\mathbf{r}(\mathbf{x}) = \mathbf{1} -$ flx

We first establish that the corresponding map admits a unique fixed point for any $\gamma > 0$, and show that it is ℓ_1-contractive for $\gamma \leqslant \frac{1}{2}$.

Proposition 19. *Consider*

$$\mathbf{p}(t) \mapsto \mathbf{f}(\mathbf{p}(t)) = \mathbf{p}(t+1) \textit{ where} \tag{4.29a}$$

$$\mathbf{p}(t+1) = \big(\mathrm{diag}(\mathbb{1} - \gamma\mathbf{p}(t)) + \mathbf{C}^\mathsf{T}\,\mathrm{diag}(\gamma\mathbf{p}(t))\big)\,\mathbf{p}(t). \tag{4.29b}$$

[5]That $\frac{1}{n}\mathbb{1}$ is a fixed point can be verified directly, whereas the fact that there is no other fixed point can be argued in a similar manner as [88, Theorem 2].

For any $\gamma > 0$, there is a unique fixed point $\mathbf{p}^\star$, where

$$p_i^\star = \frac{\sqrt{c_i}}{\sum_{i=1}^{n} \sqrt{c_i}}, \quad i = 1, \dots, n. \tag{4.30}$$

For $0 < \gamma \leqslant \frac{1}{2}$, $\mathbf{f}$ is ℓ_1-contractive and in this case $\mathbf{p}^\star$ is an attractive fixed point.

Proof. The fixed-point condition

$$\gamma \mathbf{p}^\star \odot \mathbf{p}^\star = \mathbf{C}^\mathsf{T} \gamma \mathbf{p}^\star \odot \mathbf{p}^\star$$

implies that $p_i^\star$ must equal $\kappa\sqrt{c_i}$, for each i and some $\kappa > 0$. Thus, the fixed point is always unique and is as claimed. For $0 < \gamma \leqslant \frac{1}{2}$, the Jacobian $\mathrm{d}\mathbf{f}$

$$\boldsymbol{\delta} \mapsto \underbrace{\left(\operatorname{diag}(1 - 2\gamma\mathbf{p}) + \mathbf{C}^\mathsf{T} \operatorname{diag}(2\gamma\mathbf{p})\right)}_{\mathbf{Q}^\mathsf{T}(\mathbf{p})} \boldsymbol{\delta}$$

is element-wise non-negative, inherits irreducibility from $\mathbf{C}^\mathsf{T}$ in $\mathcal{S}_{n-1}^{o}$, and as before, $\mathbf{f}$ is ℓ_1-contractive. $\square$

Once again, for $\gamma \in [\frac{1}{2}, 1]$, analysis can be done on a case by case basis and no general conclusion can be drawn. Similar to the comment in Section 4.4.1, we can find a closed-form expression for $\max_{\mathbf{p} \in \mathcal{S}_{n-1}} \|\mathrm{d}\mathbf{f}|_{\mathcal{T}}\|_{(1)}$ for $\gamma \in (\frac{1}{2}, 1]$. Then requiring $\max_{\mathbf{p} \in \mathcal{S}_{n-1}} \|\mathrm{d}\mathbf{f}|_{\mathcal{T}}\|_{(1)} < 1$, it can be shown that if $\mathbf{C}$ has zero diagonal (a standard assumption in DeGroot-Friedkin literature), then for $\frac{1}{2} < \gamma < \frac{1}{2}\left(1 - \min_{i \neq j} C_{ij}\right)^{-1}$, the map $\mathbf{f}$ is guaranteed to be ℓ_1-nonexpansive.

4.5 Continuous-time Framework

The framework presented extends naturally to continuous-time. Indeed, a continuous-time analog of (4.5) as a dynamical system on $\mathcal{S}_{n-1}$ is given by

$$\dot{\mathbf{p}}(t) = \mathbf{L}^{\mathsf{T}}(\mathbf{I} - \mathrm{diag}(\mathbf{r}(\mathbf{p}(t))))\mathbf{p}(t), \tag{4.31}$$

where $\mathbf{L} = \mathbf{C} - \mathbf{I}$ is a Laplacian matrix satisfying $\mathbf{L}\mathbb{1} = 0$. It is clear that $(\mathbf{I} - \mathrm{diag}(\mathbf{r}(\mathbf{p}(t))))\mathbf{L}$ is a Laplacian matrix as $(\mathbf{I} - \mathrm{diag}(\mathbf{r}(\mathbf{p}(t))))\mathbf{L}\mathbb{1} = 0$. The scaling by $\mathrm{diag}(\mathbf{r}(\mathbf{p}(t)))$ can be interpreted to play a similar role–it promotes or discourages staying at a state i in accordance with the current value of the corresponding occupation probability p_i. The special case when $\mathbf{r}(\mathbf{p}) = \mathbf{p}$ was recently considered in [17].

Lemma 20. *If $\mathbf{p}^\star$ is a fixed point of the continuous time model in 4.31 and Jacobian of the map has positive entries at this point, then $\mathbf{p}^\star$ is locally stable.*

Proof. For stability analysis of 4.31, we start by linearizing the nonlinear model using the taylor expansion ($f(\mathbf{p} + \delta) - f(\mathbf{p}) \approx \dot{f}(\mathbf{p})\delta$).

$$\begin{aligned}\dot{\mathbf{p}}(t) &= L^{\mathsf{T}}(I - diag(\mathbf{r}(\mathbf{p}(t))))\mathbf{p}(t) \\ &= f(\mathbf{p})\end{aligned}$$

Hence, we have

$$
\begin{aligned}
\mathrm{f}(\mathbf{p}+\boldsymbol{\delta})-\mathrm{f}(\mathbf{p}) &= \mathrm{L}^{\mathsf{T}}(\mathrm{I}-\mathrm{diag}(\mathbf{r}(\mathbf{p}+\boldsymbol{\delta})))(\mathbf{p}+\boldsymbol{\delta})-\mathrm{L}^{\mathsf{T}}(\mathrm{I}-\mathrm{diag}(\mathbf{r}(\mathbf{p})))\mathbf{p} \\
&= \mathrm{L}^{\mathsf{T}}(\mathbf{p}+\boldsymbol{\delta}-\mathbf{r}\mathbf{p}-\mathbf{r}\boldsymbol{\delta}-\boldsymbol{\delta}^2\dot{\mathbf{r}}-\boldsymbol{\delta}\dot{\mathbf{r}}\mathbf{p}-\mathbf{p}+\mathbf{r}\mathbf{p}) \\
&= \mathrm{L}^{\mathsf{T}}\mathrm{diag}(1-\mathbf{r}(\mathbf{p})-\dot{\mathbf{r}}(\mathbf{p})\mathbf{p})\boldsymbol{\delta} \\
&= \mathrm{M}\delta.
\end{aligned}
$$

Therefore, the linearized model and its solution has the general form of

$$
\begin{aligned}
&\dot{\boldsymbol{\delta}}(t) = \mathrm{M}\boldsymbol{\delta}(t), \\
&\boldsymbol{\delta}(t) = e^{(\mathrm{M}t)}\boldsymbol{\delta}_0.
\end{aligned}
$$

Discretization of the solution is as follow

$$
\begin{aligned}
&\delta(t+\Delta) = e^{(\mathrm{M}\Delta)}\delta(t), \\
&\delta(t+\Delta) = (\mathrm{I}+\mathrm{M}\Delta)\delta(t).
\end{aligned}
$$

Thus, from 6, we know that if Jacobian of the map (in this case $e^{(\mathrm{M}\Delta)}$) has positive entries then map is contractive in ℓ_1-norm.

$\square$

Note that if $\mathrm{M}\Delta$ be a Metzler matrix (matrix in which all the off-diagonal components are nonnegative (equal to or greater than zero)), then we know that entries of the Jacobian would be nonnegative (exponential of the Metzler matrix is a nonnegative matrix). It means that for stability analysis of 4.31, we only need to check that $\mathrm{diag}(1-\mathbf{r}(\mathbf{p})-\dot{\mathbf{r}}(\mathbf{p})\mathbf{p})$ has positive diagonal elements.

4.6 Groupings

It is quite interesting to speculate about the effect of colluding sub-group in opinion forming. Indeed, everyday experience suggests that opinion is often reinforced within groups of like-minded individuals that draw confidence upon the collective wisdom, or lack of. To account for such interactions, we use a stochastic matrix W to model the joint influence between group members by weighing their collective states via $\mathbf{r}(W\mathbf{p})$, which should be contrasted with individual-reinforcement of opinion/confidence modeled by $\mathbf{r}(\mathbf{p})$. This is independent and in addition to $\mathbf{C}$, which is used to model information flow over the total influence network. A reasonable choice for W is to be block diagonal where the blocks correspond to different subgroups of interacting individuals. The special case where W is identity matrix reduces to the earlier setting.

In fact, what we propose herein is an "interacting particle" analogue for nonlinear Markov chains, modeled as follows:

$$\begin{aligned} \mathbf{p}(t+1) &= \mathbf{\Pi}(\mathbf{p}(t))^{\mathsf{T}}\mathbf{p}(t) \\ &= \big(\operatorname{diag}(\mathbf{r}(W\mathbf{p}(t))) + \mathbf{C}^{\mathsf{T}}(\mathbf{I} - \operatorname{diag}(\mathbf{r}(W\mathbf{p}(t))))\big)\,\mathbf{p}(t). \end{aligned} \tag{4.32}$$

In particular, using a fixed-point argument as in [53], we establish existence results for the cases $\mathbf{r}(x) = x$ and $\mathbf{r}(x) = 1 - e^{-x}$, and a general stochastic matrix W.

Proposition 21. *Let $\mathbf{r}(x) = x$ or $\mathbf{r}(x) = 1 - e^{-x}$, and W a stochastic matrix. Assume that $\mathbf{c}_k < \frac{1}{2}$ for all k. The Markov nonlinear model* (4.32)*, has at least one fixed point in the interior of probability simplex $\mathcal{S}_{n-1}$.*

Proof. Any fixed point of (4.32) must satisfy

$$\mathbf{p}_j = F_j(\mathbf{p}) := \frac{1}{1 + \frac{\sum_{k \neq j} \mathbf{c}_k/(1-\mathbf{r}_k)}{\mathbf{c}_j/(1-\mathbf{r}_j)}}.$$

Since

$$\sum_{k \neq j} \frac{\mathbf{c}_k}{\mathbf{c}_j(1-\mathbf{r}_k)} > \sum_{k \neq j} \frac{\mathbf{c}_k}{\mathbf{c}_j} > 1,$$

there exists $\epsilon > 0$ small enough such that

$$\left(\sum_{k \neq j} \frac{\mathbf{c}_k}{\mathbf{c}_j(1-\mathbf{r}_k)} - 1\right)\epsilon - \sum_{k \neq j} \frac{\mathbf{c}_k}{\mathbf{c}_j(1-\mathbf{r}_k)}\epsilon^2 > 0.$$

It follows

$$\frac{1}{1 + \sum_{k \neq j} \frac{\mathbf{c}_k}{\mathbf{c}_j(1-\mathbf{r}_k)}\epsilon} < 1 - \epsilon.$$

Combining the above we obtain

$$F_j(\mathbf{p}) \leqslant \frac{1}{1 + \sum_{k \neq j} \frac{\mathbf{c}_k}{\mathbf{c}_j(1-\mathbf{r}_k)}\epsilon} < 1 - \epsilon.$$

On the other hand, given

$$\mathbf{p} \in \mathcal{S}_\epsilon := \{\mathbf{p} \in \mathcal{S}_{n-1} \mid \mathbf{p}_i \leqslant 1 - \epsilon,\ \forall i = 1, \ldots, n\},$$

it is easy to see $\mathbf{r}(W\mathbf{p}) \in \mathcal{S}_\epsilon$ due to the facts that $\mathbf{r}(x) \leqslant x$ and W is stochastic. Thus, $F(\mathcal{S}_\epsilon) \subset \mathcal{S}_\epsilon$. Clearly, F is continuous. Therefore, by Brouwer fixed-point theorem, there exists $\mathbf{p}^\star$ such that $\mathbf{p}^\star = F(\mathbf{p}^\star)$. □

The ”nonlocal interaction” matrix W may in general introduce negative off-diagonal elements in $\mathrm{d}\mathbf{f}$. The theory in Section 4.2 applies on a case by case basis, but no general conclusion can be drawn at this point regarding global stability of particular class of models as we did earlier. Indeed, for $\mathbf{r}(x) = 1 - e^{-x}$, a matrix representation of the differential (4.8) becomes

$$\begin{aligned}\mathbf{Q}(\mathbf{p})^{\mathsf{T}} &= \operatorname{diag}(\mathbb{1} - e^{-W\mathbf{p}}) + \mathbf{C}^{\mathsf{T}} \operatorname{diag}(e^{-W\mathbf{p}}) \\ &\quad + (\mathbf{I} - \mathbf{C}^{\mathsf{T}}) \operatorname{diag}(\mathbf{p} \odot e^{-W\mathbf{p}})W.\end{aligned}$$

This, in general, has negative entries, which however doesn’t imply that the fixed point is unstable. The theory in Section 4.2 applies and attractiveness of equilibria can be ascertained by e.g., explicitly computing the ℓ_1-gain of $\mathrm{d}\mathbf{f}|_{\mathcal{T}}$.

Below is an example in $\mathcal{S}_2$. We take $\mathbf{r}(x) = 1 - e^{-Wx}$,

$$\mathbf{C} = \begin{bmatrix} 0.8 & 0.1 & 0.1 \\ 0.4 & 0.2 & 0.4 \\ 0.4 & 0.4 & 0.2 \end{bmatrix} \tag{4.33}$$

and

$$W = \begin{bmatrix} 0.5 & 0.5 & 0 \\ 0.5 & 0.5 & 0 \\ 0 & 0 & 1 \end{bmatrix}. \tag{4.34}$$

Numerically (Fig. 4.6), we see that the system has a unique fixed point, $\mathbf{p}^{\star} = (0.6975, 0.1744, 0.1282)^{\mathsf{T}}$, which is stable. This results are consistent with element-wise positiveness of the Jacobian of (4.32)

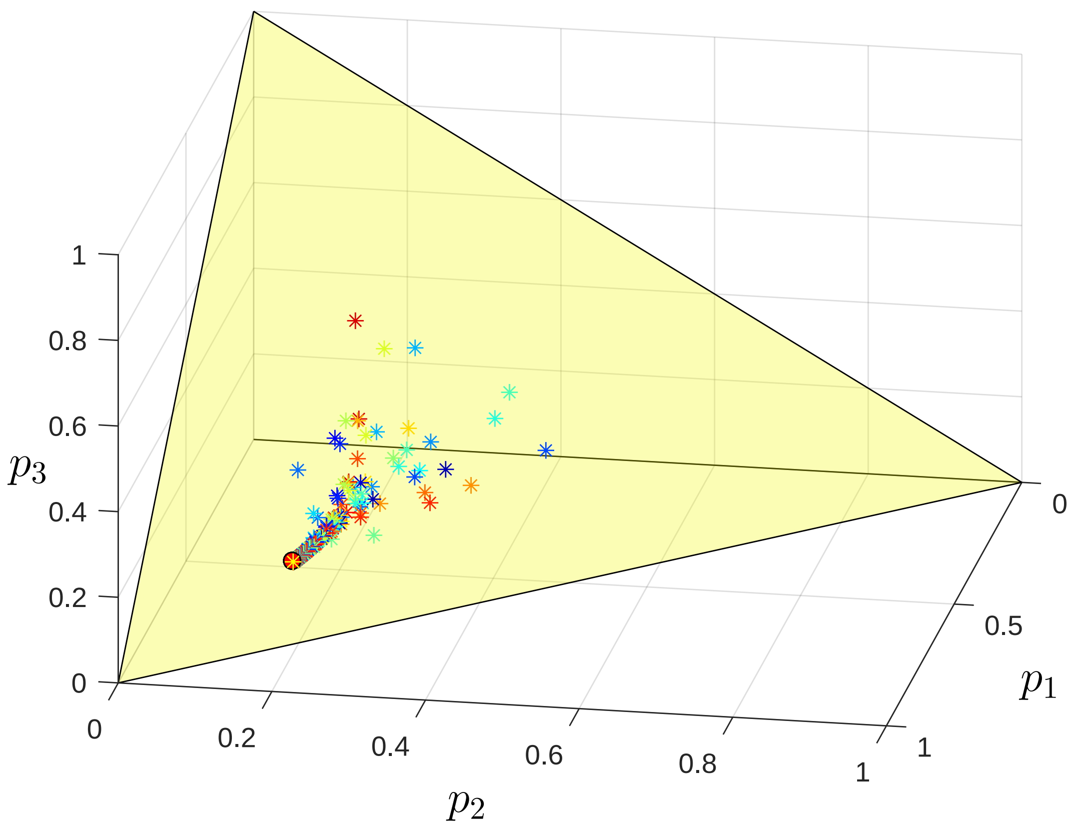

Figure 4.6: For the 3-state model (4.32) with influence matrix $\mathbf{C}$ and W given by (4.33) and (4.34), trajectories converge to the unique fixed point $\mathbf{p}^\star = (0.6975, 0.1744, 0.1282)^\mathsf{T}$.

which is evaluated at $\mathbf{p}^\star$,

$$\mathrm{d}\mathbf{f}|_{\mathbf{p}^\star} = \begin{bmatrix} 0.8932 & 0.2812 & 0.3068 \\ 0.0872 & 0.5052 & 0.3068 \\ 0.0196 & 0.2136 & 0.3865 \end{bmatrix}.$$

It is worth mentioning that simulation with the same $\mathbf{C}$ but this time with $W = \mathrm{I}_{3\times 3}$ gives $\mathbf{p}^\star = (0.8014, 0.0993, 0.0993)^\mathsf{T}$. Hence, as expected, the influence between member of the sub-group has a strengthening effect.

4.7 Connection to Interacting particles systems

Consider a collection of N weakly interacting particles, in which each particle evolves as a continuous time pure jump cadlag stochastic process taking values in a finite state space $\mathcal{X} = \{1, \cdots, d\}$. The evolution of this collection of particles is described by an N-dimensional time-homogeneous Markov process $= \{X^{i,N}\}_{i=1,\cdots,N}$, where for $t \geqslant 0$, $X^{i,N}(t)$ represents the state of the i_{th} particle at time t. The jump intensity of any given particle depends on the configuration of other particles only through the empirical measure

$$\mu^N(t) = \frac{1}{N}\sum_{i=1}^{N} \delta_{X^{i,N}}(t), t \in [0, \infty) \tag{4.35}$$

where δ_a is the Diract measure at a. Consequently, a typical particle's effect on the dynamics of the given particle is of order $\frac{1}{N}$.

Note that $\mu^N(t)$ is a random variable with values in the space $(\mathcal{S}_{n-1})_N(\mathcal{X}) = \mathcal{S}_{n-1}(\mathcal{X}) \cap \frac{1}{N}\mathcal{Z}^d$, where $(\mathcal{S}_{n-1})_N(\mathcal{X})$ is the space of probability measures on $\mathcal{X}$, equipped with the usual topology of weak convergence. The jump intensities of all particles will have the same functional form. Thus, if the initial particle distribution of $X^N(0) = \{X^{i,N}(0)\}_{i=1,\cdots,N}$ is exchangeable, then at any time $t > 0$, $X^N(t) = \{X^{i,N}(t)\}_{i=1,\cdots,N}$ is also exchangeable.

Roughly speaking, such a result states that on any fixed time interval $[0, T]$, the particles become asymptotically independent as $N \to \infty$, and that for each fixed t the distribution of a typical particle converges to a probability measure $p(t)$, which coincides with the limit in probability of the sequence of empirical measures $\{\mu^N(t)\}_{N\in\mathcal{N}}$ as $N \to \infty$. Under suitable conditions, the function $t \to p(t)$ can be characterized as the unique solution of a nonlinear differential equation on $\mathcal{S}_{n-1}(\mathcal{X})$ of the form 4.5a where for each $p \in \mathcal{S}_{n-1}(\mathcal{X})$, $\Pi(p)$ is a rate matrix for a Markov chain on X. This differential equation admits an interpretation as the forward equation of a ”nonlinear” jump Markov process that represents the evolution of the typical particle. In the context of weakly interacting diffusions, this limit equation is also referred to as the McKean-Vlasov limit.

4.8 Summary

We presented conditions that guarantee global attractiveness of equilibria of nonlinear stochastic maps; these are Theorems 6 and 14 and Propositions 11, 12, and 13 in Section 4.2. The criteria can be effectively used in certain cases where structural features can be exploited. Interest stems from modeling dynamical interactions over social networks. In Sections 4.3 and 4.4, we highlight application of the theory in representative examples where the complementing statements of Section 4.2 are pertinent, respectively. Section 4.6 presents a natural generalization of opinion models where the dynamics are modified by local interactions between subgroupings of the interacting agents. We expect that the development herein, i.e., both the theory as well as the new class of exponential models that we present in Sections 4.3 and 4.6 to provide impetus for further advances. In particular, a research direction of practical significance is to quantify the effect of uncertainty and disturbances in such models. In general, it is of interest to quantify the effect of bias/disturbance in the dynamic response (e.g., shift in the position and nature of equilibria).

Chapter 5

Macroscopic Network Circulation for Planar Graphs

5.1 Introduction

Time asymmetry of traffic flow in city streets is unmistakable, as it flows in one direction around city squares and one-way in many city streets as well. Yet, from a macroscopic vantage point, circulation may or may not be evident. Flux from one part of town to another may average out with flux in the opposite direction. When this is not the case, it is of interest to identify the nature and to quantify any large scale imbalance in global circulation. Likewise, in another example that motivated this work, it is of interest to detect circulatory action potentials in the heart electrical conduction system. Such large scale imbalance patterns, peered via a collection of sensors, underly self-sustaining cardiac rhythm abnormalities1. Thus, herein, we seek to define and identify macroscopic circulation in a network/graph that captures flow asymmetry at large scale.

The mathematical setting used to contemplate model flows on graphs is that of a stationary discrete-time Markov model, where the probability flux represents a vector field on the network of the nodes and edges of a Markov chain. In this setting, the famous Cheeger inequality relates the likelihood of transitioning between two parts in a 2-partition of the nodes, across, in either direction, as well as the rate of mixing, to spectral properties of the graph Laplacian. As a 2-partition aims to capture bottlenecks that impede mixing, the Cheeger constant duly takes into account the relatively size of the boundary between the two parts. In a similar manner, contemplating the elements of circulatory imbalance, we are led naturally to a 3-partition of the network. After all, in a 2-partition, the probability current across the boundary, at stationarity, balances out. Tell-tale signs of circulatory asymmetry requires at least three parts. In general, flux-imbalance at the micro or macro level may manifest *only when more that two components interact and exchange "mass."* For a 3-state partitioning of a network into parts A, B, and C, the net flow from $\mathsf{A} \to \mathsf{B}$ (which is considered positive when the net flux is in the direction of B), by detailed-balance, must equal to the net flux from $\mathsf{B} \to \mathsf{C}$, and must also equal the net flux from $\mathsf{C} \to \mathsf{A}$. Thereby, the asymmetry manifests itself as a network circulation current. For reasons similar to those underlying the Cheeger constant, careful consideration of the size and regularity of the boundary between the three parts is warranted and may need to be duly restricted.

Graph theory has impacted many fields in mathematics, physics, network science, biology, medicine, and engineering [8, 63, 71]. Typically, applications relate to clustering, community detection, parallel computation, and so on. Yet the concept of circulation discussed at present does not appear to have been studied at any length. Thus, a main contribution of the present work is motivate and study circulation in graphs and the topology of corresponding partitions. Further, a computational framework is developed that applies to embedded planar graphs; for general graphs macroscopic circulation and the corresponding graph partitioning remain challenging combinatorial problems.

The structure of the chapter is as follows. In section 5.2, we discuss connection between probability currents and flow fields on graphs. In section 5.3, we highlight the concept of macroscopic circulation in the context of Markov chains. The setting of Markov chains is not restricted by the dimensionality of possible embedding of the respective graph, but the formulation of global circulation in general requires further refinement. In section 5.4, we discuss planar graph and the decomposition of flows accordingly. In section 5.5, we introduce an algorithm for calculating scalar potential supported on the dual graph and propose a method for partitioning the graph into three parts and calculating macroscopic circulation. The issue of embedding is revisited in section 5.6 where it is explained that a given graph may have non-equivalent embeddings, leading to different values for the macroscopic circulation. In sections 5.6.1 and 5.7, we detail additional illuminating examples. For convenience, the important notations used in this chapter are summarized in Table 5.1.

Table 5.1: Table of notations.

Symbols	Definitions
N	number of the nodes, $\mathsf{N} \geqslant 3$
$\mathcal{V} = \{v_1, \dots, v_\mathsf{N}\}$	node set
$\mathcal{E}$	edge set
$\mathcal{F}$	face set
$\mathcal{G} := (\mathcal{V}, \mathcal{E})$	directed graph
$\mathcal{G}^*$	dual of graph $\mathcal{G}$
$\mathcal{G}_\mathsf{F}$	directed graph with the adjacency matrix having the zero pattern of F
$\mathcal{G}_\mathsf{F}^{\mathrm{chordal}}$	triangulated graph $\mathcal{G}_\mathsf{F}$
π_{ij}	transition probability between every two nodes i, j
Π	transition probability matrix
π^T	the (unique left/row Frobenius-Perron) eigenvector of Π with eigenvalue 1
	$\pi = [\pi_i]_{i=1}^{\mathsf{N}}$ is the column stationary probability vector of the Markov chain
P	probability current matrix
F	net flux on $\mathcal{G}$
$\mathcal{W}$	vector filed
ϕ	scalar potential
$\boldsymbol{\psi}$	vector potential
$\partial_\mathcal{B}^\mathcal{A}$	boundary between sets $\mathcal{A}$ and $\mathcal{B}$ which is defined as $\{e = (v_a, v_b) \in \mathcal{E} \mid v_a \in \mathcal{A}, v_b \in \mathcal{B}\}$
$\oplus$, $\circ$	entry-wise Boolean addition and multiplication of characteristic vectors, respectively
$\mathbb{1}, \mathbf{0}$	(column) vectors with all 1's and all 0's, respectively
$S(n,k)$	Stirling number of the second kind: $S(n,k) = \frac{1}{k!}\sum_{i=0}^{k}(-1)^i\binom{n}{i}(k-i)^n$
	(number of ways to partition a set of n labeled objects into k nonempty unlabeled subsets)

5.2 Probability currents & flow fields on graphs

We explain flows on graphs in the context of Markov chains. These can be thought as a canonical model to represent flows on discrete spaces in the form of probability currents induced by the Markov structure.

Consider a time-homogeneous, discrete-time, N-state finite Markov chain X_t, with $t \in \mathbb{N}$, with states $\mathcal{V} = \{v_1, \ldots, v_N\}$, comprised of the nodes of a network, and transition probabilities π_{ij}, i.e.,

$$\mathbb{P}\{X_{t+1} = v_j \mid X_t = v_i\} = \pi_{ij}.$$

We assume that the Markov chain is ergodic and hence, irreducible and aperiodic. Thus, the matrix $\Pi := [\pi_{ij}]_{i,j=1}^N$ has non-negative entries and is such that $\Pi\mathbb{1} = \mathbb{1}$, where $\mathbb{1}$ denotes a column vector with all entries equal to 1. The ergodicity assumption implies that for a sufficiently large integer k (e.g., $k = N$), Π^k has all entries positive. The dimensionality of vectors and matrices will be explicit, unless their dimension is clear from the context. The Markov chain is associated to a graph $\mathcal{G} := (\mathcal{V}, \mathcal{E})$, where the (directed) edge set $\mathcal{E}$ is specified by the allowed transitions, i.e.,

$$\mathcal{E} = \{e = (v_i, v_j) \mid \pi_{ij} \neq 0\}.$$

Throughout, $\mathcal{G}$ is assumed to be strongly connected as it follows from the ergodicity assumption of the Markov chain.

Let now $\pi = [\pi_i]_{i=1}^N$, where $\mathbb{1}^T\pi = 1$, denote the stationary probability (column) vector of the Markov chain. Thus, π^T is the (unique left/row Frobenius-Perron) eigenvector of Π with eigenvalue 1, i.e.,

$$\pi^T\Pi = \pi^T.$$

Throughout, $(\cdot)^T$ denotes transposition and $\mathrm{diag}(\pi_1, \ldots, \pi_N) = \mathrm{diag}(\pi)$ denotes a diagonal matrix with the specified diagonal entries. Thence,

$$P := \mathrm{diag}(\pi_1, \ldots, \pi_N)\Pi \tag{5.1}$$

represent probability current $p_{ij} = \pi_i \pi_{ij}$ from vertex v_i to v_j. Probability currents quantify *flux* on $\mathcal{G}$.

Our aim in this chapter is to identify (large scale) imbalance in the *net flux* across $\mathcal{G}$, and to this end, we will be working mostly with the anti-symmetric part of P (modulo a factor of $1/2$)

$$F = P - P^T. \tag{5.2}$$

Any element of matrix F is the difference between the incoming and outgoing flow for each node of $\mathcal{G}$, defined as $F_{ij} = p_{ij} - p_{ji}$, where p_{ij} is defined in 5.1. This retains information on only local flux imbalance between any two nodes, and removes all the self-loops. Note that since, $\Pi\mathbb{1} = \mathbb{1}$, it follows that $P\mathbb{1} = P^T\mathbb{1}$, and therefore, that $F\mathbb{1} = \mathbf{0}$ (the zero vector) as well. Imbalance between the incoming and outgoing flow at a node indicates sink/source character which corresponds to non-vanishing divergence in the case of vector fields. Thus, we refer to a flow field F on $\mathcal{G}$ as *"divergence free"* if and only if the local net flux imbalance between any two nodes is zero, i.e., $F\mathbb{1} = \mathbf{0}$. When F is not *divergence free*, it can be replaced by its restriction on the complement of the range of $\mathbb{1}\mathbb{1}^T$, namely, $(I - \frac{1}{N}\mathbb{1}\mathbb{1}^T)F(I - \frac{1}{N}\mathbb{1}\mathbb{1}^T)$, so that $F\mathbb{1} = 0$; this relates to a projection onto the space of divergence free flows. For further discussion on such a decomposition see Section 5.4.2.

Once again, consider a "divergence free" *flow field* F on $\mathcal{G}$. Besides the fact that

$$F = -F^T \tag{5.3a}$$

$$F\mathbb{1} = \mathbf{0}, \tag{5.3b}$$

the positive part of F, namely, $F_+ := [\max\{F_{ij}, 0\}]_{i,j=1}^N$, has entries that are less than or equal those in P, and since $\mathbb{1}^T P \mathbb{1} = 1$,

$$\mathbb{1}^T F_+ \mathbb{1} \leqslant 1. \tag{5.3c}$$

It turns out that (5.3a-5.3c) characterize divergence-free flow fields on graphs. I.e., any antisymmetric matrix with the above properties originates from a Markovian probability structure. We state the precise result below.

Proposition 22. *Consider an* $N \times N$ *matrix* F *and assume that (5.3a-5.3c) hold. Then* F *originates as a divergence-free flow-field on a graph* $\mathcal{G} = (\mathcal{V}, \mathcal{E})$*, with* $|\mathcal{V}| = N$*, associated with a Markov probability structure.*

Proof. If (5.3c) holds with equality, let $P = F_+$, otherwise define

$$P := M + F_+, \tag{5.4}$$

for a symmetric matrix $M = M^T$, of the same size, with nonnegative entries such that

$$\mathbb{1}^T M \mathbb{1} = 1 - \mathbb{1}^T F_+ \mathbb{1},$$

ensuring that $\pi^T := \mathbb{1}^T P$ has all entries positive. This is clearly possible from the standing assumptions. Now, verify that

$$\Pi = \mathrm{diag}(\pi_{v_1}, \dots, \pi_{v_N})^{-1} P \tag{5.5}$$

is a transition probability matrix that leads to the divergence-free flow field F. Specifically, i) Π has non-negative entries. ii) In view of $\pi^T = \mathbb{1}^T P$ and (5.5), $\pi^T \Pi = \pi^T$ holds. iii) Note that $F = F_+ - F_+^T$ and hence, $F_+ \mathbb{1} = F_+^T \mathbb{1}$ from (5.3b). It follows that $P\mathbb{1} = P^T \mathbb{1}$, and from (5.5) the definition $\pi^T = \mathbb{1}^T P$, that $\Pi \mathbb{1} = \mathbb{1}$. iv) Lastly, $P - P^T = F_+ - F_+^T = F$. □

5.3 Macroscopic circulation on graphs

Consider an $N \times N$ antisymmetric matrix F of net fluxes that defines a divergence-free flow field on a (simple) graph $\mathcal{G}$. We seek a suitable definition of (maximal) *macroscopic circulation* by partitioning the states into three subsets A, B, and C, in such a way so as to maximize the flux between the parts. We discuss first the simplest case, of three states, and proceed to define the concept of circulation and flow-density in general.

Three-state example

We consider a three-state Markov chain ($N = 3$) in Fig. 5.1, where for convenience we label the three nodes as A, B, C, i.e., $\mathcal{V} = \{A, B, C\}$. The net flux matrix on $\mathcal{G}$ (anti-symmetric part of the probability current matrix P, modulo a factor of $1/2$) is

$$F = \begin{bmatrix} 0 & -\gamma & \gamma \\ \gamma & 0 & -\gamma \\ -\gamma & \gamma & 0 \end{bmatrix},$$

with the directionality encoded in the sign of γ. Obviously, the off-diagonal entries of F must have the same magnitude, since $F\mathbb{1} = 0$. Evidently, the value $|\gamma|$ quantifies circulation in this example. The weighted oriented graph of net fluxes is shown in Fig. 5.2. For the case of a three-state Markov chain, a close-form expression for γ can be obtained in terms of Π, though this is immaterial and not to be expected in general. □

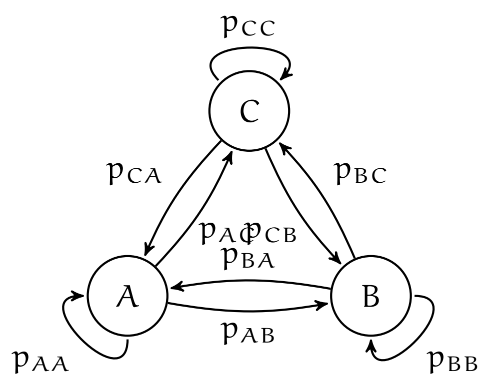

Figure 5.1: Probability currents in a 3-state Markov chain.

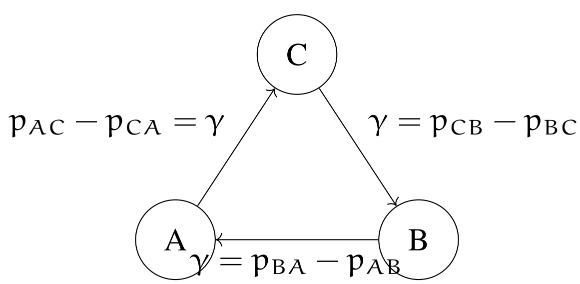

Figure 5.2: Weighted oriented graph of net fluxes.

General case

We now consider the general case with N states, as before, and data for net flux between nodes in F. We seek partitioning the graph into three subsets of nodes

$$\mathcal{A}, \mathcal{B}, \mathcal{C} \subset \mathcal{V}$$

that are pairwise non-intersecting with

$$\mathcal{V} = \mathcal{A} \cup \mathcal{B} \cup \mathcal{C}.$$

Such a triple of subsets of $\mathcal{V}$ will be referred to as a 3-partition.

Define the characteristic (column) vector $I_\mathcal{S}$ of a set $\mathcal{S} \subseteq \mathcal{V}$, with $\mathcal{V}$ ordered, as follows: the ν^{th} entry of $I_\mathcal{S}$ is equal to 1 when $\nu \in \mathcal{S}$ and 0 otherwise. It is convenient to define entry-wise Boolean addition and multiplication of characteristic vectors, $\oplus$ and $\circ$, respectively, and also the notation $\mathbb{1}, \mathbf{0}$ to denote the (column) vectors with all 1's and all 0's, respectively.

Lemma 23. $(\mathcal{A}, \mathcal{B}, \mathcal{C})$ *is a 3-partition of* $\mathcal{V}$ *if and only if*

$$I_\mathcal{A} \oplus I_\mathcal{B} \oplus I_\mathcal{C} = \mathbb{1}, \tag{5.6a}$$

$$I_\mathcal{A} \circ I_\mathcal{B} = I_\mathcal{B} \circ I_\mathcal{C} = I_\mathcal{C} \circ I_\mathcal{A} = \mathbf{0}, \tag{5.6b}$$

Proof. Relation (5.6a) is equivalent to $\mathcal{V} = \mathcal{A} \cup \mathcal{B} \cup \mathcal{C}$. Then, (5.6b) is equivalent to the pair-wise non-intersection condition. □

Given a flow field (net-probability flux) matrix F, as before, and a 3-partition $(\mathcal{A}, \mathcal{B}, \mathcal{C})$ of the (ordered) vertex set $\mathcal{V}$, then $I_\mathcal{A}^T F I_\mathcal{B}$ is the (signed) flux directed from $\mathcal{A}$ to $\mathcal{B}$. That is, if $I_\mathcal{A}^T F I_\mathcal{B} < 0$, the net flux, summed over all edges connecting directly $\mathcal{A}$ and $\mathcal{B}$, is directed from $\mathcal{B}$ into $\mathcal{A}$. Thus,

$$\mathsf{I}_{\mathcal{A}}^{\mathsf{T}}\mathsf{F}\mathsf{I}_{\mathcal{B}} = -\mathsf{I}_{\mathcal{B}}^{\mathsf{T}}\mathsf{F}\mathsf{I}_{\mathcal{A}},$$

while the absolute value $|\mathsf{I}_{\mathcal{A}}^{\mathsf{T}}\mathsf{F}\mathsf{I}_{\mathcal{B}}|$ is the total net flux between the two parts.

Lemma 24. *For any 3-partition* $(\mathcal{A}, \mathcal{B}, \mathcal{C})$ *of the (ordered) vertex set* $\mathcal{V}$*,*

$$\mathsf{I}_{\mathcal{A}}^{\mathsf{T}}\mathsf{F}\mathsf{I}_{\mathcal{B}} = \mathsf{I}_{\mathcal{B}}^{\mathsf{T}}\mathsf{F}\mathsf{I}_{\mathcal{C}} = \mathsf{I}_{\mathcal{C}}^{\mathsf{T}}\mathsf{F}\mathsf{I}_{\mathcal{A}}.$$

Proof. Note that $\mathsf{I}_{\mathcal{A}}^{\mathsf{T}}\mathsf{F}\mathsf{I}_{\mathcal{A}} = 0$, since F is antisymmetric, and that $\mathsf{I}_{\mathcal{A}} \oplus \mathsf{I}_{\mathcal{B}\cup\mathcal{C}} = \mathsf{I}_{\mathcal{A}\cup\mathcal{B}\cup\mathcal{C}} = \mathbb{1}$. Then,

$$\begin{aligned}
\mathsf{I}_{\mathcal{A}}^{\mathsf{T}}\mathsf{F}\mathsf{I}_{\mathcal{B}} + \mathsf{I}_{\mathcal{A}}^{\mathsf{T}}\mathsf{F}\mathsf{I}_{\mathcal{C}} &= \mathsf{I}_{\mathcal{A}}^{\mathsf{T}}\mathsf{F}\mathsf{I}_{\mathcal{B}\cup\mathcal{C}} \\
&= \mathsf{I}_{\mathcal{A}}^{\mathsf{T}}\mathsf{F}\mathsf{I}_{\mathcal{B}\cup\mathcal{C}} + \mathsf{I}_{\mathcal{A}}^{\mathsf{T}}\mathsf{F}\mathsf{I}_{\mathcal{A}} \\
&= \mathsf{I}_{\mathcal{A}}^{\mathsf{T}}\mathsf{F}\mathbb{1} = 0.
\end{aligned}$$

Thus,

$$\begin{aligned}
\mathsf{I}_{\mathcal{A}}^{\mathsf{T}}\mathsf{F}\mathsf{I}_{\mathcal{B}} &= -\mathsf{I}_{\mathcal{A}}^{\mathsf{T}}\mathsf{F}\mathsf{I}_{\mathcal{C}} \\
&= \mathsf{I}_{\mathcal{C}}^{\mathsf{T}}\mathsf{F}\mathsf{I}_{\mathcal{A}}.
\end{aligned}$$

And, similarly, $\mathsf{I}_{\mathcal{B}}^{\mathsf{T}}\mathsf{F}\mathsf{I}_{\mathcal{A}} = \mathsf{I}_{\mathcal{C}}^{\mathsf{T}}\mathsf{F}\mathsf{I}_{\mathcal{B}}$. □

In view of the above, it is natural to define the circulation

$$\mathsf{c}(\mathcal{A}, \mathcal{B}, \mathcal{C}) := |\mathsf{I}_{\mathcal{A}}^{\mathsf{T}}\mathsf{F}\mathsf{I}_{\mathcal{B}}|$$

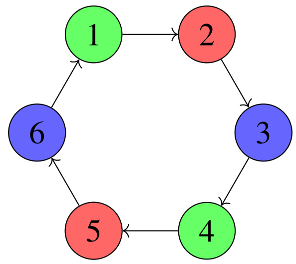

Figure 5.3: 3-partition into non-contiguous pairs.

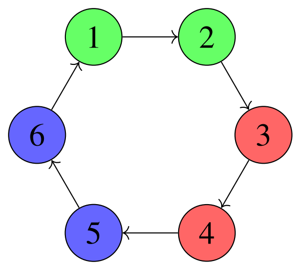

Figure 5.4: 3-partition into contiguous pairs

associated to any given 3-partition and, accordingly, the maximal macroscopic circulation

$$\mathsf{c}_{\max} := \max_{\text{3-partitions}} \mathsf{c}(\mathcal{A}, \mathcal{B}, \mathcal{C}).$$

Evidently, $\mathsf{c}(\mathcal{A}, \mathcal{B}, \mathcal{C})$ depends on the partition as well as the "divergence-free" flow field on the graph $\mathcal{G} = (\mathcal{V}, \mathcal{E})$ that is specified by the skew symmetric matrix F. Herein, we prefer to let F be specified from the context, instead of using a more cumbersome notation such as $\mathsf{c}_{\mathsf{F}}(\mathcal{A}, \mathcal{B}, \mathcal{C})$.

A moment's reflection reveals that these concepts do not take into account the topology of the partition. More specifically, the nature and size of the boundary between the parts of the partition may be relevant to the type of global feature we may want to capture. We highlight this point with the following example, and then return to define normalized notions of macroscopic circulation.

Six-state example

Consider hexagonal planar graph in Fig.'s 5.3 and 5.4. The two figures display color-coded 3-partitions, where in the first, pairs that constitute each of the three parts are not contiguous, whereas in the second, pairs of nodes in each of the three parts are neighboring and connected. The net flux matrix F is

$$\mathsf{F} = \begin{bmatrix} 0 & 1 & 0 & 0 & 0 & -1 \\ -1 & 0 & 1 & 0 & 0 & 0 \\ 0 & -1 & 0 & 1 & 0 & 0 \\ 0 & 0 & -1 & 0 & 1 & 0 \\ 0 & 0 & 0 & -1 & 0 & 1 \\ 1 & 0 & 0 & 0 & -1 & 0 \end{bmatrix} \tag{5.7}$$

Let $\mathcal{A}$ denote the green set of nodes and $\mathcal{B}$ the red. In the first of these two 3-partitions, $\mathrm{I}_{\mathcal{A}}^{\mathsf{T}}\mathsf{F}\mathrm{I}_{\mathcal{B}} = 2$, whereas in the second $\mathrm{I}_{\mathcal{A}}^{\mathsf{T}}\mathsf{F}\mathrm{I}_{\mathcal{B}} = 1$. The difference between the two is that the "circulatory flux" in the first 3-partition is counted *twice* due to the fact that the boundary between the parts $\mathcal{A}$ and $\mathcal{B}$, denoted by $\partial_{\mathcal{B}}^{\mathcal{A}}$ has size 2, as it consists of two edges, and is traversed "twice" by any complete transport around a cycle. In the second choice for a 3-partition, $\partial_{\mathcal{B}}^{\mathcal{A}} = 1$. □

The above examples suggest normalizing the flux between any two parts of a partition, by dividing by the size of the corresponding boundaries. That is, normalizing $\mathrm{I}_{\mathcal{A}}^{\mathsf{T}}\mathsf{F}\mathrm{I}_{\mathcal{B}}$ by dividing with the size of the boundary, namely, $|\partial_{\mathcal{B}}^{\mathcal{A}}|$ which denotes the cardinality of the set

$$\partial_{\mathcal{B}}^{\mathcal{A}} := \{(\nu_i, \nu_j) \mid \nu_i \in \mathcal{A},\ \nu_j \in \mathcal{B},\ \text{and } (\nu_i, \nu_j) \in \mathcal{E}\}$$

of edges between the two parts $\mathcal{A}$, $\mathcal{B}$, brings us to a notion of *density flux* associated with the boundary separating two parts of any partition,

$$\mathsf{f}(\partial^{\mathcal{A}}_{\mathcal{B}}) := \frac{|\mathrm{I}^{\mathsf{T}}_{\mathcal{A}}\mathsf{F}\mathrm{I}_{\mathcal{B}}|}{|\partial^{\mathcal{A}}_{\mathcal{B}}|}.$$

Accordingly, the minimal density flux of the partition, is

$$\mathsf{f}_{\min}(\mathcal{A}, \mathcal{B}, \mathcal{C}) := \min\{\mathsf{f}(\partial^{\mathcal{A}}_{\mathcal{B}}), \mathsf{f}(\partial^{\mathcal{B}}_{\mathcal{C}}), \mathsf{f}(\partial^{\mathcal{C}}_{\mathcal{A}})\}, \tag{5.8}$$

and similarly for the maximal. This approach leads us to a combinatorial problem. In fact, for a graph with n vertices, the total number of possible cases to consider for solving (5.8) is equal to Stirling number of the second kind, $S(n, 3)$ [73]. Thus, below, we focus on planar graphs and explain how to compute suitable notions of macroscopic circulation via a scalar potential supported on the dual graph.

5.4 Planar graphs and network circulation

We assume that geographic proximity of nodes is dictated by an actual embedding of a graph into a linear metric space, specifically $\mathbb{R}^2$. Graphs that can be embedded in $\mathbb{R}^2$, without intersection of edges, are called *planar*. In this case flow fields have a strong resemblance to planar vector fields.

For planar vector fields there is a well known decomposition into gradient flow and curl that captures circulation. In fact, circulation can be conveniently quantified by a scalar potential. In a similar manner, for planar graphs, circulation relates to a scalar potential on the vertex set of a dual graph as we will explain shortly.[1] We proceed to review some facts on planar graphs, as well

[1]The dual graph $\mathcal{G}^*$ of a planar graph $\mathcal{G}$ is a planar graph that each of its vertices corresponds to a face of $\mathcal{G}$ and each of whose faces corresponds to a graph vertex of $\mathcal{G}$. Two nodes in $\mathcal{G}^*$ are connected by an edge if the corresponding faces in $\mathcal{G}$ have an edge as a boundary.

as elements of the Helmholtz-Hodge decomposition of vector fields that provides insight into the corresponding decomposition of flow fields on graphs.

5.4.1 Planar graphs

A graph is referred to as *planar* when it can be drawn on the plane in a way that no edges cross each other and intersect only at their endpoints (vertices). The study of planar graphs goes back to Euler who showed that, for simple and connected planar graphs on the simply connected space $\mathbb{R}^2$, i.e., with zero genus g, the Euler characteristic[2] $\chi(g) = 2$ in (5.9)

$$\begin{aligned} |\mathcal{V}| - |\mathcal{E}| + |\mathcal{F}| &= \chi(g) \\ \chi(g) &= 2 - 2g \end{aligned} \tag{5.9}$$

where $\mathcal{F}$ is the face[3] set. Euler formula is not sufficient to ensure planarity. A condition that fully characterizes planarity was given in 1930's by Kuratowski and Wagner in the form of absence of two specific subgraphs, K_5 or $K_{3,3}$ [56, 76, 79, 84].

The next important consideration is how to embed a planar graph in $\mathbb{R}^2$. For this we refer to [67]. It turns out that there may exist several "nonequivalent embeddings" [38, 86]. As we explain below, network circulation depends on the particular embedding.

Every planar graph can be drawn on a sphere (and vice versa) via stereographic projection. This amounts to identifying points on $\mathbb{R}^2$ with points on the (Riemann) sphere by corresponding the "north pole" with the "point at ∞" and any other pair in line with the north pole (the line containing a point on the sphere and the corresponding projection on $\mathbb{R}^2$) (see Fig. 5.5).

[2]Euler characteristic is a topological invariant, a number that describes a topological space's shape or structure regardless of the way it is bent.

[3]The exterior of the graph needs to be counted as a face, and it is referred to as the outside face.

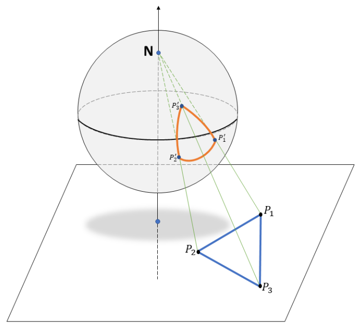

Figure 5.5: Stereographic Projection.

For any planar graph $\mathcal{G}$, and any face f of $\mathcal{G}$, the graph can be redrawn on the plane in such a way that f is the "outside face" of $\mathcal{G}$. This can be effected by rotating the projection of the graph onto the Riemann sphere so that the image of the face contains the north pole. But, besides sliding and rotating the graph projection on the Riemann sphere, other transformations are possible that may change the local ordering of vertices, leading to non-equivalent embeddings of the graph on $\mathbb{R}^2$.

More precisely, for our purposes, two graph embeddings are said to be *equivalent* if their corresponding projections onto the sphere can be continuously rotated (and the corresponding vertices shifted onto the sphere without crossing edges) so as to match. The equivalence of two graphs is exemplified in Fig. 5.6. For the reasons we just explained, that the positioning of the north pole leads to equivalent embeddings, there are $|\mathcal{F}|$ isomorphic embeddings for every planar graph, as stated next.

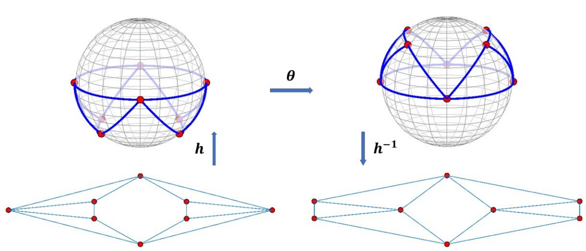

Figure 5.6: Isomorphic graphs and sequence of graph morphisms; θ and h are rotation and projection maps, respectively.

Lemma 25. *There are $|\mathcal{F}|$ isomorphic embeddings for every planar graph.*

Proof. Figure 5.6 exemplifies the equivalence between two planar embeddings, as discussed leading into the lemma. More specifically, consider a graph $\mathcal{G}$ with a given embedding $h : \mathbb{R}^2 \to S^2$ that maps $\mathcal{G}$ to $\mathcal{G}_s$ on sphere S^2. A homeomorphism $\theta : S^2 \to S^2$ rotates the position of nodes and edges of $\mathcal{G}_s$ on the outside of S^2, placing the "north pole" within any of the $|\mathcal{F}|$ possible faces. Then, $h^{-1} \circ \theta \circ h$ produces an equivalent graph embedding. $\square$

5.4.2 Helmholtz-Hodge decomposition

We now turn to a brief overview of concepts of vector fields. The Helmholtz-Hodge decomposition simplifies the analysis by bringing up important properties such as incompressibility and vorticity that can thereby be studied directly [49, 50].

According to the *Helmholtz-Hodge decomposition Theorem*, the space of a vector field can be uniquely decomposed into mutually L^2-orthogonal sub-spaces using potential functions [11]. These components can be calculated as the gradient of a scalar potential ϕ and curl of a vector potential $\boldsymbol{\psi}$, namely,

$$\mathcal{W} = \nabla\phi + \nabla \times \boldsymbol{\psi} + \mathfrak{h},$$

where $\nabla\phi$ is the curl-free component (i.e., $\nabla \times \nabla\phi = 0$) of the vector field $\mathcal{W}$, and $\nabla \times \boldsymbol{\psi}$ is its divergence-free component (i.e., $\nabla \cdot \nabla \times \boldsymbol{\psi} = 0$), whereas the harmonic component $\mathfrak{h}$ is both divergence-free and curl-free.

The curl-free component: Since the divergence of a curl is zero, we can compute ϕ, the scalar potential associated with the curl-free component of the vector field $\mathcal{W}$, as the solution of the following Poisson equation.

$$\nabla \cdot \mathcal{W} = \nabla \cdot \nabla \phi = \nabla^2 \phi$$

where the last equality holds because the divergence of a gradient is the Laplacian.

The divergence-free component: Since the vorticity (normal component of the surface curl) of a gradient field vanishes, the following identity holds: $\hat{n} \,.\, (\nabla \times \mathcal{W}) = \hat{n} \,.\, (\nabla \times \psi)$. Using the fact that vorticity of the surface curl of a scalar potential is just the surface Laplacian of the potential, we have

$$\hat{n} \,.\, (\nabla \times \mathcal{W}) = \Delta \psi \tag{5.10}$$

where $\hat{n}$ is the normal vector. Equation (5.10) is obeyed if the scalar field ψ is a solution of the above Poisson equation.

In the case of vector fields on $\mathbb{R}^2$, the curl can be expressed as $\Psi = J \nabla \psi$, where J is an antisymmetric matrix and ψ a scalar potential. It follows (Stokes' theorem) that the flux crossing any curve connecting two points a and b on $\mathbb{R}^2$ is given by the difference of the endpoint potentials. As a consequence we have the following.

Proposition 26. *The flux across the path connecting the extrema of a curl potential field is maximum.*

Proof. With J the operator that rotates a vector on $\mathbb{R}^2$ counter-clockwise by $\pi/2$, the flux across any path linking a and b is

$$I = \int_a^b J \nabla \psi \,.\, J ds = \int_a^b \nabla \psi \,.\, ds = \psi(b) - \psi(a). \tag{5.11}$$

Hence,

$$\max(I) = \max_{a,b\in\mathbb{R}^2}(\psi(b) - \psi(a)). \tag{5.12}$$

□

The analogue of Theorem 26 over discrete vector fields on graphs is discussed next.

5.4.3 Planar Net Flux Graph

Starting with an antisymmetric net flux matrix $F = [F_{ij}]_{i,j}$ in (5.2) of a Markov chain on a planar graph, we consider the graph with adjacency matrix having the zero pattern of F; the space of vertices and edges are the collection of the nodes and edges, respectively, that have corresponding non-zero elements in F, $\mathcal{V}_F = \{v_i \in \mathcal{V} | F_{ij} \neq 0 \text{ for some } v_j \in \mathcal{V}\}$, $\mathcal{E}_F = \{e_{ij} \in \mathcal{E} \mid F_{ij} \neq 0\}$. In addition we specify a sign function $\sigma : \mathcal{V}_F \times \mathcal{V}_F \to \{-1, 1\}$ that assigns an orientation, specifically $\sigma(i,j) = \mathrm{sign}(F_{ij})$ for all non-zero elements of the net flux matrix, and define the directed graph $\mathcal{G}_F(\mathcal{V}_F, \mathcal{E}_F, \sigma)$. The vector of edge flow weights

$$\mathcal{W} = (w_{ij})_{i,j}$$

corresponding to edges $e_{ij} \in \mathcal{E}_F$ with values $w_{ij} = |F_{ij}|$ represents the flow field. The space of all flow fields is denoted by $\mathcal{U}_F$ and assumes a Helmholtz-Hodge decomposition,

$$\mathcal{U}_F = \mathcal{U}_F^{\text{curl}} \oplus \mathcal{U}_F^{\text{harmonic}} \oplus \mathcal{U}_F^{\text{gradient}},$$

where $\mathcal{U}_F^{\text{gradient}}$ and $\mathcal{U}_F^{\text{curl}}$ are curl-free and divergent-free components and $\oplus$ denotes the direct sum of vector spaces. If $\mathcal{W}_{\text{curl}}, \mathcal{W}_{\text{harmonic}}, \mathcal{W}_{\text{gradient}}$ denote projections of $\mathcal{W}$ in the respective components, then clearly $\mathcal{W}_{\text{gradient}} = \mathbf{0}$, since by assumption F has no "sources."

We wish to capture circulation in a similar manner as in planar flow fields and thereby we seek a curl potential ψ. The harmonic component $\mathcal{W}_{\text{harmonic}}$ relates to circulation about "holes" (non-triangular faces [59]) in the graph. Thus, before we proceed, we triangulate $\mathcal{G}_{\mathsf{F}}$, and generate a new graph $\mathcal{G}_{\mathsf{F}}^{\text{chordal}}$ so as to remove holes and ensure that the harmonic component is zero.

5.4.4 Triangular Planar Graph

The curl component of the flow field is defined on triangles, i.e., cycles of length 3 [59]. The cycle graphs of more than 3 vertices are considered as holes and their edge flow as harmonic components of the flow field.

To remove the harmonics, we replace the holes that are not bounded by triangles with chordal subgraphs. That is, we add minimum number of chords, which are the edges with zero flux that are not part of the cycle but each connects two vertices of the cycle. This way, we generate a planar chordal graph such that every chordless cycle subgraph is a triangle. Fig. 5.10 shows a triangulated graph with two different embeddings (original graphs are shown in Fig. 5.9). It can be seen that graph triangulation strongly depends on the embedding.

The corresponding potential function ψ is now defined on the graph's faces, and hence, can be assigned to the nodes of the dual graph, $(\mathcal{G}_{\mathsf{F}}^{\text{chordal}})^*$. The maximum flux, in complete analogy with (5.12), is then obtained by identifying those vertices of the dual graph with minimum and maximum curl potentials.

5.4.5 Non-planar Graphs

Graphs that cannot be drawn on a plane or sphere without edge crossings, i.e., non-planar, can always be drawn on a surface of higher genus [87]. A surface is said to be of genus $\mathsf{g} \in \{0, 1, 2 \ldots\}$ if it is topologically homeomorphic to a sphere with g handles [46]. For instance, the genus of a sphere is 0, and that of a torus is 1. Accordingly, a graph is said to have genus g if it can be drawn without crossings on a surface of genus g, but not on one of genus $\mathsf{g} - 1$. It can be easily seen that K_5 and $K_{3,3}$ are graphs of genus 1 (toroidal graphs); Fig. 5.7 exemplifies $K_{3,3}$ drawn on the torus T^2. The graph is drawn by assigning points and continuous, non-intersecting (except at end-points) paths corresponding to the vertices and edges of the graph, respectively. The dual of a non-planar graph can also be drawn on the torus in a similar fashion to a planar graph.

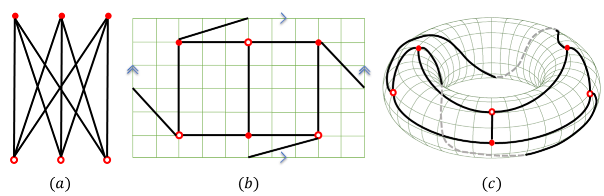

Figure 5.7: A toroidal graph ($K_{3,3}$): (a) Embedding on $\mathbb{R}^2$; (b) The projective plane; (c) Embedding on a torus.

The decomposition of a continuous vector field on the torus (as a manifold) is more complicated than on a sphere. In this case, the divergence-free component $\mathcal{U}_{\mathsf{F}}^{\mathrm{curl}}$, can be partitioned into a toroidal and a poloidal part [10, 74] –a restricted form of the usual Helmholtz decomposition. We contend that an analogous decomposition of a flow field of genus 1 graph can be similarly obtained; the corresponding poloidal component is once again generated by a scalar potential (as in the case of planar graphs) whereas the poloidal component is harmonic and represents flux/circulation around holes (of the torus). A detailed analysis on how to compute maximal graph circulation for graphs of genus 1 is not available at present.

5.5 Graph Partitioning

We summarize the insights gained and highlight the steps needed in Algorithm 1 which helps obtain a 3-partition corresponding to maximal circulation by providing the curl potential ψ on the vertices of its dual graph (i.e., faces of the original graph) and how to numerically calculate these. The outcome depends on the embedding of $\mathcal{G}_F$ (cf. Section 5.6).

Algorithm 1: Finding curl potential extrema

Input:
An embedded strongly connected, aperiodic, planar, directed graph $\mathcal{G}$ with a transition matrix Π.

Offline Preprocessing:
1. Calculate the net flux matrix F from (5.2).
2. Construct and triangulate $\mathcal{G}_F$ as described in Section 5.4.3, to generate $\mathcal{G}_F^{\mathrm{chordal}}$.
3. Find dual graph $(\mathcal{G}_F^{\mathrm{chordal}})^*$.
4. Set the potential ψ for the outside face to zero.

Computations:
Find ψ for vertices of the dual graph using (5.11), i.e., obtain ψ so that the difference between values at the nodes of the dual graph (corresponding to faces of the primal) equals the flux of the corresponding edge of the primal graph, $\psi(\mathrm{face}_{\mathrm{left}}) - \psi(\mathrm{face}_{\mathrm{right}}) = F_{ij}$ assuming a consistent orientation.

Output:
Two faces of the primal with potential extrema.

Knowing ψ allows carving 3-partitions that entail maximal circulation. Indeed, any set of two paths on the dual graph between the points of ψ-extrema separates the graph in the three regions, A, B and C, discussed earlier. This is summarized next.

Theorem 27. *Consider a divergence-free flow field W on the edges of a strongly connected directed graph. Algorithm 1 generates the chordal directed graph $\mathcal{G}_F^{\mathrm{chordal}}$ and its dual with an associated curl potential ψ. There exist paths in the dual graph connecting two chosen extrema points of ψ that provide a 3-partition with maximal macroscopic circulation.*

Proof. Completion of the graph into a chordal graph is the first step of the algorithm and was explained before. We compute ψ as follows. We assign 0 at the vertex of the dual of the chordal graph corresponding to the outside face, and proceed to assign values to the remaining vertices of the dual graph so that the difference between values of adjacent vertices equals the (signed, e.g., in the counter-clockwise sense) flux on the corresponding edge of the primal graph. We now explain the last part of the theorem.

Since $\mathcal{G}_{\mathsf{F}}^{\text{chordal}}$ is triangular, its dual is 3-edge-connected [44]. By Menger theorem [26, 64], for 3-edge-connected graphs every pair of vertices has 3 edge-disjoint paths in between. Now consider a pair of vertices on the dual graph, v_{min}^{*} and v_{max}^{*}, corresponding to the minimum and maximum of ψ, respectively. There are 3 edge-disjoint paths P_1, P_2, and P_3, connecting v_{min}^{*} and v_{max}^{*}. These paths can generate three cycles as follows.

$$C_{ij} = P_i \cup P_j, \ (1 \leqslant i < j \leqslant 3)$$

where $C_{ij} \in \mathcal{C}$, and $\mathcal{C}$ is a family of cycles in $(\mathcal{G}_{\mathsf{F}}^{\text{chordal}})^{*}$.

If paths P_1, P_2, and P_3 are also internally disjoint, then they will generate three cycles C_{12}, C_{23}, and C_{13}. If C_{12} and C_{23} are contractible, by 3-path condition [22, 66, 80], C_{13} is also contractible. We only need to show that if P_2 lies between P_1 and P_3, then C_{13} is surface separating and[4] $\mathtt{int}(C_{13}) = \mathtt{int}(C_{23}) \cup \mathtt{int}(C_{12}) \cup P_2$. It follows from Euler's formula that the genus of $\mathtt{int}(C_{13}) \cup C_{13}$ is zero, and thus C_{13} is contractible.

Since C_{ij}'s are also *discrete Jordan curves* and equivalent to the bonds of $\mathcal{G}_{\mathsf{F}}^{\text{chordal}}$ [16, 58, 87], by properly selecting interior or exterior of those cycles, these delineate three disjoint and connected sets of primal vertices. Then, by (5.12), the flow that crosses their shared boundaries (i.e., P_1, P_2, and P_3) is maximal.

[4] $\mathtt{int}(\cdot)$ and $\mathtt{ext}(\cdot)$ denote interior and exterior, respectively.

If P_1, P_2, P_3 are edge-disjoint paths between v^*_{min} and v^*_{max}, but not internally disjoint, there exists cycles C_{ij}'s that are self-intersecting. That is, the $\mathrm{int}(C_{ij})$ is not path-connected and, hence, not contractible. $\square$

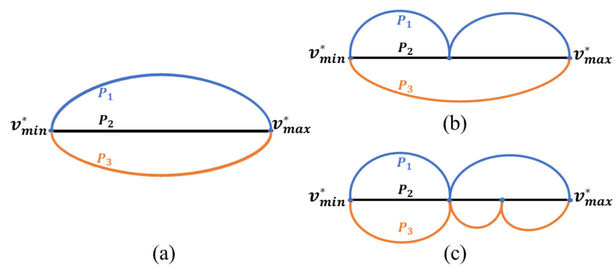

Figure 5.8: Cases of 3 edge-disjoint paths between v^*_{min} and v^*_{max}: P_1, P_2, P_3 are (a) internally disjoint, (b,c) not internally disjoint.

Fig. 5.8 exemplifies cases discussed in the above proof. In case (a) the three cycles $C_{12} = P_1 \cup P_2, C_{23} = P_2 \cup P_3$, and $C_{13} = P_1 \cup P_3$ are contractible. Therefore, all 3-partitions, $\mathrm{int}(C_{12}), \mathrm{int}(C_{23}), \mathrm{ext}(C_{13})$ are connected. The cases (b,c) correspond to cycles that are self-intersecting. Specifically, in Fig. 5.8(b) only C_{12} is self-intersecting, whereas in Fig. 5.8(c) all three cycles are self-intersecting. Accordingly, the corresponding 3-partitions may not be connected.

Corollary 28. *If there exist 3 edge-disjoint paths that are vertex-disjoint, then each 3-partition is connected.*

Fig. 5.11 exemplifies Theorem 27 for a planar graph with two non-equivalent embeddings, where P_1, P_2, P_3 are marked with different colors and the 3-partitions are marked using different colors (red, blue, green) and shapes (□, ○, △). In the next section we explain how the output of algorithm 1, and consequently the partitioning, depends on the embedding.

Table 5.2: Two embeddings of a graph with non-isomorphic corresponding duals.

$\mathcal{G}_1^*$ $\mathcal{G}_2^*$

5.6 Effect of Embedding on Partitioning

Whitney showed that 3-connected graphs have unique embedding, and consequently unique dual graph [86]. But in general it is possible that if we consider two different embeddings $\mathcal{G}_1, \mathcal{G}_2$ of a planar graph $\mathcal{G}$, the duals $\mathcal{G}_1^*, \mathcal{G}_2^*$ become non-isomorphic, Table 5.2. And this may result into a different output of algorithm 1.

5.6.1 Example

Given transition matrix for a planar graph as in (5.13), net flux matrix is calculated using equation (5.2). Fig. 5.9 indicates two possible graphs which are constructed based on calculated net flux matrix in (5.14). These two embeddings of a connected planar graph are related by flipping at separating pair[5]. As described in 5.4.3, graphs are triangulated, $\mathcal{G}_1', \mathcal{G}_2'$ in Fig. 5.11.

$$\Pi = \begin{bmatrix} 0 & 0.25 & 0 & 0 & 0.25 & 0 & 0.25 & 0.25 \\ 0.333 & 0 & 0.333 & 0.333 & 0 & 0 & 0 & 0 \\ 0 & 0.25 & 0 & 0.25 & 0 & 0.25 & 0 & 0.25 \\ 0 & 0.333 & 0.333 & 0 & 0.333 & 0 & 0 & 0 \\ 0.333 & 0.333 & 0 & 0.333 & 0 & 0 & 0 & 0 \\ 0 & 0 & 0.333 & 0 & 0 & 0 & 0.333 & 0.333 \\ 0.5 & 0 & 0 & 0 & 0 & 0.5 & 0 & 0 \\ 0.25 & 0 & 0.25 & 0 & 0 & 0.25 & 0.25 & 0 \end{bmatrix} \tag{5.13}$$

[5]In graph theory, a vertex separator for nonadjacent vertices a and b is a vertex subset $S \subset V$ such that the removal of S from the graph separates a and b into distinct connected components.

Figure 5.9: Two possible embeddings, constructed based on net flux matrix in (5.14).

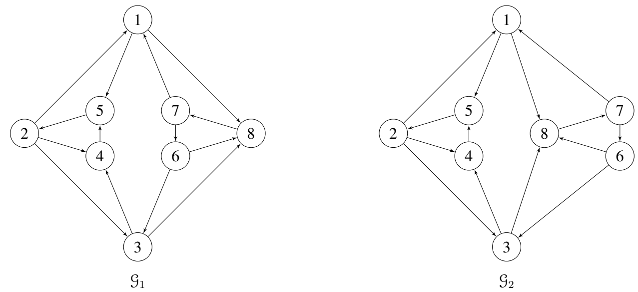

Figure 5.10: Triangulated of the graphs in Fig. 5.9.

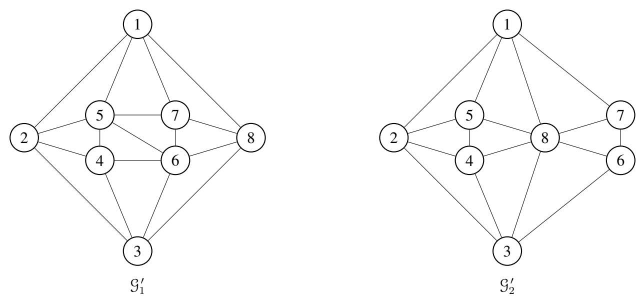

$$\mathsf{F} = \begin{bmatrix} 0 & -0.0076 & 0 & 0 & 0.014 & 0 & -0.016 & 0.0096 \\ 0.0076 & 0 & 0.0082 & 0.0099 & -0.0256 & 0 & 0 & 0 \\ 0 & -0.0082 & 0 & 0.0017 & 0 & -0.0025 & 0 & 0.009 \\ 0 & -0.0099 & -0.0017 & 0 & 0.0116 & 0 & 0 & 0 \\ -0.014 & 0.0256 & 0 & -0.0116 & 0 & 0 & 0 & 0 \\ 0 & 0 & 0.0025 & 0 & 0 & 0 & -0.014 & 0.0115 \\ 0.016 & 0 & 0 & 0 & 0 & 0.014 & 0 & -0.03 \\ -0.0096 & 0 & -0.009 & 0 & 0 & -0.0115 & 0.03 & 0 \end{bmatrix} \tag{5.14}$$

Figure 5.11: Triangulated and dual of the graphs in Fig. 5.9 and their 3-partitions.

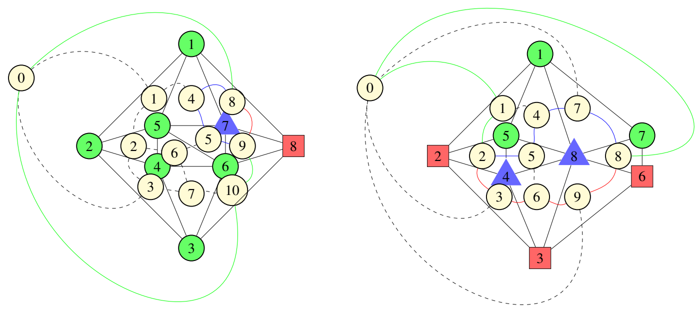

Based on Algorithm 1, a vector of curl potentials for each triangulated graph is calculated,

$$\begin{aligned}
&\psi_1=[0, -0.0076, 0.0181, 0.0082, 0.0064, 0.0064, 0.0064, 0.0064, -0.0096, 0.0205, 0.009]^{\mathsf{T}}, \\
&\psi_2=[0, -0.0076, 0.0181, 0.0082, 0.0064, 0.0064, 0.0064, 0.016, -0.014, -0.0025]^{\mathsf{T}}.
\end{aligned} \tag{5.15}$$

where ψ_{i_j} corresponds to the curl potential of the j^{th} face of graph $\mathcal{G}_i'$, $i \in \{1, 2\}$. The faces with maximum and minimum potential for $\mathcal{G}_1'$ and $\mathcal{G}_2'$ are $\{f_8, f_9\}$ and $\{f_2, f_8\}$, respectively. Applying Theorem 27, the 3-partitions for them are $\{\{6\}, \{7\}, \{1, 2, 3, 4, 5, 8\}\}$ and $\{\{4, 8\}, \{2, 3, 6\}, \{1, 5, 7\}\}$, respectively.

This example highlights that the output of Algorithm 1 and consequently the partitioning of a graph varies with the embedding. Hence, in order to determine faces with extremum potentials we need to specify the embedding along with the transition matrix. To specify the embedding, we need to conduct a rotation system; there exists a unique such rotation system for every locally oriented graph embedding [43].

5.7 Application of Network Circulation in Cardiology

While graph theory has been widely used to model biological systems, in the field of cardiac electrophysiology, its application is fairly new. Perhaps one of the first applications of directed networks in studying the excitation of the human heart [83]. In this section, we briefly discuss the application of network circulation in cardiac conduction system for a specific case known as "reentry."

Reentry is a mechanism of pathologic impulse conduction and describes a self-sustaining cardiac rhythm abnormality. In fact, reentry may account for most tachyarrhythmias found in patients that could lead to life-threatening arrhythmias and sudden cardiac death [42, 51, 54]. A model for reentry is shown in Fig. 5.12. In normal conduction, a single action potential [29] travels down each branch and through a common, connecting pathway. In reentry, the action potential propagates in a circus-like closed loop manner and continuously depolarizes the cardiac muscles around the abnormal area.

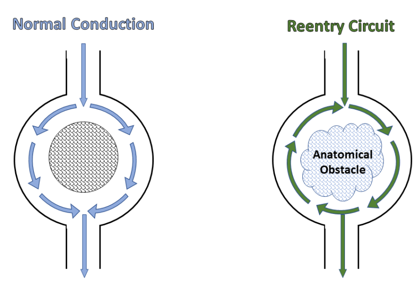

Figure 5.12: Normal conductoin and reentry circuit.

Reentry can take place within a small local region within the heart or it can occur between the atria and ventricles (global reentry) (see Fig. 5.13) and can cause atria and/or ventricular tachycardia. Local reentry could be as a result of conduction blocks, whereas global reentry is formed due to an accessory pathway[6]. A well-know complication that occur in the latter case is Wolff-Parkinson-White (WPW) pattern that can transition into ventricular tachycardia and sudden death without prompt diagnosis and treatment [54].

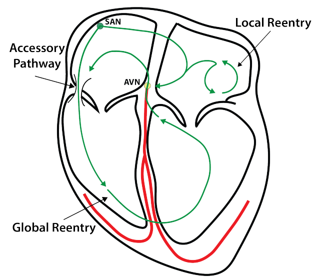

Figure 5.13: Local and global reentry in heart.

A permanent treatment for such cases is a cardiac ablation by destroying the abnormal conduction pathways with heat. Many complications can occur from cardiac ablation and it is crucial to locate the abnormal conduction pathways by precise cardiac mapping [18, 51]. The proposed macroscopic circulation concept in this chapter can be used as a diagnostic tool for detecting the source of arrhythmias and potential target cells for ablation.

5.8 Summary

In this work we introduced a notion of circulation and explored this concept for planar graphs where computations are simple. We shown how circulation for planar graphs relates to partitioning of the graph into three parts. We proposed an algorithm to effectively partition the planar graph and calculate circulation. It will be of great interest to consider whether such concepts can be quantified by spectral properties of the graph Laplacian as is the case for geometric properties in the case of the Cheeger inequality.

[6]Accessory pathways are muscle bridges connecting the atria and the ventricle, also called Kent bundles.

Chapter 6

Conclusions and Future Work

- The purpose of Chapter 3 is analysis of DeGroot-Friedkin model. In our approach, we used local inverse function theorem and Hadamard theorem to establish the existence and uniqueness of the fixed point. Another interesting direction of research for studying DeGroot-Friedkin model could be geometrical analysis, the reason is that the fixed point of the model could be interpreted as intersection of a system of hyperbola equations. We also found the closed form solution for the fixed point of the map for the special case of three individuals discussing on the sequence of issues. Future research may also focus on finding closed form solution of the fixed point for the general case of having a group of n individuals.

- In Chapter 4, we proposed a groups of nonlinear Markov chain models to capture social interactions in a group of people who discuss on a sequence of issues. In our setting, despite DeGroot-Friedkin model, individuals don't need to wait for opinion consensus on a particular issue s before updating their self-confidence. This setting allows individuals to update their self-confidence during the discussion. In addition, in this setting the random walk adapts the return probability of each state so as to promote or discourage residence in states with high marginal probability. We developed stability theory which allows drawing general conclusions on attractiveness of equilibria of nonlinear evolution models on probability simplices, i.e., stochastic evolutions. Besides the current interest in modeling dynamical interactions over social networks, the theory applies more broadly as similar models are pertinent in other types of interaction. Also, we extended our proposed models to study effect of colluding subgroup in opinion forming.

Future research should focus on the effect of uncertainty and disturbances in such models. We can also expand the analysis to the continuous-time setting. Continuous-time frame has several possible merits. Stability analysis in continuous-time turns out to be simpler than for the discrete-time evolution. On the other hand, analysis of the continuous-time dynamics may provide valuable insight into the dynamics of the discrete-time evolution. Also, modification of the proposed models in order to count for stubborn agents in the group is another relevant topic of research.

- In Chapter 5, We have introduced maximal graph circulation of ”divergence free” flows on graphs and related this with suitable 3-partitions. The 3-partitions can be seen as ”communities” (of nodes, cells, etc.) on the path that supports the maximizing circulatory current. Where as computational issues for general graphs remain a combinatorial challenge, planar graphs are amenable to a systematic analysis framework. Planar graphs are of great importance in cadriac electrophysiology, since the heart muscle may be seen as homeomorphic to a sphere where planar graphs can be projected. This last application was a motivating example for the work presented, and it is our hope that the concepts laid out in this work will facilitate the development of diagnostic tools for detecting the source of arrhythmias and potential target cells for ablation.

  A natural next step in this direction of research is to calculate macroscopic circulation for general graphs. Although we have demonstrated the advantages of planar graphs and the fact that calculating circulation for the special case of planar graph is simple. But in practice, many problems are modeled with general graphs and also in the proposed algorithm for calculating circulation we need to first check graph planarity but for large graphs this is not preferable. Further, the proposed algorithm does not always preserve connectivity of partitions. Of our interest is to study the effects of partitions' connectivity in macroscopic circulation.

Bibliography

[1] R. P. Abelson. Mathematical models of the distribution of attitudes under controversy. *Contributions to mathematical psychology*, 1964.

[2] O. Abrahamsson, D. Danev, and E. G. Larsson. Opinion dynamics with random actions and a stubborn agent. In *2019 53rd Asilomar Conference on Signals, Systems, and Computers*, pages 1486–1490. IEEE, 2019.

[3] D. Acemoğlu, G. Como, F. Fagnani, and A. Ozdaglar. Opinion fluctuations and disagreement in social networks. *Mathematics of Operations Research*, 38(1):1–27, 2013.

[4] S. Alemzadeh and M. Mesbahi. Influence models on layered uncertain networks: A guaranteed-cost design perspective. *arXiv preprint arXiv:1807.06612*, 2018.

[5] C. Altafini. Consensus problems on networks with antagonistic interactions. *IEEE Transactions on Automatic Control*, 58(4):935–946, 2013.

[6] R. Andersen, F. Chung, and K. Lang. Using pagerank to locally partition a graph. *Internet Mathematics*, 4(1):35–64, 2007.

[7] R. Andersen, F. Chung, and K. Lang. Local partitioning for directed graphs using pagerank. *Internet Mathematics*, 5(1-2):3–22, 2008.

[8] S. Arora, S. Rao, and U. Vazirani. Expander flows, geometric embeddings and graph partitioning. *Journal of the ACM (JACM)*, 56(2):5, 2009.

[9] Z. Askarzadeh, R. Fu, A. Halder, Y. Chen, and T. T. Georgiou. Stability theory of stochastic models in opinion dynamics. *IEEE Transactions on Automatic Control*, 2019.

[10] M. Berger and G. Hornig. A generalized poloidal–toroidal decomposition and an absolute measure of helicity. *Journal of Physics A: Mathematical and Theoretical*, 51(49), 2018.

[11] H. Bhatia, G. Norgard, V. Pascucci, and P.-T. Bremer. The Helmholtz-Hodge decomposition-a survey. *IEEE Transactions on Visualization and Computer Graphics*, 19(8):1386–1404, 2012.

[12] F. Bullo, J. Cortes, and S. Martinez. *Distributed control of robotic networks: a mathematical approach to motion coordination algorithms*, volume 27. Princeton University Press, 2009.

[13] Y. Cao, W. Yu, W. Ren, and G. Chen. An overview of recent progress in the study of distributed multi-agent coordination. *IEEE Transactions on Industrial informatics*, 9(1):427–438, 2013.

[14] S. Chaudhuri and A. Middey. The applicability of bipartite graph model for thunderstorms forecast over Kolkata. *Advances in Meteorology*, 2009.

[15] G. Chen, X. Duan, N. E. Friedkin, and F. Bullo. Social power dynamics over switching and stochastic influence networks. *IEEE Transactions on Automatic Control*, 64(2):582–597, 2018.

[16] L. Chen. A note on the discrete Jordan curve theorem (revised), 2013.

[17] X. Chen, J. Liu, M.-A. Belabbas, Z. Xu, and T. Başar. Distributed evaluation and convergence of self-appraisals in social networks. *IEEE Transactions on Automatic Control*, 62(1):291–304, 2017.

[18] R. Cheng, M. Chang, and C. Yuan Ng. Risks from catheter ablation of atrial fibrillation: A review of methods, efficacy, and safety. *Journal of atrial fibrillation*, 4(6):455, 2012.

[19] G. Como. On resilient control of dynamical flow networks. *Annual Reviews in Control*, 43:80–90, 2017.

[20] G. Como, E. Lovisari, and K. Savla. Throughput optimality and overload behavior of dynamical flow networks under monotone distributed routing. *IEEE Transactions on Control of Network Systems*, 2(1):57–67, 2015.

[21] S. Coogan. A contractive approach to separable lyapunov functions for monotone systems. *arXiv preprint arXiv:1704.04218*, 2017.

[22] É. C. De Verdière. Algorithms for embedded graphs, 2014.

[23] G. Deffuant, D. Neau, F. Amblard, and G. Weisbuch. Mixing beliefs among interacting agents. *Advances in Complex Systems*, 3(01n04):87–98, 2000.

[24] M. H. DeGroot. Reaching a consensus. *Journal of the American Statistical Association*, 69(345):118–121, 1974.

[25] R. L. Dobrushin. Central limit theorem for nonstationary Markov chains. I. *Theory of Probability & Its Applications*, 1(1):65–80, 1956.

[26] C. Doczkal. Short proof of Menger's theorem in coq (proof pearl). *HAL-02086931*, 2019.

[27] Y. Dong, Z. Ding, L. Martínez, and F. Herrera. Managing consensus based on leadership in opinion dynamics. *Information Sciences*, 397:187–205, 2017.

[28] Fan Chung. Laplacians and the cheeger inequality for directed graphs. *Annals of Combinatorics*, 9(1):1–19, 2005.

[29] J. Feher. 5.5 - The Cardiac Action Potential. In *Quantitative Human Physiology*, pages 528 – 536. Academic Press, Boston, second edition, 2012.

[30] F. Forni and R. Sepulchre. A differential lyapunov framework for contraction analysis. *IEEE Transactions on Automatic Control*, 59(3):614–628, 2014.

[31] F. Forni and R. Sepulchre. Differentially positive systems. *IEEE Transactions on Automatic Control*, 61(2):346–359, 2016.

[32] N. E. Friedkin. The attitude-behavior linkage in behavioral cascades. *Social Psychology Quarterly*, 73(2):196–213, 2010.

[33] N. E. Friedkin. A formal theory of reflected appraisals in the evolution of power. *Administrative Science Quarterly*, 56(4):501–529, 2011.

[34] N. E. Friedkin. The problem of social control and coordination of complex systems in sociology: A look at the community cleavage problem. *IEEE Control Systems*, 35(3):40–51, 2015.

[35] N. E. Friedkin and E. C. Johnsen. Social influence and opinions. *Journal of Mathematical Sociology*, 15(3-4):193–206, 1990.

[36] N. E. Friedkin and E. C. Johnsen. Social influence and opinions. *The Journal of Mathematical Sociology*, 15(3-4):193–206, 1990.

[37] N. Friendkin and E. Johnsen. Social influence networks and opinion change. *Adv Group Proc*, 16:1–29, 1999.

[38] A. Gagarin, W. Kocay, and D. Neilson. Embeddings of small graphs on the torus. *Cubo Mat. Edu.*, 5, 2003.

[39] S. Galam, Y. Gefen, and Y. Shapir. Sociophysics: A new approach of sociological collective behaviour. i. mean-behaviour description of a strike. *Journal of Mathematical Sociology*, 9(1):1–13, 1982.

[40] M. R. Garey, D. S. Johnson, and L. Stockmeyer. Some simplified np-complete problems. In *Proceedings of the sixth annual ACM symposium on Theory of computing*, pages 47–63, 1974.

[41] S. Gaubert and Z. Qu. Dobrushin's ergodicity coefficient for markov operators on cones. *Integral Equations and Operator Theory*, 81(1):127–150, 2015.

[42] A. Goyal, B. Senst, P. Bhyan, and et al. Reentry arrhythmia, September 2020.

[43] J. L. Gross and T. W. Tucker. *Topological graph theory*. Courier Corporation, 2001.

[44] J. L. Gross and J. Yellen. *Handbook of graph theory*. CRC press, 2003.

[45] A. Halder. Degroot-friedkin map in opinion dynamics is mirror descent. *IEEE Control Systems Letters*, 2019.

[46] A. Hatcher. *Algebraic topology*. Cambridge Univ. Press, Cambridge, 2005.

[47] R. Hegselmann, S. König, S. Kurz, C. Niemann, and J. Rambau. Optimal opinion control: The campaign problem. *arXiv preprint arXiv:1410.8419*, 2014.

[48] R. Hegselmann, U. Krause, et al. Opinion dynamics and bounded confidence models, analysis, and simulation. *Journal of artificial societies and social simulation*, 5(3), 2002.

[49] H. Helmholtz. Uber integrale der Hydrodynamischen Gleichungen, Welche den Wirbelbewegungen Entsprechen. *Journal fur die reine und angewandte Mathematik*, 1858(55):25–55, January 1858.

[50] W. V. D. Hodge. *The theory and applications of harmonic integrals*. Cambridge University Press, 1941.

[51] H. D. Huang, J. W. Waks, F. M. Contreras-Valdes, C. Haffajee, A. E. Buxton, and M. E. Josephson. Incidence and risk factors for symptomatic heart failure after catheter ablation of atrial fibrillation and atrial flutter. *EP Europace*, 18(4):521–530, 08 2015.

[52] P. Jia, N. E. Friedkin, and F. Bullo. Opinion dynamics and social power evolution: A single-timescale model. *arXiv preprint arXiv:1712.02452*, 2017.

[53] P. Jia, A. MirTabatabaei, N. E. Friedkin, and F. Bullo. Opinion dynamics and the evolution of social power in influence networks. *SIAM review*, 57(3):367–397, 2015.

[54] J. Kaplan, A. Kanwal, and V. Lala. Reentrant arrhythmia, 2020.

[55] V. N. Kolokoltsov. *Nonlinear Markov processes and kinetic equations*, volume 182. Cambridge University Press, 2010.

[56] K. Kuratowski. Sur le problème des courbes gauches en topologie. *Fundamenta Mathematicae*, 15(1):271–283, 1930.

[57] T. Leighton and S. Rao. An approximate max-flow min-cut theorem for uniform multicommodity flow problems with applications to approximation algorithms. Technical report, MASSACHUSETTS INST OF TECH CAMBRIDGE MICROSYSTEMS RESEARCH CENTER, 1989.

[58] Li Chen. Discrete Jordan curve theorem. In *Vision Geometry VIII*, pages 82–94. International Society for Optics and Photonics, SPIE, September 1999.

[59] L. Lim. Hodge laplacians on graphs. *SIAM Rev.*, 62:685–715, 2019.

[60] I. R. Manchester and J.-J. E. Slotine. On existence of separable contraction metrics for monotone nonlinear systems. *IFAC-PapersOnLine*, 50(1):8226–8231, 2017.

[61] Y. Mao, S. Bouloki, and E. Akyol. Spread of information with confirmation bias in cyber-social networks. *IEEE Transactions on Network Science and Engineering*, 2018.

[62] A. A. Markov. Extension of the law of large numbers to dependent quantities. *Izv. Fiz.-Matem. Obsch. Kazan Univ.(2nd Ser)*, 15:135–156, 1906.

[63] O. Mason and M. Verwoerd. Graph theory and networks in biology. *IET systems biology*, 1(2):89–119, 2007.

[64] K. Menger. Zur allgemeinen kurventheorie. *Fundamenta Mathematicae*, 10(1):96–115, 1927.

[65] A. Mirtabatabaei, P. Jia, N. E. Friedkin, and F. Bullo. On the reflected appraisals dynamics of influence networks with stubborn agents. In *American Control Conference (ACC), 2014*, pages 3978–3983. IEEE, 2014.

[66] B. Mohar and C. Thomassen. *Graphs on surfaces*, volume 16. Johns Hopkins University Press Baltimore, 2001.

[67] G. Nemhauser and L. Wolsey. Integer programming and combinatorial optimization. In *Wiley, 1988*. Springer, 1999.

[68] H. Noorazar. Recent advances in opinion propagation dynamics: a 2020 survey. *The European Physical Journal Plus*, 135(6):1–20, 2020.

[69] H. Noorazar, K. R. Vixie, A. Talebanpour, and Y. Hu. From classical to modern opinion dynamics. *International Journal of Modern Physics C*, 31(07):2050101, 2020.

[70] S. E. Parsegov, A. V. Proskurnikov, R. Tempo, and N. E. Friedkin. Novel multidimensional models of opinion dynamics in social networks. *IEEE Transactions on Automatic Control*, 2016.

[71] G. Pavlopoulos, M. Secrier, and C. Moschopoulos. Using graph theory to analyze biological networks. *BioData Mining*, 4(10), 2011.

[72] J. D. Phillips, W. Schwanghart, and T. Heckmann. Graph theory in the Geosciences. *Earth-Science Reviews*, 143:147 – 160, 2015.

[73] J. Quaintance. *Combinatorial Identities for Stirling Numbers: The Unpublished Notes of H W Gould*. World Scientific, 2015.

[74] F. Razafindrazaka, P. Yevtushenko, K. Poelke, F. Polthier, and L. Goubergrits. Hodge decomposition of wall shear stress vector fields characterizing biological flows. *Royal Society Open Science*, 6, 2019.

[75] G. Russo, M. Di Bernardo, and E. D. Sontag. A contraction approach to the hierarchical analysis and design of networked systems. *IEEE Transactions on Automatic Control*, 58(5):1328–1331, 2013.

[76] S. Sarvottamananda. Lecture notes in planar graphs, planarity testing and embedding, October 2014.

[77] E. Seneta. Markov and the creation of Markov chains. In *Markov Anniversary Meeting*, pages 1–20. Boson Books, Raleigh, North Carolina,, 2006.

[78] K. Sznajd-Weron and J. Sznajd. Opinion evolution in closed community. *International Journal of Modern Physics C*, 11(06):1157–1165, 2000.

[79] C. Thomassen. Planarity and duality of finite and infinite graphs. *Journal of Combinatorial Theory, Series B*, 29(2):244–271, 1980.

[80] C. Thomassen. Embeddings of graphs with no short noncontractible cycles. *Journal of Combinatorial Theory, Series B*, 48(2):155–177, 1990.

[81] T. Vaidya, T. Chotibut, and G. Piliouras. Broken detailed balance and non-equilibrium dynamics in noisy social learning models. *Physica A: Statistical Mechanics and its Applications*, 570:125818, 2021.

[82] T. Vaidya, C. Murguia, and G. Piliouras. Learning agents in black–scholes financial markets. *Royal Society open science*, 7(10):201188, 2020.

[83] N. Vandersickel, E. Van Nieuwenhuyse, N. Van Cleemput, J. Goedgebeur, M. El Haddad, J. De Neve, A. Demolder, T. Strisciuglio, M. Duytschaever, and A. V. Panfilov. Directed networks as a novel way to describe and analyze cardiac excitation: Directed graph mapping. *Frontiers in Physiology*, 10:1138, 2019.

[84] K. Wagner. Uber eine Erweiterung eines Satzes von Kuratowski. *Deutsche Mathematik*, 2:280–285, 1937.

[85] D. Wang, W. Chen, and L. Qiu. Multi-leader selection in complex networks. In *2016 IEEE 55th Conference on Decision and Control (CDC)*, pages 1751–1756. IEEE, 2016.

[86] H. Whitney. Congruent graphs and the connectivity of graphs. In *H. Whitney Collected Papers*, pages 61–79. Springer, 1992.

[87] R. J. Wilson. *Introduction to graph theory*. Pearson Education India, 1979.

[88] Z. Xu, J. Liu, and T. Başar. On a modified Degroot-Friedkin model of opinion dynamics. In *American Control Conference (ACC), 2015*, pages 1047–1052. IEEE, 2015.

[89] M. Ye, J. Liu, B. D. Anderson, C. Yu, and T. Başar. On the analysis of the degroot-friedkin model with dynamic relative interaction matrices. *IFAC-PapersOnLine*, 50(1):11902–11907, 2017.

[90] A. Zagouras, A. A. Argiriou, H. A. Flocas, G. Economou, and S. Fotopoulos. An advanced method for classifying atmospheric circulation types based on prototypes connectivity graph. *Atmospheric Research*, 118:180 – 192, 2012.

[91] Z. Zhang and M.-Y. Chow. Convergence analysis of the incremental cost consensus algorithm under different communication network topologies in a smart grid. *IEEE Transactions on Power Systems*, 27(4):1761–1768, 2012.

[92] Q. Zhou, Z. Wu, A. H. Altalhi, and F. Herrera. A two-step communication opinion dynamics model with self-persistence and influence index for social networks based on the degroot model. *Information Sciences*, 519:363–381, 2020.